Energy Research and Development Division
FINAL PROJECT REPORT

POTENTIAL IMPACTS OF FUTURE GEOLOGICAL STORAGE OF CO_2 ON THE GROUNDWATER RESOURCES IN CALIFORNIA'S CENTRAL VALLEY

Simulations of Deep Basin Pressure Changes and Effect on Shallow Water Resources

Prepared for: California Energy Commission
Prepared by: Lawrence Berkeley National Laboratory

MAY 2013
CEC-500-2014-028

PREPARED BY:

Primary Author(s):
Nigel Quinn
Haruku Wainwright
Preston Jordan
Quanlin Zhou
Jens Berkholzer

Lawrence Berkeley National Laboratory
1 Cyclotron Road
Berkeley, CA 94720

Contract Number: 500-09-034

Prepared for:

California Energy Commission

Joe O'Hagan
Contract Manager

Aleecia Gutierrez
Office Manager
Energy Generation Research Office

Laurie ten Hope
Deputy Director
ENERGY RESEARCH AND DEVELOPMENT DIVISION

Robert P. Oglesby
Executive Director

DISCLAIMER

This report was prepared as the result of work sponsored by the California Energy Commission. It does not necessarily represent the views of the Energy Commission, its employees or the State of California. The Energy Commission, the State of California, its employees, contractors and subcontractors make no warranty, express or implied, and assume no legal liability for the information in this report; nor does any party represent that the uses of this information will not infringe upon privately owned rights. This report has not been approved or disapproved by the California Energy Commission nor has the California Energy Commission passed upon the accuracy or adequacy of the information in this report.

ACKNOWLEDGEMENTS

Funding for this work was provided by the California Energy Commission, as part of "Work for Others" funding for Lawrence Berkeley National Laboratory. The authors thank the California Energy Commission for supporting this research through California's Public Interest Energy Research Program. The uncertainty quantification methods used in Section 4 were partially developed under the National Risk Assessment Partnership (NRAP), supported by the Assistant Secretary for Fossil Energy, Office of Sequestration, Hydrogen, and Clean Coal Fuels, of the U.S. Department of Energy, under Contract No. DE-AC02-05CH11231.

The authors wish to thank Marco Bianchi and Dan Hawkes of Lawrence Berkeley National Laboratory for a careful review of the manuscript and the suggestion of improvements. Thanks are also due to Jeff Wagoner from Lawrence Livermore National Laboratory for developing the geologic framework model of the southern San Joaquin Basin. The authors would also like to thank Claudia Faunt from the U.S. Geological Survey in San Diego, California for her help and support with extracting the Kern Subarea model from the CVHM MODFLOW application. We had the privilege of working with the new Farm Process software while still under development by Randy Hanson and got to test the new subsidence algorithm which separates elastic and inelastic subsidence and the new deformable mesh algorithm. Randy's quick attention to bug fixes was much appreciated. Also we are thankful to Hoang Tran from Aquaveo Inc. who gave valuable lessons in the workings of GMS and provided valuable help with the output post-processing. The U.S. Bureau of Reclamation's MPGIS group, in particular Diane Williams, was helpful in assisting with the data output conversion process from Earthvision.

PREFACE

The California Energy Commission Energy Research and Development Division supports public interest energy research and development that will help improve the quality of life in California by bringing environmentally safe, affordable, and reliable energy services and products to the marketplace.

The Energy Research and Development Division conducts public interest research, development, and demonstration (RD&D) projects to benefit California.

The Energy Research and Development Division strives to conduct the most promising public interest energy research by partnering with RD&D entities, including individuals, businesses, utilities, and public or private research institutions.

Energy Research and Development Division funding efforts are focused on the following RD&D program areas:

- Buildings End-Use Energy Efficiency
- Energy Innovations Small Grants
- Energy-Related Environmental Research
- Energy Systems Integration
- Environmentally Preferred Advanced Generation
- Industrial/Agricultural/Water End-Use Energy Efficiency
- Renewable Energy Technologies
- Transportation

Potential Impacts of Future Geological Storage of CO_2 on the Groundwater Resources in California's Central Valley: Simulations of Deep Basin Pressure Changes and Effect on Shallow Water Resources is the final report for the Potential Impacts of Future Geological Storage of CO_2 on the Groundwater Resources in California's Central Valley: Simulations of Deep Basin Pressure Changes and Effect on Shallow Water Resources project (contract number 500-09-034) conducted by Lawrence Berkeley National Laboratory. The information from this project contributes to Energy Research and Development Division's Industrial/Agricultural/Water End-Use Energy Efficiency Program.

For more information about the Energy Research and Development Division, please visit the Energy Commission's website at www.energy.ca.gov/research/ or contact the Energy Commission at 916-327-1551.

ABSTRACT

This study investigated the potential impacts of the injection and storage of large quantities of carbon dioxide on shallow water resources in California's southern San Joaquin Basin, including the possibility that if such injection was properly planned it might help mitigate the land subsidence impacts related to over-pumping of groundwater. The project used simulation studies to investigate whether the basin-scale pressure changes and brine displacement caused by future carbon dioxide storage in the deep sediments could impact the groundwater-surface water systems in the area. Two simulation models were developed. The Deep Basin Reservoir Simulation Model was developed for accurately simulating the multiphase processes of carbon dioxide and brine flow occurring in deep sequestration reservoirs. The Shallow Water Resources Impact Simulation Model was developed for accurately predicting the impact of deep carbon dioxide sequestration on a stressed water system, including evaluation of carbon dioxide-related impacts in the context of the long-term groundwater and subsidence trends occurring in the area as a result of other water stresses such as pumping and irrigation. The Deep Basin Reservoir Simulation Model showed that the caprock and overlying geological units had sufficient barrier attributes to prevent pressure propagation from the injection layer to the shallow aquifers. The Shallow Water Resources Impact Simulation Model simulation results showed that deep carbon dioxide injection would create only minor head change and surface uplift in the shallow model layers. Overall the simulation results suggested that even large carbon dioxide storage projects should have minimal impact on shallow groundwater and surface water systems if thick layers of shales and sands separated the deep CO_2 injection layers from shallow aquifers. Researchers believed this study justified devoting resources to evaluating the potential impact from localized pathways or from induced seismicity to more thoroughly investigate the feasibility of carbon dioxide storage in the southern San Joaquin Basin.

Keywords: geologic carbon sequestration, groundwater, saline aquifers

Please use the following citation for this report:

Quinn, Nigel; Haruko Wainwright; Preston Jordan; Quanlin Zhou; Jens Birkholzer. (Lawrence Berkeley National Laboratory). 2013. ***Potential Impacts of Future Geological Storage of CO_2 on the Groundwater Resources in California's Central Valley: Simulations of Deep Basin Pressure Changes and Effect on Shallow Water Resources.*** California Energy Commission. Publication number: CEC-500-2014-028.

TABLE OF CONTENTS

ACKNOWLEDGEMENTS ..... **i**

PREFACE ..... **ii**

ABSTRACT ..... **iii**

TABLE OF CONTENTS ..... **iv**

LIST OF FIGURES ..... **vi**

LIST OF TABLES ..... **xi**

EXECUTIVE SUMMARY **1**

Introduction 1

Project Purpose 2

Project Approach 2

Project Benefits 3

CHAPTER 1: **5**

Introduction **5**

1.1 Background and Objective 5

1.2 Methodology and Project Tasks 7

CHAPTER 2: Southern San Joaquin Valley **16**

2.1 Description of Population, Agriculture, and Water Resources 16

2.2 CO_2 Emissions and Storage Potential 18

CHAPTER 3: **21**

Development of Geologic and Hydrogeologic Framework **21**

3.1 Hydrogeology of the Southern San Joaquin Basin 21

3.2 Data Sources and Methods 25

3.3 Brief Description of Geomodels 26

CHAPTER 4: The Deep Basin Reservoir Simulation Model **31**

4.1 Model Description 31

4.1.1 Model Domain and Setup 31

4.1.2 Numerical Model 34

4.1.3 System Responses of Interest 35
4.2 Base-Case Results 37
4.2.1 Deep Injection Reservoir 37
4.2.2 Shallow Groundwater Resources 38
4.2.3 Land Surface Uplift 39
4.3 Uncertainty Quantification 40
4.3.1 Parameter Range and Distribution 40
4.3.2 Pressure Profiles 41
4.3.3 Fluxes at Eastern Boundary 42
4.3.4 Land-Surface Uplift 43
4.4 Compartmentalized Reservoir 44
4.4.1 Deep Injection Reservoir 46
4.4.2 Land Surface Uplift 47
4.5 Summary Results from Deep Basin Reservoir Simulation Model 49
CHAPTER 5: 50
The Shallow Water Resources Impact Simulation Model 50
5.1 Selection of Suitable Shallow Simulation Model 50
5.1.1 Model Mesh 51
5.1.2 Stream-Aquifer Interactions 52
5.1.3 Evapotranspiration 53
5.1.4 Deficit Irrigation 53
5.1.5 Simulation of Ggroundwater Wells 53
5.1.6 Subsidence 54
5.2. Description of CVHM-FMP Attributes 54
5.2.1 Hydrologic and Land Use Data Inputs 55
5.2.2 Lithologic Data Inputs and CVHM-FMP3 Model Topology 58
5.2.3 Shallow Model Subsidence Simulation 60
5.2.4 Water Budget Analysis 61

5.2.5 Model Calibration against Monitoring Well Data 62

5.3 Modification of CVHM-FMP to Build Shallow Water Resources Impact Simulation Model 65

5.3.1 Development of Kern Sub-Basin Model 65

5.3.2 Vertical Extension of Kern Sub-Basin Model 66

5.4 Model Results 68

5.4.1 CO_2 Injection Scenario 68

5.4.2 Observation Locations 69

5.4.3 Vertical Profiles of Head and Displacement Response at Vedder Injection Location 70

5.4.4 Time Evolution of Head and Displacement Response at Vedder Injection Location 74

5.4.5 Time Evolution of Head and Displacement Response at Other Locations 81

5.4.6 Contour Plots of Head at 0.1, 10, 25 and 50 Years 91

5.4.7 Contour Plots of Displacement at 10, 25 and 50 Years 96

5.5 Summary Results from Shallow Water Resources Impact Simulation Model 102

CHAPTER 6: 104

Conclusions and Outlook 104

REFERENCES 107

LIST OF FIGURES

Figure 1: Schematic Showing Different Regions of Influence Related to CO_2 Storage (from Birkholzer et al., 2009) 6

Figure 2: Geologic Cross Section through the San Joaquin Valley 8

Figure 3: Initial Plan for Coupling the Simulation Model for CO_2 Storage Impacts in Deep Sediments and the Shallow Groundwater Management Model 9

Figure 4: 3-D Depiction of the 50 km by 50 km Geologic Framework Model for the Kimberlina Project, with the Planned Kimberlina Injection Location in the Center 11

Figure 5: Generalized Cross Section (A-A') Showing the Vertical Discretization of the CVHM Model in the San Joaquin Basin, California (Source: Faunt et al., 2009a) 13

Figure 6: Use of Hydrographic Water Budget Areas by Both CVHM and C2VSIM Models to Simulate Groundwater and Surface Water Hydrology of the Central Valley (Faunt et al., 2009a) 14

Figure 7: Map of Kern County Water Districts Showing Dependence on Three Major Conveyance Systems: the California Aqueduct, Which Runs along the Western Margin of the Southern San Joaquin Basin, the Friant Kern Canal, Which Runs North to South along the Eastern Margin of the Basin, and the Cross Valley Canal, Which Allows California Aqueduct Water to Deliver Surplus Flow to the Friant Kern Canal (KCWA, 2013) 17

Figure 8: Total Annual CO_2 Emissions from Large Stationary Sources in WESTCARB Region (from U.S. DOE, 2012) 18

Figure 9: Mapping of Large Stationary CO_2 Emitters with Geologic Storage Potential in California. Red Circle Marks our Study Area in the Southern San Joaquin Basin 20

Figure 10: Planview of San Joaquin Basin with Focus Area in the South 22

Figure 11: Generalized Stratigraphic Section for the Southern San Joaquin Basin (Hosford Scheirer, 2007) 25

Figure 12: Extent of the Two Geomodels Used in this Study 27

Figure 13: Cut-Away View of the 84 km by 112 km Regional Model at the Location of the Planned Kimberlina Injection (Vertical Yellow Line) 28

Figure 14: Cut-Away View of the Rotated 103 km by 168 km Regional Model 28

Figure 15: Projection of the Extent of the Vedder Formation (in Yellow) on Top of the Underlying Formations (in Brown) 29

Figure 16: Projection of the Extent of the Stevens Formation (in Yellow) on Top of the Underlying Formations (in Brown) 30

Figure 17: Various Cross-Sections of the Geological Model in a Fence Diagram 30

Figure 18: Vedder Sandstone Reservoir: (a) Areal Extent and Faults, (b) Thickness (in m), and (c) Top Elevation (in m) 33

Figure 19: Estimated Depth-Dependent (a) V Sand Permeability and (b) V Sand Porosity 34

Figure 20: 2D Plan View of Simulation Mesh 35

Figure 21: Evolution of Pressure Buildup (Top Row in MPa) and CO_2 Saturation (Bottom Row) at 20, 50, 100 and 200 yr after Start of CO_2 Injection (Left to Right Columns) 39

Figure 22: Evolution of Pressure Buildup (in 10^{-3} MPa) in the Shallow Aquifer at 25, 50, 100 and 200 Years from Left to Right 39

Figure 23: Surface Uplift at 25, 50, 100, and 200 Years from Left to Right 40

Figure 24: Pressure Increase along a Vertical Column at the Location Adjacent to the Injection Location 42

Figure 25: (a) Flux and (b) Migration Distance at the Eastern Boundary in the Updipping Vedder Formation 43

Figure 26: Land-Surface Uplift above the Injection Point 44

Figure 27: CO_2 Storage Scenarios for Different Systems; Open, Closed and Semi-Closed System from the Top 45

Figure 28: Domain for the Compartmentalized (closed) System 45

Figure 29: Evolution of Pressure Buildup (Top Row in MPa) and CO_2 Saturation (Bottom Row) at 20, 50, 100 and 200 yr after Start of CO_2 Injection (Left to Right Columns) for the Compartmentalized Reservoir 46

Figure 30: Pressure Increase along the Vertical Columns at the Location Adjacent to the Injection Location for the Compartmentalized Reservoir 47

Figure 31: Base Case Results: Land-Surface Uplift in Top Model Layer in the Compartmentalized Reservoir. 48

Figure 32: Land Surface Uplift above Injection Point for the Compartmentalized Reservoir 48

Figure 33: Conceptual Water Flow Diagram Showing the Relative Fluxes Related to Atmosphere, aquifer and Stream Channels Components in the MODFLOW-FMP Pre-Processor (Schmid et al., 2006; http://water.usgs.gov/nrp/gwsoftware/mf2k-fmp/tm6A17.pdf) 52

Figure 34: Historical Effective Precipitation for the Kern Sub-Basin Model through 2010 Estimated by the Kern County Water Agency (KCWA, 2013) 56

Figure 35: Gross Water Supplies and Net Crop Water Requirements within the Kern Sub-Basin Estimated by the Kern County Water Agency (KCWA, 2013) 56

Figure 36: Irrigated Acreage Estimated by the Kern County Water Agency – the Major Water Purveyor for the Region Covered by the Kern Sub-Basin Model (KCWA, 2013) 57

Figure 37: Main Crop Distribution for 2010 within the Kern Sub-Basin (KCWA, 2013) 57

Figure 38: Groundwater Pumping Estimated by the Kern County Water Agency for the Kern Sub-Basin (KCWA, 2013) 58

Figure 39: Texture Distributions for Three Layers within the 10 Layer CVHM-FMP3 Model for the Kern Sub-Basin. (a) Model Top 50 ft Layer; (b) Corcoran Clay Aquitard Layer; (c) Model Layer 6. 59

Figure 40: Map of Subsidence in the Central Valley Showing the Concentration of Problems in the Kern Sub-Basin Simulated by the CVHM-FMP3 Model. 60

Figure 41: Major Land Subsidence Areas in the Kern Sub-Basin Mostly Due to Water Level Declines over Time 61

Figure 42: Water Budgets for Component Subareas within the Kern Sub-Basin 62

Figure 43: Depth to Shallow Groundwater in the Kern Sub-Basin (KCWA, 2013) 64

Figure 44: Groundwater Quality in the Confined Aquifer below the Corcoran Clay in the Model Kern Sub-Basin 64

Figure 45: Depth to Groundwater in the Unconfined (above Corcoran) Aquifer (KCWA, 2013) 65

Figure 46: 3-D View Showing the 15 Vertical Formations of the Deep Geomodel Mapped to CVHM-FMP3 67

Figure 47: 3-D Rendering of the CVHM-FMP3 Model Showing Surface Features with an Overlay of the Model Rectangular 1 Mile by 1 Mile Mesh 67

Figure 48: CVHM-FMP3 Model Imported into GMS 68

Figure 49: Plan View of Injection Locations and Observation Locations 69

Figure 50: East-West Cross Section Showing Vedder Formation in Red, with Vedder Injection Well as Vertical Black Line. 70

Figure 51: Diagonal Cross Section Showing Stevens Formation in Turquoise and Vedder Formation in Red, with Stevens Injection Well as Vertical Black Line 70

Figure 52: Head Profiles for the Vedder and Stevens Formation Injection Simulation Observed at the Vedder Site for 0.1, 10, 25 and 50 Year Simulations 72

Figure 53: Displacement Profiles for the Vedder and Stevens Formation Injection Simulation Observed at the Vedder Site for 10, 25, and 50-Year Simulations 73

Figure 54: Head and Vertical Displacement in Layer 6 Comparing Vedder Formation and Combined Vedder and Stevens Formation Injection Scenarios with the Base (No Injection) Scenario 75

Figure 55: Head and Vertical Displacement in Layer 9 Comparing Vedder Formation and Combined Vedder and Stevens Formation Injection Scenarios with the Base (No Injection) Scenario. 76

Figure 56: Head and Vertical Displacement in Layer 11 Comparing Vedder Formation and Combined Vedder and Stevens Formation Injection Scenarios with the Base (No Injection) Scenario 78

Figure 57: Head and Vertical Displacement in Layer 21 Comparing Vedder Formation and Combined Vedder and Stevens Formation Injection Scenarios with the Base (No Injection) Scenario 79

Figure 58: Head and Vertical Displacement in Layer 26 Comparing Vedder Formation and Combined Vedder and Stevens Formation Injection Scenarios with the Base (No Injection) Scenario 80

Figure 59: Pressure Head and Vertical Displacement in Layer 6 at the Vedder "Hydro" Observation Location. Vedder "Hydro" is about 4 km Updip of the Vedder Formation Injection to the East 82

Figure 60: Pressure Head and Vertical Displacement in Layer 6 at the Vedder "Geo" Observation Location. Vedder "Geo" is about 14 km Updip of the Vedder Formation Injection to the East 83

Figure 61: Pressure Head and Vertical Displacement in Layer 6 at the Stevens "Hydro" Observation Location. Stevens "Hydro" is about 4 km West of the Stevens Formation Injection 84

Figure 62: Pressure Head and Vertical Displacement in Layer 6 at the Stevens "Geo" Observation Location 85

Figure 63: Pressure Head and Vertical Displacement in Layer 21 at the Vedder "Hydro" Observation Location 87

Figure 64: Pressure Head and Vertical Displacement in Layer 11 at the Vedder "Geo" Observation Location 88

Figure 65: Pressure Head and Vertical Displacement in Layer 22 at the Stevens "Hydro" Observation Location. 89

Figure 66: Pressure Head and Vertical Displacement in Layer 23 at the Stevens "Geo" Observation Location 90

Figure 67: Baseline Head Contours (Meters) for Layer 6 at 0.1 Years, 10 Years, 25 years, and 50 Years 92

Figure 68: Baseline Head Contours (Meters) for Layer 10 at 0.1 Years, 10 Years, 25 years, and 50 Years 93

Figure 69: Baseline Head Contours (Meters) for Layer 21 at 0.1 Years, 10 Years, 25 Years, and 50 Years 94

Figure 70: Vedder Injection Head Contours (Meters) for Layer 21 at 0.1 Years, 10 Years, 25 Years, and 50 Years 95

Figure 71: Vedder and Stevens Injection Head Contours (Meters) for Layer 21 at 0.1 Years, 10 Years, 25 Years, and 50 Years 96

Figure 72: Baseline Vertical Displacement Contours (Meters) for Layer 6 at 10 Years, 25 years, and 50 Years 98

Figure 73: Baseline Vertical Displacement Contours (Meters) for Layer 21 at 10 Years, 25 Years, and 50 Years 99

Figure 74: Vedder Injection Vertical Displacement Contours (Meters) for Layer 21 at 10 Years, 25 Years, and 50 Years 100

Figure 75: Vedder and Stevens Injection Vertical Displacement Contours (Meters) for Layer 21 at 10 Years, 25 Years, and 50 Years 101

LIST OF TABLES

Table 1: Hydrogeologic Properties Assigned to Each Formation: k_h and k_v are Horizontal and Vertical Permeability, Φ is Porosity, β_P is Pore Compressibility, α is the Van Genuchten Parameter for Entry Capillary Pressure, and m is the Van Genuchten Parameter for Pore-Size Distribution 32

EXECUTIVE SUMMARY

Introduction

A promising measure for mitigating climate change is to store large volumes of carbon dioxide (CO_2) captured from large point-source carbon emitters in deep saline aquifers. The thick sediments of California's Central Valley have been identified as prime targets for future geological carbon sequestration (GCS). The Sacramento and San Joaquin River basins have thick sedimentary sections at sufficient depth, and include multiple saline aquifers and oil and gas reservoirs that may be able to accept large volumes of injected CO_2. Widespread shale seals found in the basins would serve as structural trapping, ensuring the natural long-term confinement of injected CO_2. There have also been significant geological data collected from oil and gas operations in these basins.

California's Central Valley is home to over six million people and generates over $20 billion in agricultural crops annually. The agricultural and urban development in the area depends on an intricate surface water distribution system that routes water from surrounding watersheds to the Central Valley and on the presence of extensive aquifers that provide substantial amounts of freshwater and are increasingly being used as buffers for fluctuations in surface water supplies. Managing the Central Valley's water resources has been a challenging task in light of limited water availability from drought and climate change, increasing demands, environmental concerns about wetlands, endangered species and water quality, as well as land subsidence caused by groundwater pumping. Any water resources impacts of large-scale CO_2 storage need to be evaluated before industrial-size storage projects get under way.

An extremely large amounts of CO_2 will need to be injected and sequestered underground for this technology to contribute significantly to climate change mitigation. Storing these additional fluids in deep saline aquifers causes pressure changes and displacement of native brines, affecting subsurface volumes that can be significantly larger than the CO_2 plume itself. Environmental impacts on groundwater resources may result if the deep parts of the basin communicate effectively with shallower units.

Numerous research studies have been conducted in the United States and worldwide over the last decade or so evaluating under which hydrogeological conditions the injected volumes of CO_2 could be safely stored over hundreds or even thousands of years. The topic of reservoir pressurization due to large-scale CO_2 storage has recently received increasing attention. Researchers are addressing questions about pressure-driven caprock fracturing and/or fault reactivation in addition to concerns about potential brine migration and related impacts on shallower groundwater resources. Large-scale pressurization could also be an issue for activities involving exploitation of subsurface resources in the area, such as oil and gas or geothermal energy or may affect neighboring CO_2 storage sites that reside in the same formation. Pressure management via extraction of native brines has been proposed to mitigate pressure concerns but the cost for pumping, treatment, and disposal of these brines can be prohibitive.

Project Purpose

The pupose of this study is to evaluate the potential impact of large-scale CO_2 sequestration in California, with specific focus on the water resources in the southern San Joaquin River Valley. The study involved two distinct, but related projects. The first project utilized production and pressure data from oil reservoirs in the San Joaquin Valley as a reverse analog to the potential pressure impact of CO_2 injection. Results from this project were summarized in a companion report. The second project used simulation studies to investigate whether the basin-scale pressure changes and brine displacement caused by future CO_2 storage in the deep sediments could impact the groundwater-surface water systems in the area. This report summarizes the second project, which aimed to address the following questions:

- Will vertical pressure propagation through thick layers of shale and sands have a significant impact on shallow water resources?
- Is brine displacement an issue through thick layers of shale and sands for shallow water resources?
- What deformations are to be expected from deep CO_2 storage, and would land surface uplift be a concern for shallow water resources?

Project Approach

Researchers developed two separate, but complementary simulation models that covered the entire vertical thickness of interest, from deep sequestration reservoirs to shallow water resources. The first model was the Deep Basin Reservoir Simulation Model, which was extended upward to include relevant shallow layers, albeit with much less level of detail. The second model was the Shallow Water Resources Impact Simulation Model, which was extended downward to include additional deep sediments of interest for geologic carbon sequestration. Both models were applied in parallel efforts to look into CO_2 storage impacts.

The Deep Basin Reservoir Simulation Model was developed for accurately simulating the multiphase processes of CO_2 and brine flow occurring in deep sequestration reservoirs. The scale of this model was extended to include shallow groundwater resources and was expected to provide reasonable estimates of shallow pressure changes and land-surface impacts of CO_2 injection, but did not account for the complex water stresses important for shallow water resources and groundwater management and did not model any dynamic trends except those induced by CO_2 sequestration. Simulations with this model were conducted for a range of parameter uncertainty cases to accurately predict the impact of CO_2 injection on pressure buildup and brine displacement in deep sediments and to obtain reasonable estimates of shallow pressure changes and land-surface impacts. The model essentially served as a validation tool for the Shallow Water Resources Impact Simulation Model and was also used to conduct uncertainty quantification and analysis of alternative storage scenarios.

The Shallow Water Resources Impact Simulation Model was developed for accurately predicting the impact of deep CO_2 sequestration on a stressed water system using an accurate and well-calibrated simulation tool for water resources in the area that allowed evaluation of CO_2-related impacts in the context of the long-term groundwater and subsidence trends occurring in the area as a result of other water stresses such as pumping and irrigation.

Simulations with this model were conducted for selected carbon sequestration scenarios to predict CO_2-related impacts in the context of long-term groundwater and subsidence trends occurring in the area from other water stresses such as pumping and irrigation.

Project Results

The Deep Basin Reservoir Simulation Model showed that the caprock and overlying geological units had sufficient barrier attributes to prevent pressure propagation from the injection layer to the shallow aquifers. The updipping structure of the injection layer created a hydrological connection with shallow surface aquifers several tens of kilometers east of the injection location but the pressure increase and brine flux decreased significantly before reaching this connection. Researchers concluded that the potential concerns associated with CO_2 storage would be relatively minor except possibly for land surface uplift effects. The Deep Basin Reservoir Simulation Model did not account for any of the dynamic shallow water resources changes in the region caused by groundwater pumping and other water management practices so the researchers' conclusions were not based on a direct comparison of CO_2 injection impacts with other ongoing water system stresses.

The Shallow Water Resources Impact Simulation Model simulation results showed that deep CO_2 injection would create only minor head change and surface uplift in the shallow model layers, which was consistent with the findings from the Deep Basin Reservoir Simulation Model. The projected changes in shallow groundwater levels and surface displacement caused by CO_2 injection were much smaller than the significant groundwater drawdown and land subsidence effects that can result from ongoing pumping in shallow aquifers. The projected long-term subsidence would be slightly offset by the uplift provided by deep well injection of CO_2. This minor uplift was unlikely to cause any damage to existing conveyance facilities or to disrupt agricultural activities in any significant way. If carefully planned such uplift could work against unwanted subsidence and could have a positive effect. These conclusions were partly site-specific because the geologic units in this study were capable of preventing substantial vertical pressure propagation, injection of CO_2 occurs fairly deep and the overlying shallow water resources were already strongly impacted from over-pumping and thus affected by head decreases and land subsidence.

Overall the simulation results suggested that even large CO_2 storage projects should have minimal impact on shallow groundwater and surface water systems if thick layers of shales and sands separated the deep CO_2 injection layers from shallow aquifers. This study did not look into the potential for leakage of CO_2 and/or brine in localized pathways and did not consider the possibility of pressure-induced fault activation or "induced seismicity." Researchers believed this study justified devoting resources to evaluating the potential impact from localized pathways or from induced seismicity to more thoroughly investigate the feasibility and safety of CO_2 storage in the southern San Joaquin Basin.

Project Benefits

This study evaluated the potential impact of large-scale CO_2 sequestration in California, with specific focus on the water resources in the southern San Joaquin River Valley. Carbon

sequestration is a method for potentially storing captured CO_2 so that it is not released into the atmosphere. The study showed that even large CO_2 storage projects should have minimal impact on shallow groundwater and surface water systems if thick layers of shales and sands separated the deep CO_2 injection layers from shallow aquifers. Successful carbon sequestration could help reduce the amount of greenhouse gases that contribute to climate change.

CHAPTER 1: Introduction

1.1 Background and Objective

A promising measure for mitigating climate change is to store large volumes of CO_2 captured from large point-source carbon emitters in deep saline aquifers. In California, the thick sediments of the Central Valley have been identified as prime targets for future geological carbon sequestration (GCS). Both the Sacramento and San Joaquin River basins have thick sedimentary sections at sufficient depth, including multiple saline aquifers and oil and gas reservoirs, which guarantee a large injection volume. Widespread shale seals found in the basins would serve as structural trapping, ensuring the natural long-term confinement of injected CO_2. In addition, there have been significant geological data collected from oil and gas operations, which enable us to conduct environmental assessments with sufficient reliability (e.g., PIER Collaborative Report, 2006).

California's Central Valley is currently the home to over six million people, and generates over $20 billion in agricultural crops each year. The agricultural and urban development in the area depends on an intricate surface water distribution system that routes water from surrounding watersheds to the Central Valley, and on the presence of extensive aquifers that provide substantial amounts of freshwater and are increasingly being used as buffers for fluctuations in surface water supplies. Managing the Central Valley's water resources has already been a challenging task in light of limited water availability (a result of drought and climate change), increasing demands, environmental concerns about wetlands, endangered species, and water quality, as well as land subsidence caused by groundwater pumping. In such a vulnerable and valuable system, any water resources impacts of large-scale CO_2 storage need to be evaluated and assessed before industrial-size storage projects get under way.

What are the hydrological concerns about CO_2 sequestration in the Central Valley? One primary concern results from the extremely large amounts of CO_2 that must be injected and sequestered underground if this technology is to contribute significantly to climate change mitigation (on the order of millions of tons per year per storage site). Storing these additional fluids in deep saline aquifers causes pressure changes and displacement of native brines, affecting subsurface volumes that can be significantly larger than the CO_2 plume itself (Figure 1). Environmental impacts on groundwater resources may result if the deep parts of the basin communicate effectively with shallower units. As one possible communication path, the large-scale pressure perturbation within a storage formation may extend updip to a freshwater aquifer used for domestic or commercial water supply. In such cases, CO_2 storage at depth could impact the shallower portions of the aquifer, which could experience pressure increase and water-table rise, changes in discharge and recharge zones, and changes in water quality. Even if separated from deep storage formations by sequences of low-permeability seals, freshwater resources may be hydraulically communicating with deeper layers, and the pressure buildup at depth would then provide a driving force for upward brine migration. This can happen, for example, through local high-permeability flow paths such as faults and abandoned boreholes. Also, seals

may pinch out or have higher permeabilities locally, allowing for interlayer migration vertically. Finally, land-surface deformation or uplift can be expected in response to CO_2 injection. This may change surface and near-subsurface flow patterns even without a direct impact from pressure propagation and brine displacement.

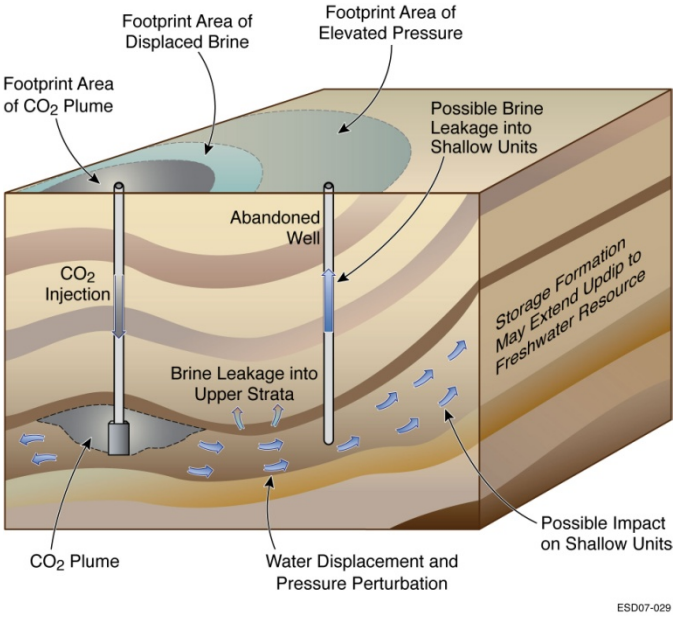

Figure 1: Schematic Showing Different Regions of Influence Related to CO_2 Storage (from Birkholzer et al., 2009)

Over the last decade or so, numerous research studies have been conducted in the United States (and worldwide) evaluating under which hydrogeological conditions the injected volumes of CO_2 can be safely stored over hundreds (or even thousands) of years. For example, many of these studies address issues such as the long-term efficiency of various CO_2 trapping mechanisms (e.g., structural trapping of CO_2 under sealing layers, dissolution of CO_2 into formation water, and mineral trapping as CO_2 reacts with the rock), and the detection and mitigation of potential CO_2 and brine leakage through localized pathways. Initially, less emphasis was placed on the understanding of large-scale pressure changes and the fate of the native brines or brackish waters being displaced by the injected volumes of CO_2. As discussed above, industrial-scale injection of CO_2 affects subsurface volumes much larger than the CO_2 plume. Thus, even if the injected CO_2 itself were safely trapped in suitable geological structures, large-scale pressure buildup and related brine displacement may affect valuable groundwater resources.

The topic of reservoir pressurization due to large-scale CO_2 storage has recently received increasing attention. In addition to concerns about potential brine migration and related impact on shallower groundwater resources, researchers are also addressing questions about pressure-driven caprock fracturing and/or fault reactivation (e.g., Rutqvist et al., 2007, 2008; Rutqvist, 2012). Large-scale pressurization can also be an issue for activities involving exploitation of subsurface resources in the area, such as oil and gas or geothermal energy, or may affect

neighboring CO_2 storage sites that reside in the same formation. Regarding the latter, the potential for pressure interference between GCS operations was illustrated in a regional-scale simulation for the Illinois Basin in the USA (Birkholzer and Zhou, 2009; Zhou and Birkholzer, 2011). Such interference not only leads to cumulative effects of pressurization, but also has regulatory implications, since permitting needs to be conducted based on a multi-site evaluation (Birkholzer and Zhou, 2009). Pressure management via extraction of native brines has been proposed to mitigate pressure concerns (e.g., Court et al., 2011; Bergmo et al., 2011; Birkholzer et al., 2012), but the cost for pumping, treatment, and disposal of these brines can be prohibitive.

In 2010, the California Energy Commission, via its PIER program, commissioned a study to evaluate the potential impact of large-scale CO_2 sequestration in California, with specific focus on the water resources in the southern San Joaquin River Valley. The study work comprised two distinct, but related projects: The first project utilized production and pressure data from oil reservoirs in the San Joaquin Valley as a reverse analog to the potential pressure impact of CO_2 injection. Results from this project are summarized in a companion report. The second project investigated (via simulation studies) whether the basin-scale pressure changes and brine displacement caused by future CO_2 storage in the deep sediments could have an impact on the groundwater-surface water systems in the area. The current report summarizes the simulation studies conducted in the second project. The objective of this second project was to address the following questions:

- Will vertical pressure propagation through thick layers of shale and sands have a significant impact on shallow water resources?
- Is brine displacement an issue through thick layers of shale and sands for shallow water resources?
- What deformations are to be expected from deep CO_2 storage, and would land surface uplift be a concern for shallow water resources?

This study does not look into the potential for and the impact of leakage of CO_2 and/or brine in localized pathways, such as improperly abandoned wells or undetected permeable faults. A companion study launched in 2012 conducts research to assess the potential groundwater quality impacts of localized leakage from deep storage aquifers into shallow potable aquifers, with focus on selected aquifer materials from field sites in California's San Joaquin Valley (funded by California Energy Commission under Project Title: Assessment of Potentially Deleterious Effect of CCS Operations on Groundwater Quality). Another topic not addressed in this study is the potential for pressure-induced fault activation, or "induced seismicity"; however, the simulation conducted in this study can provide a starting point for evaluating induced seismicity potential.

1.2 Methodology and Project Tasks

At the onset of the project, the simulation plan was to couple two different types of simulation models (via data transfer) of dynamic boundary conditions at a common interface. Geologic

CO_2 sequestration occurs in deep sediments at depths ranging from >800 m to several thousand meters, a depth generally not included in shallow water resources and groundwater management models. In turn, the simulation models used to predict the multi-phase behavior of CO_2 migration and brine displacement in CO_2 storage reservoirs most likely do not consider shallow sediments, and if they do, they rarely account for the complex processes important for shallow water resources and groundwater management (e.g., precipitation, evapotranspiration, irrigation, groundwater pumping).

A typical schematic cross section through the San Joaquin Valley is shown in Figure 2. The deep sediments overlying the crystalline bedrock would be the main target of future CO_2 storage in the area. These sediments deposited in a marine environment form a succession of thick, porous and permeable, mostly saline aquifers separated by laterally persistent aquitards represented by marine shales. The overlying continental deposits, derived by erosion of the rock from the surrounding mountains, have an average thickness of about 750 m. Comprised primarily of sand and gravel interbedded with silt and clay; they form an extensive freshwater aquifer system with immense importance as groundwater resource for California. The groundwater management models in use by water agencies and consultants typically focus on the aquifer system in the thick continental sediments, while excluding the underlying mostly marine deposits (where CO_2 might be stored). On the other hand, the simulation models assessing the potential impact of CO_2 geological storage have comprised the deep sediments in great detail, but have not sufficiently accounted for the shallower groundwater system.

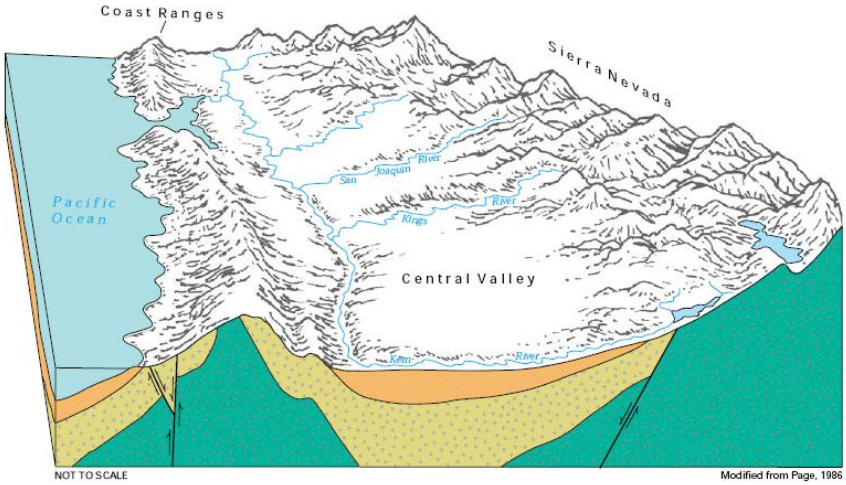

Figure 2: Geologic Cross Section through the San Joaquin Valley

The structural trough formed by uplift of crystalline rock (green) has been partially filled by thick marine (yellow) and continental sediments (light-brown) (USGS, 1995).

In order to evaluate the potential impact of basin-scale pressure changes and brine displacement on the shallow groundwater-surface water systems during CO_2 storage, we intended to simulate the CO_2 injection and migration processes in the deeper sediments with a deep basin reservoir simulation model, extract prediction results at the top of the deep-sediment model, and use these prediction results as a dynamic boundary condition at the bottom of an appropriate water-resources management model. The deep-sediment model and

the shallow-water-resources management model would not overlap, but share a common boundary condition. This initial coupling plan is depicted schematically in Figure 3.

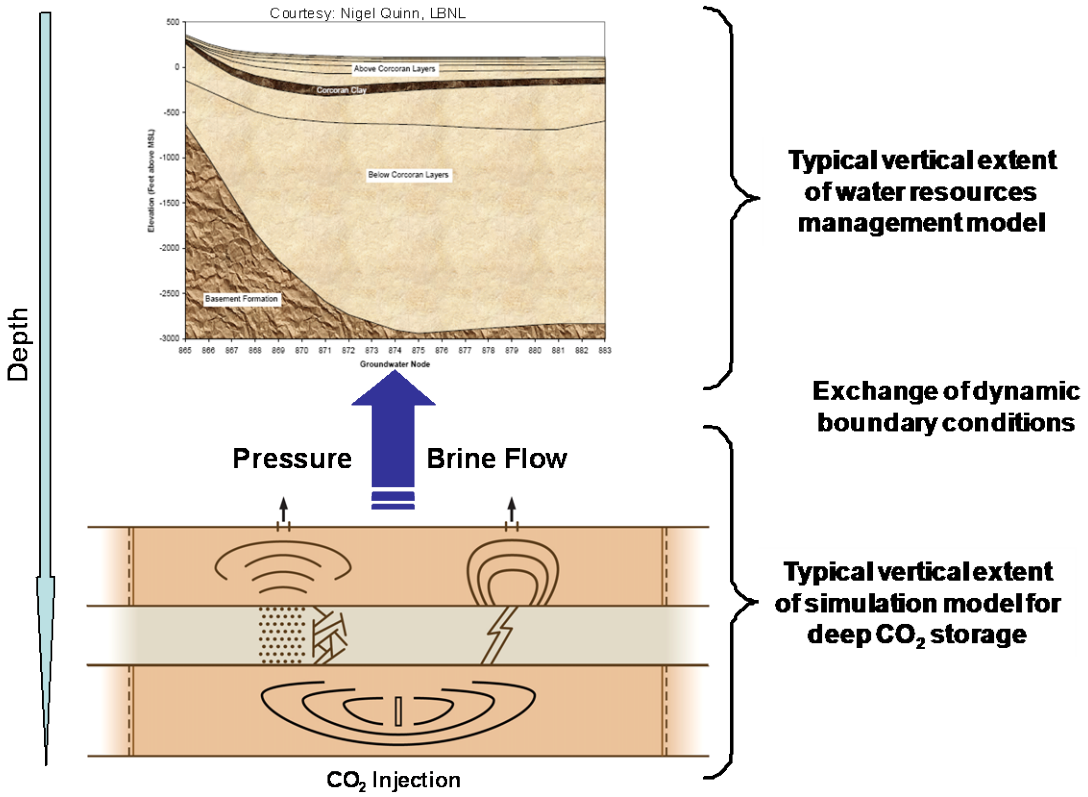

Figure 3: Initial Plan for Coupling the Simulation Model for CO_2 Storage Impacts in Deep Sediments and the Shallow Groundwater Management Model

Initial testing of the dynamic boundary treatment suggested early on in the project that an alternative methodology would be preferable, to avoid inconsistencies between the two models in terms of initial conditions, boundary conditions, and simulated processes. We eventually decided to develop two separate but complementary simulations models that both covered the entire vertical thickness of interest, from deep sequestration reservoirs to shallow water resources. The first model is the "Deep Basin Reservoir Simulation Model," which was extended upward to include relevant shallow layers, albeit with much less level of detail. The second model is the "Shallow Water Resources Impact Simulation Model," which was extended downward to include additional deep sediments, among those sandstone units of interest for geologic carbon sequestration. Both models were applied in parallel efforts to look into CO_2 storage impacts, but the focus of one model was very different from the other.

The "Deep Basin Reservoir Simulation Model" was developed for accurately simulating the multiphase processes of CO_2 and brine flow occurring in deep sequestration reservoirs. This model honors the observed geology at a large number of geologic logs in the model domain and incorporates all salient geological features, such as explicit representation of fault zones and the complex sand/shale interbedding within the injection reservoir. The TOUGH2 simulator used for this model allows for unstructured gridding, which is used to provide adequate mesh

refinement to the areas near the injection wells, and also allows for exact geometrical representation of the steeply dipping formations in the deep sediments of the southern San Joaquin River Basin. While this model was extended to include shallow groundwater resources and is expected to provide reasonable estimates of shallow pressure changes and land-surface impacts of CO_2 injection, it does not account for the complex water stresses important for shallow water resources and groundwater management, and does not model any dynamic trends except those induced by CO_2 sequestration. The model essentially serves as a validation tool for the "Shallow Water Resources Impact Simulation Model," and, in addition, because it is computationally much more efficient than the other model, we use it to conduct uncertainty quantification and analysis of alternative storage scenarios. See Section 4 for details on the model and simulation results.

The "Shallow Water Resources Impact Simulation Model" was developed for accurately predicting the impact of deep CO_2 sequestration on a stressed water system, using an accurate and well-calibrated simulation tool for water resources in the area. This means that CO_2-related impacts can be evaluated in the context of the long-term groundwater and subsidence trends occurring in the area as a result of other water stresses (e.g., pumping and irrigation). In other words, the model can be used (1) to evaluate the future water-level changes in the freshwater aquifers from ongoing water management with or without CO_2 sequestration, (2) to evaluate similar trends for land-surface deformation with and without CO_2 sequestration, and (3) to discuss potential for changes in recharge and discharge areas, and possible impacts on stream flows, wetlands, and water uses. While the model was extended to include deep sand and shale layers, it approximates the multiphase behavior of CO_2 and brine with a single-phase simulation tool that represents CO_2 injection as equivalent-volume water injection. Single-phase models have been shown to give reasonable estimates for the pressure behavior in deep CO_2 storage reservoirs (Cihan et al., 2013). Due to gridding limitations, this model neglects some salient geological features of the deep sediments, such as explicit representation of fault zones and the complex sand/shale interbedding within the injection reservoir. First-order consistency between the models was ensured by comparison with the "Deep Basin Reservoir Simulation Model." See Section 5 for details on the model and simulation results.

One of the first tasks in this project was to identify suitable deep and shallow models as a starting point for the simulation work. As to the deep "Deep Basin Reservoir Simulation Model," our project benefitted from plans for a CO_2 storage demonstration project in the Bakersfield/Visalia area, to be conducted by WESTCARB, one of DOE's seven Carbon Sequestration Regional Partnerships. This project envisioned injection of 250,000 tonnes of CO_2 per year over four years into the deep Vedder Formation (at a depth of approximately 2,300 m) at the Kimberlina power plant, located about 30 km north of Bakersfield. While the project never materialized for various reasons, the site-characterization effort for the Kimberlina project resulted in the development of an approximately 50 km by 50 km, three-dimensional geologic framework model of formations from the ground surface to the top of the basement (Figure 4; also see Section 2.3 for more detail). As part of a DOE-funded project (Birkholzer et al., 2008), researchers at LBNL used an extended version of this geologic framework model to develop a regional-scale simulation model for the deep saline aquifers in the southern San Joaquin Valley.

The simulation model was used to evaluate hypothetical large-scale CO_2 sequestration scenarios in the area, with injection of millions of tonnes of CO_2. The objective of this project was to better understand the resulting subsurface conditions in a deep formation that is compartmentalized by faults and affected by sand-shale interbedding (Birkholzer et al., 2011). While the focus of this modeling effort was on the deeper marine sand and shale sequences important for CO_2 storage, the large-scale simulation model comprised an excellent basis for developing and applying the "Deep Basin Reservoir Simulation Model" in the context of this project (Section 3).

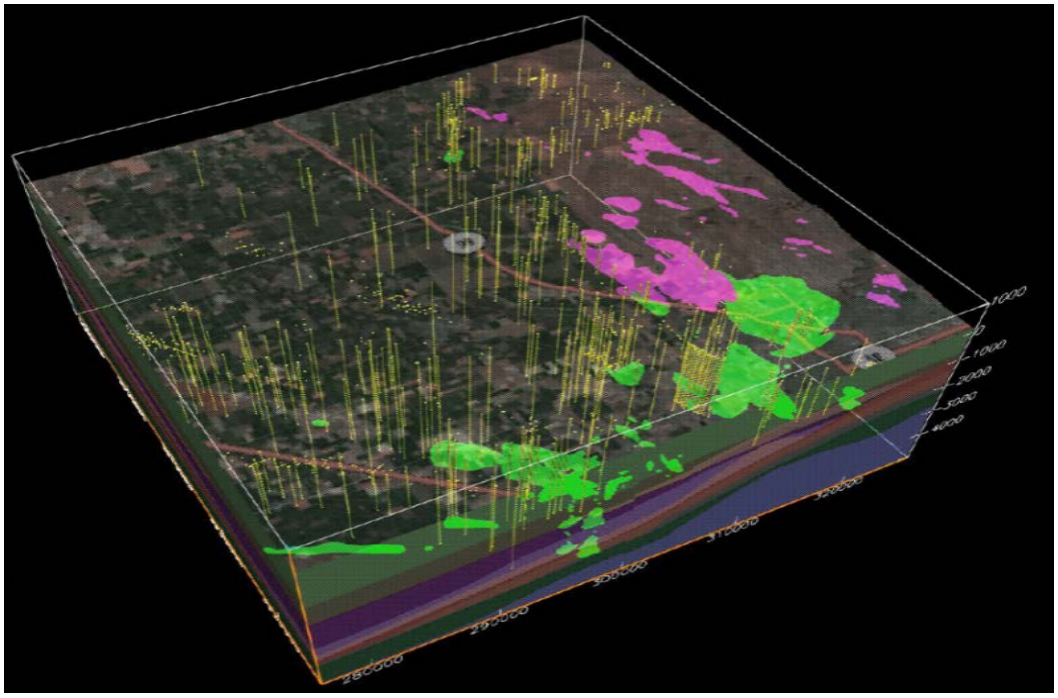

Figure 4: 3-D Depiction of the 50 km by 50 km Geologic Framework Model for the Kimberlina Project, with the Planned Kimberlina Injection Location in the Center

This model extends vertically to a depth of about 9,000 m.

A similar effort was conducted at the onset of the project to identify a good starting point for an extended "Shallow Water Resources Impact Simulation Model." Our intent was to utilize well-calibrated groundwater management models currently in use by water agencies and/or private consultants within the Basin and extend them to include deeper formations needed for modeling industrial-scale CO_2 storage. Over the past decades, several groundwater and surface water management models have been developed for different regions within California's Central Valley. A prominent model is the California Central Valley Groundwater-Surface Water Simulation Model (C2VSIM), an outgrowth of the Central Valley Groundwater Simulation Model (CVGSM), which was developed for the U.S. Bureau of Reclamation (USBR), State Water Resources Control Board (SWRCB), and California Department of Water Resources (DWR) in 1990. The latest version of this model uses a computer code developed by the DWR—the Integrated Water Flow Model (IWFM). C2VSIM simulates land-surface, groundwater and surface water flow in the alluvial portion of the entire Central Valley (Brush et al., 2008). The model was calibrated over a time period from 1922 to 2003. It now serves as the State's primary

planning tool for assessing the regional impacts of water management programs, such as conjunctive use of groundwater and surface water, future changes in surface water inflows to the Valley due to climate change (Miller et al., 2008), and the impacts of potential changes in land use within the Valley. Several more refined and local scale models have been developed within the domain of the regional-scale C2VSIM model. These models typically incorporate greater detail regarding local hydrological features and boundary conditions, as well as enhanced geological detail with respect to the description of the subsurface layers. Examples from the southern part of the San Joaquin Valley include models developed for the Tule River Basin (Harter et al., 2008), the Kaweah Delta District (Ruud et al., 2008), and the Kings Basin (Namvar et al., 2008).

Another prominent model has been developed by the U.S. Geological Survey (USGS) as part of systematic studies of groundwater in the Central Valley as part of the Regional Aquifer-System Analysis (RASA) program (Bertoldi et al., 1991; Page, 1986; Williamson et al., 1989). The original Central Valley groundwater simulation model known as CV-RASA (Central Valley Regional Aquifer Systems Analysis Model) utilized the MODFLOW-88 version of the MODFLOW code. The original model was constructed using a 6-mile mesh (36 square mile cells) and had four layers representing 1,000–3,000 ft of freshwater-bearing deposits, and the thickness of the uppermost layer ranged from 200 to 300 ft. The bottom boundary of the CV-RASA model was specified to coincide with the post-Eocene continental deposits and the lowest altitude of freshwater (Williamson et al., 1989). The base of the post-Eocene deposits ranges from less than 1,000 ft on the margins of the valley to more than 9,000 ft below land surface south of Bakersfield and averages 2,400 ft below land surface. The depth to the base of sediment saturated with freshwater (water with less than 1,000 mg/l) is highly variable and ranges from 100 to more than 4,000 ft (Planert and Williams, 1995).

The current Central Valley Hydrologic Model (CVHM) (Faunt et al., 2009c) is a direct follow-on from the CV-RASA model in terms of scale and has taken advantage of more detailed and comprehensive data collection efforts at the subregional scale. These subregional models and their associated high-resolution data files have been assimilated into GIS libraries, and the resulting coverages were used in building CVHM. The first phase of the update involved the conversion of the original MODFLOW format to MODFLOW 2000 (MF2K). The original discretization and water budgets were maintained, and several new MODFLOW packages, such as the Aquifer Subsidence package (SUB), were invoked. Taking advantage of the San Joaquin Basin subregional model (Belitz et. al, 1990), the model discretization was improved to a 1-mile resolution. The developers of the CVHM model chose to continue the model alignment with the axis of the Central Valley rather than the clockwise-rotated alignment of the subregional model.

Whereas the original CV-RASA model had four layers that increase in size with depth, the CVHM model was built with ten layers with the Corcoran Clay aquitard represented by two layers four and five (Figure 5). The top layer is set equal to 50 ft below land surface. Except where the Corcoran Clay Member of the Tulare Formation (typically referred to as the Corcoran Clay) exists, the layers range in thickness from 50 to 400 ft, increasing by 50 ft with each progressively deeper layer. The bottom boundary of both the CVHM and CV-RASA model

were specified to recognize the base of the post-Eocene continental deposits and the lowest altitude of freshwater (Williamson et al., 1989). The base of these deposits averages 2,400 ft. Use of two layers to represent the Corcoran Clay allowed the rate of drainage within the aquitard to be considered for the first time, using an improved formulation within a newly developed subsidence package. Since subsidence issues are becoming increasingly important within the Central Valley, this feature has greatly improved the model's applicability and performance. The increased layering above and beneath the Corcoran Clay improves recognition of shallow groundwater flow paths, including flow into tile drains. It also better recognizes the presence of intermediate retarding clay layers between the Corcoran Clay and the ground surface, layers which can slow the rate of fall of shallow water tables following irrigation events. The importance of agriculture to the hydrology of the basin also warranted an improvement in the temporal resolution of the model from seasonal stress periods to monthly stress periods, which better captures irrigation hydrology. The model simulation period was also extended from 1961 through 2003 and has been more recently updated through 2009 with the development of the higher resolution CVHM-2 model.

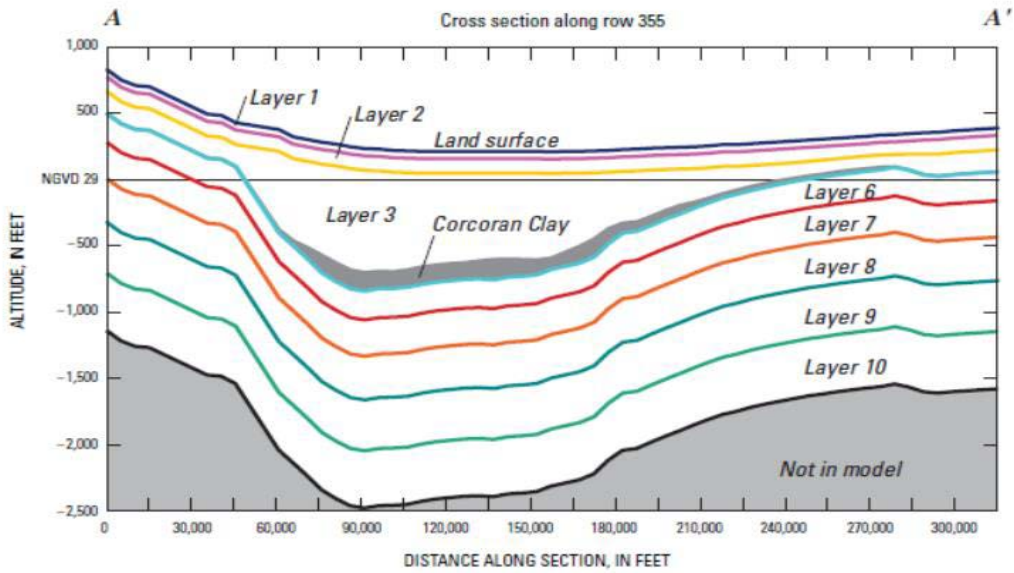

Figure 5: Generalized Cross Section (A-A') Showing the Vertical Discretization of the CVHM Model in the San Joaquin Basin, California (Source: Faunt et al., 2009a)

Recently, a more comprehensive, alternative water budget was formulated for CVHM. This water budget includes new climatic, land-use, and surface-water data including the ability to simulate direct surface-water diversion and delivery information from canals. The formulation of CVHM water-budget subregions, which formed the basis of surface water delivery and groundwater pumpage accounting, was aligned with the twenty-one hydrographic subregions developed by DWR for the State Water Plan updates and subsequently adopted for C2VSIM (Figure 6). This unusual cooperation between the USGS and the DWR extended into the development of consistent input data files for both models. This is relevant to Chapter 5 of this report, where an analysis of the two models is described which affected the choice of model for the CO_2 injection and storage analysis.

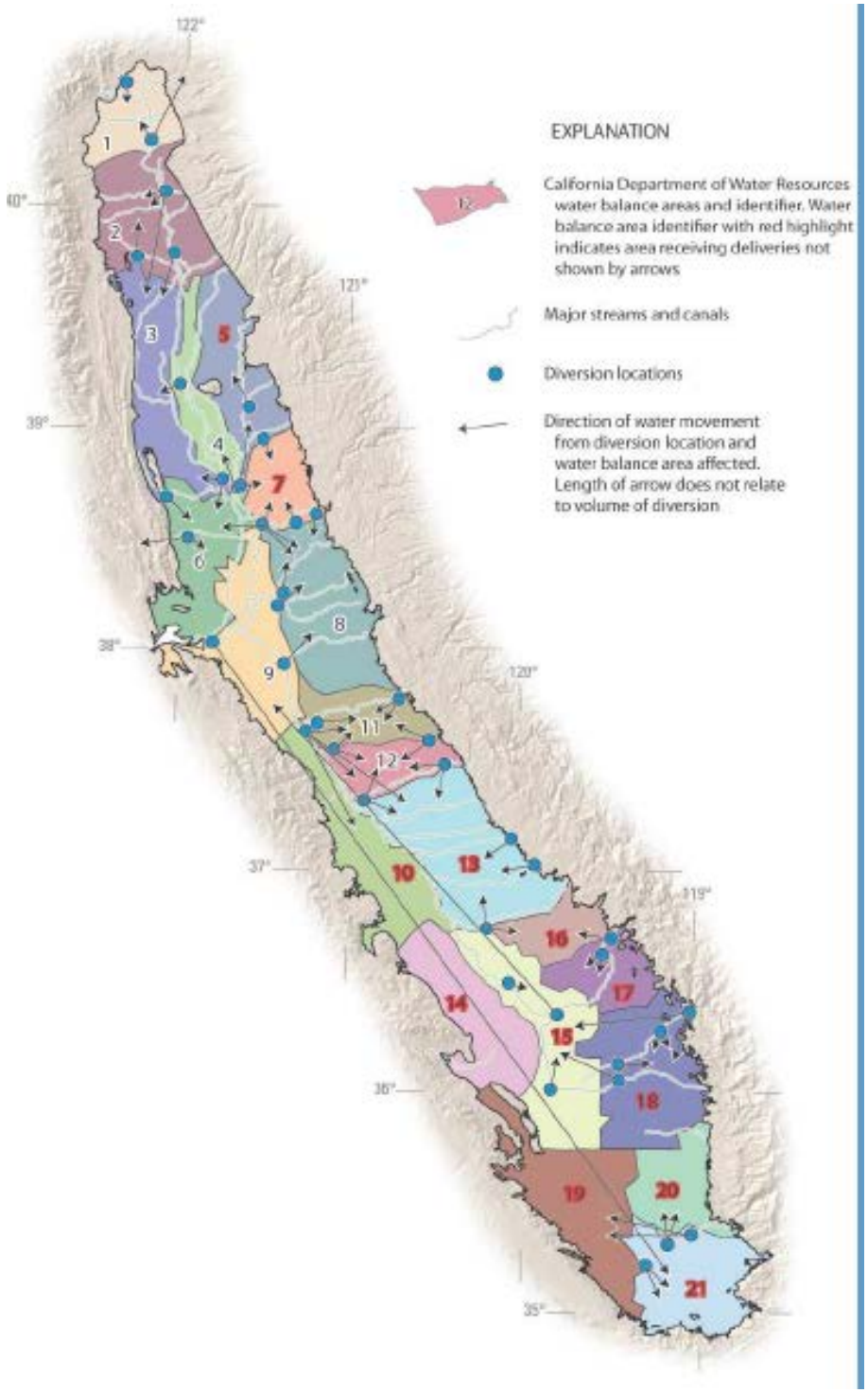

Figure 6: Use of Hydrographic Water Budget Areas by Both CVHM and C2VSIM Models to Simulate Groundwater and Surface Water Hydrology of the Central Valley (Faunt et al., 2009a)

With the background, objective, and methodology discussed above, the project comprised the following tasks:

- Extend the existing regional-scale model for the planned Kimberlina CO_2 injection and

develop the "Deep Basin Reservoir Simulation Model"

- Identify suitable existing groundwater and surface water models maintained by the DWR, USBR, USGS and/or other agencies, and select an optimal model for extension to the "Shallow Water Resources Impact Simulation Model"
- Select a range of reasonable carbon sequestration scenarios for the San Joaquin Valley,
- For a range of parameter uncertainty cases, conduct simulations with the "Deep Basin Reservoir Simulation Model," to accurately predict the impact of CO_2 injection on pressure buildup and brine displacement in deep sediments, and to obtain reasonable estimates of shallow pressure changes and land-surface impacts
- For selected scenarios, conduct simulations with the "Shallow Water Resources Impact Simulation Model," to predict CO_2-related impacts in the context of the long-term groundwater and subsidence trends occurring in the area as a result of other water stresses (e.g., pumping and irrigation)
- Discuss potential impact of industrial-scale CO_2 storage in the context of changing water resource utilization, population, land use and climate, and consider the implications of the water resource simulation results for other portions of the Central Valley

CHAPTER 2:
Southern San Joaquin Valley

2.1 Description of Population, Agriculture, and Water Resources

The San Joaquin River Basin ranks among the most important agricultural regions in the world, with over 1 million acres of irrigated cropland and an annual output valued at $4 billion. The San Joaquin River and its tributaries combine to form an important wildlife corridor that provides critical habitat for migratory and native bird populations. Damming and diversion of the river and its tributaries to support agricultural and urban development have severely impacted ecological functions. Groundwater within the valley is being used to augment surface water, resulting in significant electrical demands for pumping, widespread land subsidence, and higher salinity loads along the waterways. Salinity is now viewed by planning agencies to be one of the major constraints on future agricultural development in the area. Agricultural drainage and discharges from managed wetlands generated within the San Joaquin River Basin are the single most important determinant, apart from tidal dynamics, on the ecological health of the Bay-Delta ecosystem. The concentration of contaminants in the San Joaquin River is determined by the relative timing of reservoir releases, primarily from the eastern side of the Basin, and drainage discharges from contaminant sources on the western side. Besides ongoing impacts from the extensive agricultural system, stresses to the ecological and water systems of the San Joaquin River Basin are expected to increase due to growing urbanization, climate change, and implementation of the recent renewable energy portfolio for California. The impacts of climate change expected to emerge by mid-century include much greater frequency of heat waves, the gradual evolution of winter precipitation from snow to rain, and the ongoing northward displacement of the Pacific storm track, leading to drier conditions in southern and central California.

The focus of our study is the southern San Joaquin Valley, which exemplifies many of the water stresses discussed above. Kern County, located in the Southern San Joaquin Valley, is one of the most important vegetable producers in the U.S. with over 100,000 acres devoted to carrots, potatoes, lettuce, garlic, onions, tomatoes, bell peppers, and watermelons. Over 80 percent of the nation's carrots are grown in Kern County. Vegetable production alone in Kern County is estimated to have a value of over $460 million per year (2011). Kern County ranks third in California for agricultural production. In the past decade the dairy industry has expanded in a significant manner into Kern County. In 2011 milk production was worth $740 million relative to a total value of agricultural production of $5.4 billion.

Irrigation water supply is critical to the continued productivity of Kern County. The region receives an average rainfall of little over 6 inches per year and thus is heavily reliant on imported water from Millerton Reservoir in Fresno County, via the Friant Kern Canal, and from the Sacramento-San Joaquin Delta via the California Aqueduct and the Cross Valley Canal. Interruption of this important source of water supply or damage to these facilities could have a significant economic impact on agricultural production in the region. Aquifer subsidence,

especially in the western part of Kern County, is of great concern to the Kern County Water Agency and agencies such as the Department of Water Resources and the U.S. Bureau of Reclamation responsible for maintenance of major water conveyance facilities such as the California Aqueduct (Figure 7). Between 1977 and 2005, Kern County invested more than $300 million to build a groundwater banking infrastructure capable of storing approximately 5.7 million acre-feet of water during wet years. During dry and critically dry years, groundwater can be extracted from this water bank through direct pumping. The City of Bakersfield developed a 2,800 acre spreading basin which initiated the water banking project. In the 1990s this was expanded with the construction of the Kern Water Bank, which currently includes 20,000 acres of recharge ponds and habitat/wildlife land, and the 2,233-acre Pioneer Banking Project--created for groundwater recharge and recovery operations.

Recent legislation in support of San Joaquin River restoration will reallocate, on average, 170,000 acre-ft of Friant-Kern Canal delivery water to sustain flows in the River and assist in restoration of the salmon fishery. This reduction in contract deliveries, which is about 15 percent of the 1,150,000 acre-ft long-term average delivery to Friant Division contractors, will increase the pressure on an already overallocated water supply and the likely risk of damage to the water distribution system. Bakersfield is the county seat of Kern County and the 9th most populous cities in California. The region has diverse industries including healthcare, oil, natural gas, and agricultural-related distribution centers. The largest employers include Nestlé, Frito-Lay, State Farm, Aera Energy, Chevron, and Occidental Oil & Gas, plus regional, state, and federal agencies.

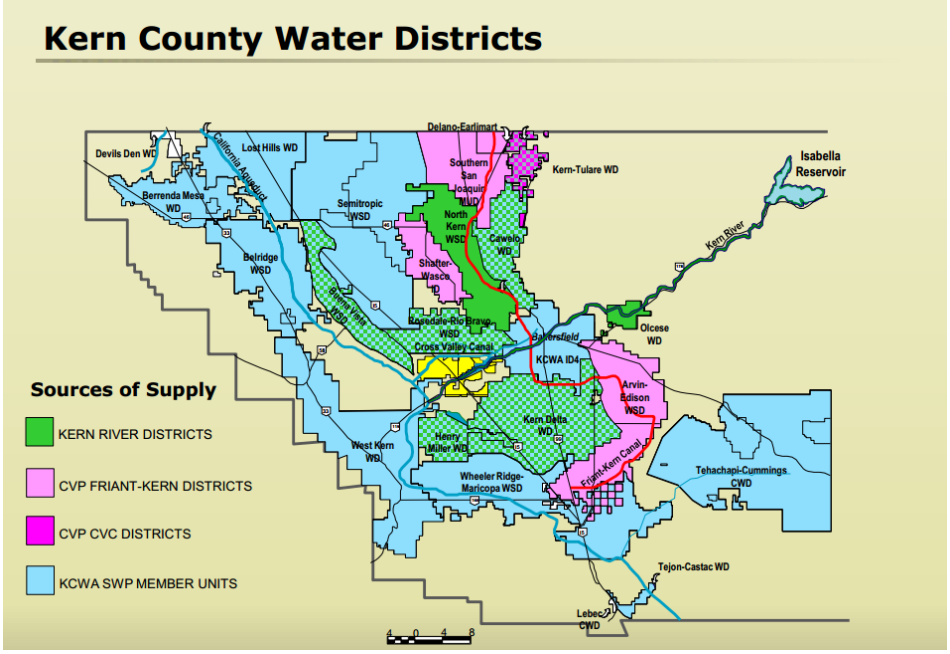

Figure 7: Map of Kern County Water Districts Showing Dependence on Three Major Conveyance Systems: the California Aqueduct, Which Runs along the Western Margin of the Southern San Joaquin Basin, the Friant Kern Canal, Which Runs North to South along the Eastern Margin of the Basin, and the Cross Valley Canal, Which Allows California Aqueduct Water to Deliver Surplus Flow to the Friant Kern Canal (KCWA, 2013)

2.2 CO_2 Emissions and Storage Potential

CO_2 sources and potential sinks for sequestration in California have been evaluated by WESTCARB, one of the seven regional partnerships established by the United States Department of Energy. WESTCARB, led by the California Energy Commission in partnership with Lawrence Berkeley and Lawrence Livermore National Laboratories, includes more than 100 members from public agencies, private companies, universities, and nonprofit organizations. WESTCARB's goals are to characterize regional opportunities for geologic carbon storage; validate promising storage options through field tests; and facilitate CO_2 utilization and geologic storage at commercial scale. The WESTCARB region includes not only California, but also Alaska, Arizona, Hawaii, Nevada, Oregon, Washington, and the Canadian province of British Columbia.

Electric power plants are the largest stationary CO_2 source type in the WESTCARB region, although the fuel mix used for power generation varies among WESTCARB states. Natural gas combined cycle plants are predominant in California. Oil refining and chemical plants are also major emission sources in California. Throughout the region, other industrial CO_2 sources include cement and lime plants, aluminum smelters, pulp and paper mills, steel mills, ethanol fermenters, and fertilizer plants. The total emissions in California from large stationary sources amount to 156 million metric tons of CO_2 per year, distributed among source types as shown in Figure 8 below.

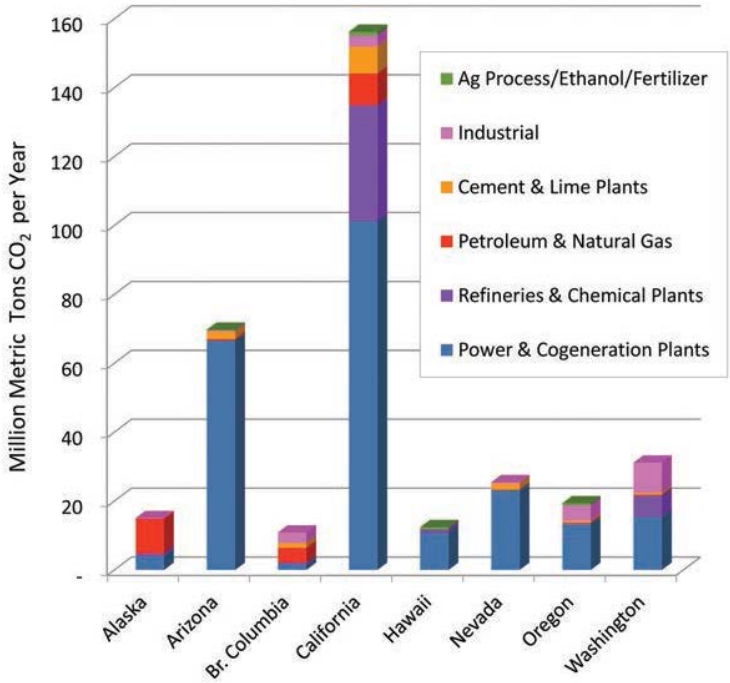

Figure 8: Total Annual CO_2 Emissions from Large Stationary Sources in WESTCARB Region (from U.S. DOE, 2012)

Figure 9 shows the location of large stationary sources within California, as well as the regional distribution of options for geologic carbon sequestration. WESTCARB's geologic characterization studies show that the saline formations in the region's broadly distributed sedimentary basins have the potential to store hundreds of years' worth of CO_2 emissions from stationary sources. In addition, major oil and gas fields represent both storage targets and opportunities for EOR and enhanced natural gas recovery. The total estimated CO_2 storage capacity in California in oil reservoirs is estimated between 0.3 billion and 1.3 billion metric tons. In gas reservoirs, the estimates are between 3.0 billion and 5.2 billion metric tons.

Regionally, California's Central Valley has the largest CO_2 storage resource potential, in the range of 2.0 billion–4.1 billion metric tons (2.2 billion–4.5 billion tons). The southern portion of the basin, the focus of our modeling study, is home to some of California's largest natural gas fields. Now largely depleted, these fields may represent opportunities for CO_2 storage following cessation of commercial natural gas production or in conjunction with the use of CO_2 for enhanced natural gas recovery, a technology currently in the research and development stage.

By far the largest storage potential, however, is in deep sedimentary basins that are broadly distributed throughout the WESTCARB region. Many contain saline formations suitable for CO_2 storage based on depth, sealing formations, and brine waters that preclude use as potable water resources. In California, Cenozoic sedimentary basins offer some of the best opportunities for geologic storage. These basins exhibit wide areal distribution, thick sedimentary sections containing multiple widespread marine sandstones, and thick, laterally persistent marine shale seals. As discussed above, in some basins, petrophysical data from oil and gas development are available to support assessments. California's Central Valley again stands out as the region with the largest storage potential, with an estimated range of 21 to 282 billion metric tons (thus far exceeding the storage capacity in depleted oil and gas reservoirs).

In summary, WESTCARB's geologic characterization studies show that the saline formations in the region's broadly distributed sedimentary basins have the potential to store hundreds of years' worth of CO_2 emissions from stationary sources. The region also offers opportunities for coupling geologic carbon storage with enhanced hydrocarbon and geothermal energy production. California's Central Valley stands out as offering a very large storage potential in proximity of major stationary emitters (see Figure 9). Our study area, the southern San Joaquin Valley, is a region in which several large CO_2 sources are co-located with significant CO_2 storage potential, both in the form of deep saline formations and ongoing/former oil and gas fields. Thick shale units provide good overlying seals at the site and surrounding areas.

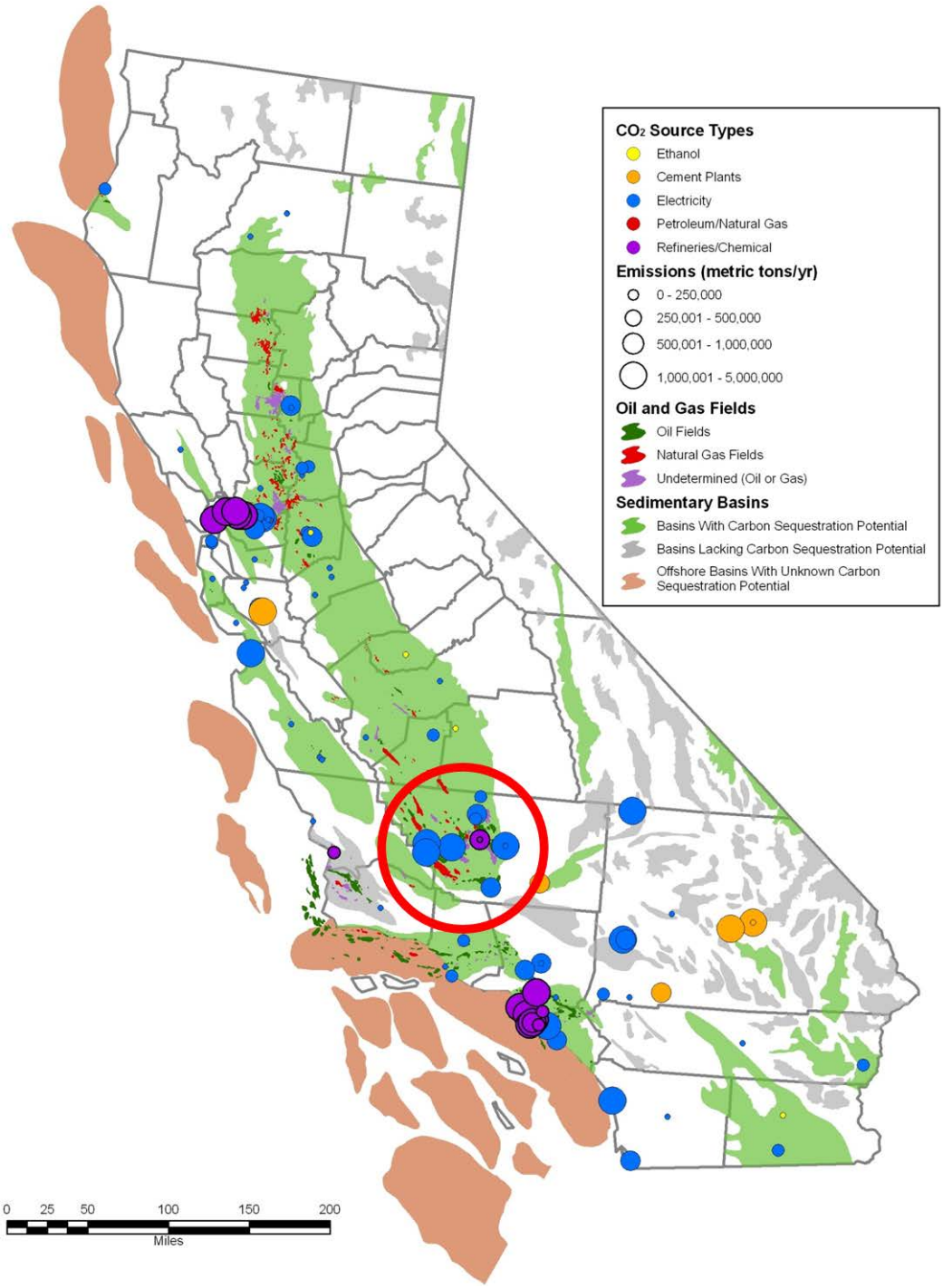

Figure 9: Mapping of Large Stationary CO_2 Emitters with Geologic Storage Potential in California. Red Circle Marks our Study Area in the Southern San Joaquin Basin

CHAPTER 3: Development of Geologic and Hydrogeologic Framework

This section describes the geologic and hydrogeologic framework model that was developed to simulate the deep sedimentary formations in both models used in this report, the "Deep Basin Reservoir Simulation Model" and the "Shallow Water Resources Impact Simulation Model." As mentioned above, our effort benefitted from previous geologic model development initially conducted for WESTCARB. The geologic model for WESTCARB centered on the planned Kimberlina pilot-scale injection, which spanned a region of 50 km by 50 km around the injection location. In 2009, this initial geologic framework model was expanded to a regional-scale basin model to accommodate the needs of a DOE-funded project gauging the potential for injecting CO_2 at industrial scale into the deep Vedder formation underlying Kimberlina (Birkholzer et al., 2008). The expanded geologic model now comprises a large region, 84 km in the eastern direction and 112 km in the northern direction. The model size was selected to incorporate the full horizontal extent of the Vedder formation. This model serves as the underlying framework for the "Deep Basin Reservoir Simulation Model" described in Section 4.

The "Shallow Water Resources Impact Simulation Model" spans a larger and slightly rotated region compared to the "Deep Basin Reservoir Simulation Model. The geologic framework model therefore needed to be expanded again, which was done as part of this study. Compared to the initial region, the model is now rotated 29 degrees counterclockwise, spanning a domain of ~103 km in the eastern direction and ~168 km in the northern direction. The steps in the development of the geomodel are described in Section 3.2 below; expansion of the model essentially entailed adding additional stratigraphic data from the California Division of Oil and Gas and Geothermal Resources (DOGGR) and also using recently available stratigraphic top data provided by the USGS. This new geomodel was then used to add geologic formations below the lowest altitude of freshwater in the domain, which forms the bottom of the CVHM-2 model, and thus develop a "Shallow Water Resources Impact Simulation Model" that incorporates shallow units important for water resources and deep units important for geologic carbon sequestration.

3.1 Hydrogeology of the Southern San Joaquin Basin

The San Joaquin Valley comprises the southern half of the Central Valley, an elongated basin located between the Sierra Nevada and the California Coast Ranges (Figure 10). The southern part of the San Joaquin Basin is filled by more than 7000 m of Tertiary marine and nonmarine sediments, which bury the downwarped western margin of the Sierra Nevada metamorphic-plutonic terrane. The stratigraphic section is generally thin and predominately continental on the east side of the basin, but thickens into largely deepwater marine facies to the west. The structure is basically a monocline dipping toward the west, characterized by block faulting and broad, open folds. A major feature of the basin is the Bakersfield Arch, a westward-plunging structural bowing on the east side of the basin. This structure plunges south-southwest into the

basin for ~25 km, separating the basin into two sub-basins. The Bakersfield Arch is the site of several major oil fields (Wagoner, 2009).

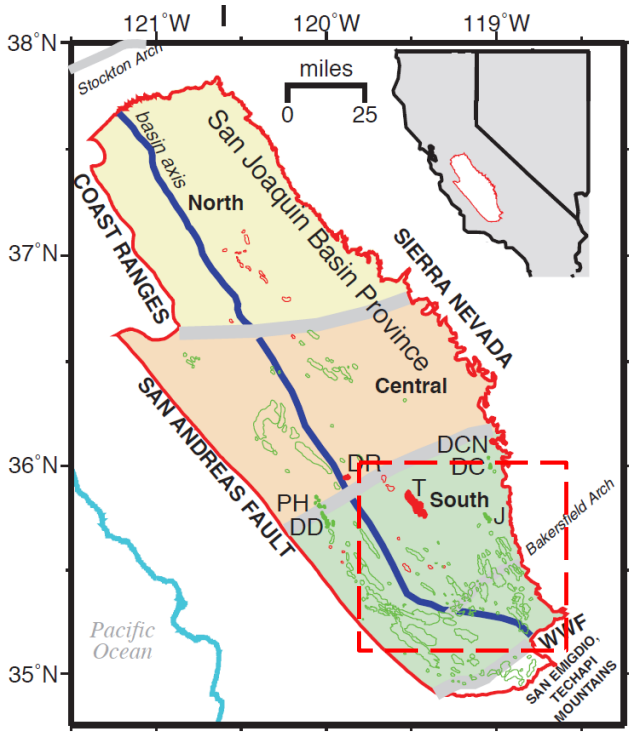

Figure 10: Planview of San Joaquin Basin with Focus Area in the South

The stratigraphic relationships of the major formations in the southern San Joaquin Valley are shown in Figure 9. The geologic framework model developed for this project included the following formations (from shallow to deep). Note that not all of these formations were treated as individual hydrogeologic units in the simulation models. The main oil- and gas-producing formations, and thus units considered as targets for potential geologic sequestration of CO_2, are the Stevens, Temblor, and Vedder formations.

Kern River Formation (Plio-Pleistocene)

Mainly nonmarine sediments. These are the youngest oil-producing sediments in the basin. This unit extends close to the surface and consists of interbedded claystone, shale, sandstone, and conglomerate.

Etchegoin Formation (Pliocene)

Unconformably overlies the Chanac Formation in the model area. Mostly fine- to coarse-grained marine sandstone and micaceous shale. The Etchegoin consists of 3 members: the basal sandstone, the Macoma Clay, and the upper sandstone.

Macoma Clay (Pliocene)

Mostly marine claystone and siltstone. This is a member of the Etchegoin Formation. Basal Etchegoin sandstone occurs stratigraphically below this fine-grained unit. This unit is mapped because it provides a useful time-stratigraphic marker.

Chanac Formation (Pliocene)

Mostly fine- to coarse-grained nonmarine sandstone, with interbedded siltstone and claystone. This deposit grades basinward into siliceous marine shale. This formation is confined to a narrow zone in the subsurface of the southeastern part of the basin. The Chanac is the nonmarine equivalent to the Santa Margarita Formation.

Santa Margarita Formation (upper Miocene)

Rests unconformably on the Fruitvale Formation. Mostly coarse-grained sandstone, with sandy shale increasing toward the base of the unit. This unit rests on progressively older sediments toward the eastern edge of the basin. This unit is time equivalent to the Stevens Sand in the central part of the basin. The formation contains both marine and nonmarine facies.

McLure Formation (upper Miocene)

Fractured marine shale. Dominant shale member of the Monterey Formation in the central part of the basin.

Stevens Sand (upper Miocene)

Fine- to coarse-grained turbidite sandstone, with interbedded hard siltstone. The sandstone is highly variable in thickness and lateral extent. In the central part of the basin, thick siliceous shales overlie the Stevens.

Fruitvale Shale (upper Miocene)

Mainly marine deep water shale. Rests unconformably on top of the Round Mountain Formation. Massive marine siltstone and shale, with streaks of sandtone. Thickens toward the center of the basin. Dominant shale member of the Monterey Formation in the southeastern part of the basin.

Round Mountain Formation (middle Miocene)

The unit is mostly hard marine siltstone and shale.

Olcese Formation (lower Miocene)

Medium- to coarse-grained sandstone. Gradational contact with the underlying Freeman Jewett Formation. The upper and lower parts of this unit are marine, while the middle portion of the Olcese is nonmarine in origin.

Freeman-Jewett Formation (lower Miocene)

Rests conformably on the Vedder Formation. Mostly hard marine shale and siltstone with thin streaks of sandstone. Grades vertically into the overlying Olcese Formation and represents the beginning of a regressive phase of the Miocene marine deposition.

Vedder Formation (lower Miocene)

Fine- to coarse-grained massive marine sandstone, with subordinate siltstone and shale. The younger Rio Bravo and Pyramid Hill sands (basal member of the overlying Freeman-Jewett Formation) have been included in this unit. This is the oldest of the significant oil-producing deposits on the eastern side of the basin. The sands included in the Vedder range from a few feet to several hundred feet thick.

Walker Formation (lower Miocene)

The Walker Formation rests on basement rocks on the east side of the basin, is continental in origin, and consists mainly of sandstone and claystone. Toward the center of the basin, the Walker interfingers with the time-equivalent Vedder Formation.

Temblor Formation (lower to middle Miocene)

This formation has a widespread distribution in the subsurface of the southern and central San Joaquin basin. The formation has several different members, with different lithologies. It represents the basinward time equivalent of the Vedder, Freeman-Jewett, and Olcese Formations.

Undifferentiated deposits (Eocene)

There are a number of Eocene formations in this part of the San Joaquin basin, but the Tumey Formation is probably the most common, and it occurs directly below the Vedder in the model area. The Tumey is a marine shale.

Basement (pre-Tertiary)

The basement in this part of the basin is mainly quartz diorite intrusive rocks.

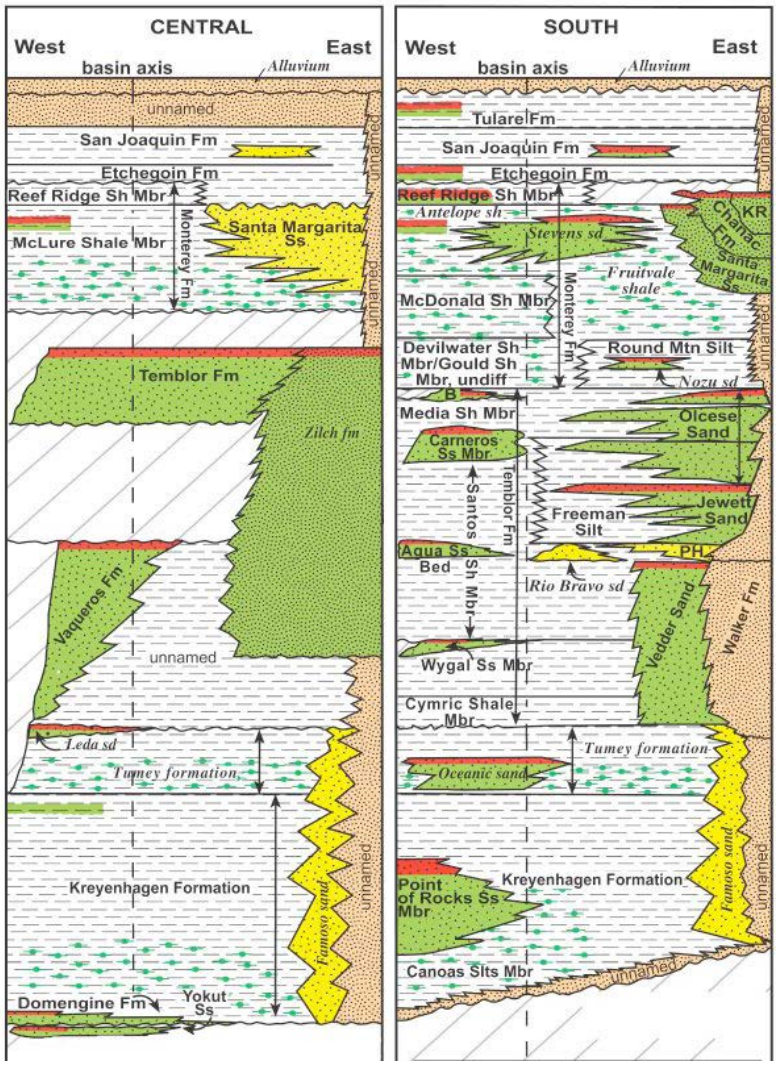

Figure 11: Generalized Stratigraphic Section for the Southern San Joaquin Basin (Hosford Scheirer, 2007)

3.2 Data Sources and Methods

The geologic units mapped for the development of the geomodels used in this study are Quaternary basin fill, Tertiary marine and continental deposits, and pre-Tertiary basement rock. Detailed geologic data, including surface maps, borehole data, and geophysical surveys, were used to define the geological setting. As listed above, sixteen stratigraphic formations were mapped, as well as >140 faults.

The topographic surface is based on a 10 m lateral resolution DEM, which was converted to a 2D grid within Earthvision. Stratigraphic tops for all of the major stratigraphic units were collected and digitized. These data were converted to elevation and 2D grids were generated for the top of each mappable unit. The fault traces were digitized from hardcopy maps. Using the assumed dip and the digitized trace, a 2D grid (xyz) was generated for each fault surface.

Most of the geologic information integrated into the geomodel is defined by borehole contacts from the oil and gas industry, available from the California Division of Oil and Gas and Geothermal Resources (DOGGR). Geologic information is available primarily for the oil and gas fields. The only publicly available data for areas outside of the fields are from wildcat exploration wells that were drilled prior to 1980. Many of these wells provide stratigraphic tops, but the data are sporadic. EOG Resources, Inc., generously provided stratigraphic information for areas near the Kimberlina power plant; these data also included seismic reflection interpretations, which are independent of the wildcat well locations. The fault data are taken from DOGGR documents on specific oil and gas fields in the basin. Our current understanding of the faulting between the oil and gas fields is poor; this is an area in which more work is required.

3.3 Brief Description of Geomodels

Figure 12 shows the domain of the two regional geomodel used in this study. The yellow box represents the domain of the geomodel used for the "Deep Basin Reservoir Simulation Model" described in Section 4. This box is about 84 km by 112 km in size. The red box represents the domain of the latest geomodel expansion to incorporate the region of the "Shallow Water Resources Impact Simulation Model" described in Section 5. This box is about 103 km by 168 km in size.

Figure 13 shows the 84 km by 112 km regional model in a cut-away view at the location of planned Kimberlina injection. Note that the stratigraphic control by available data points decreases substantially toward the center of the basin. Thus, the tops of the units are much less well constrained, especially deeper in the section. The general structural dip is to the southwest, as indicated by the well picks and the EOG seismic picks. Figure 14 shows a cut-away from the larger 103 km x 168 km regional model. While the two geomodels do not fully overlap, and one is rotated compared to the other, they share the same geological structure where they both exist.

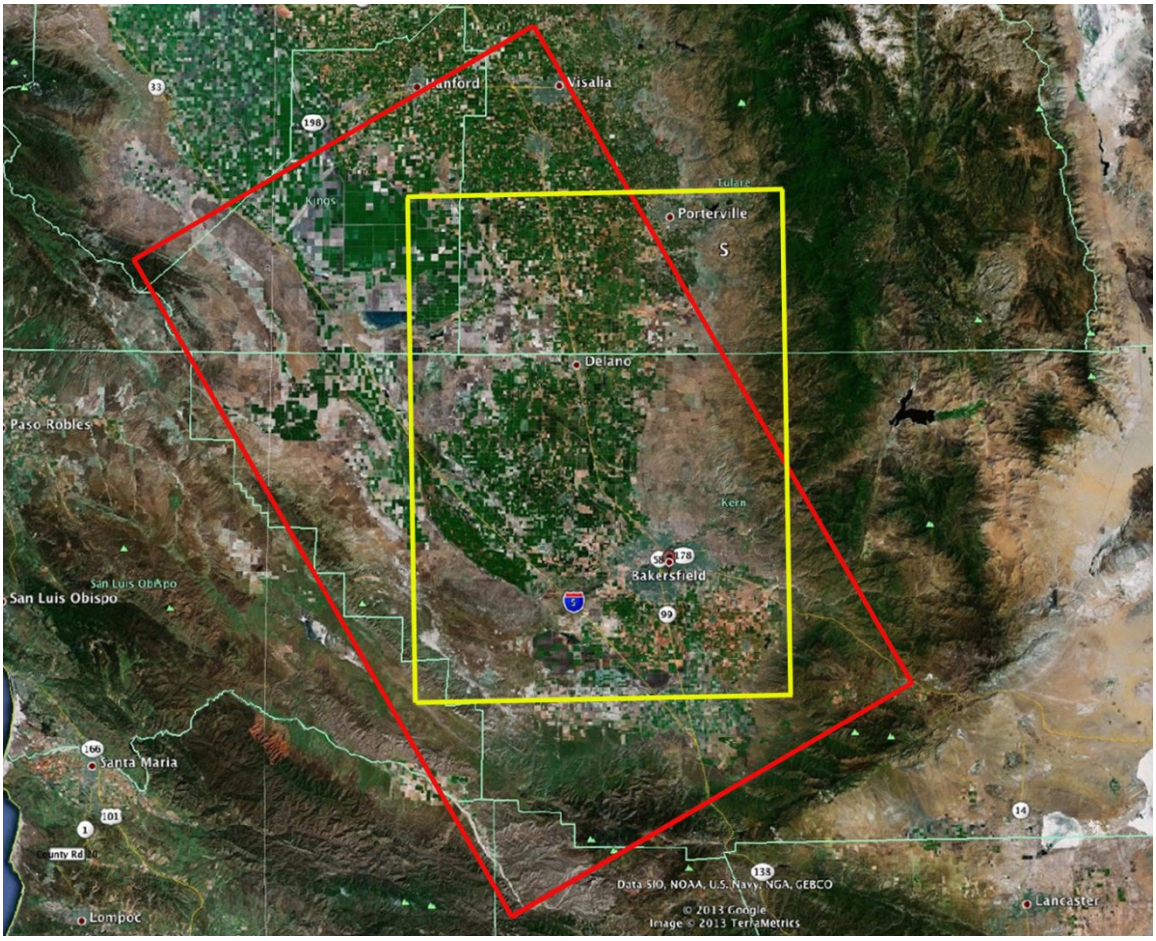

Figure 12: Extent of the Two Geomodels Used in this Study

The yellow box represents the range of the geomodel used for the “Deep Basin Reservoir Simulation Model” described in Section 4. The red box represents the range of the latest geomodel expansion to incorporate the region of the “Shallow Water Resources Impact Simulation Model” described in Section 5. This new model has incorporated additional stratigraphic data that was provided by the USGS in 2013.

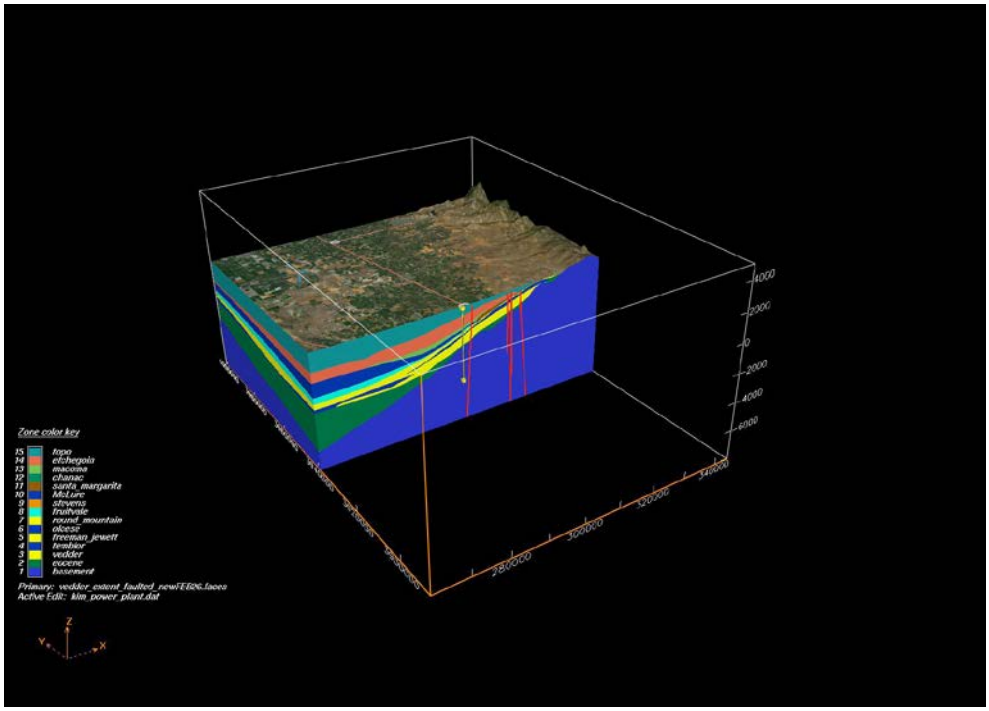

Figure 13: Cut-Away View of the 84 km by 112 km Regional Model at the Location of the Planned Kimberlina Injection (Vertical Yellow Line)

The faults are shown as subvertical red lines (4x vertical exaggeration).

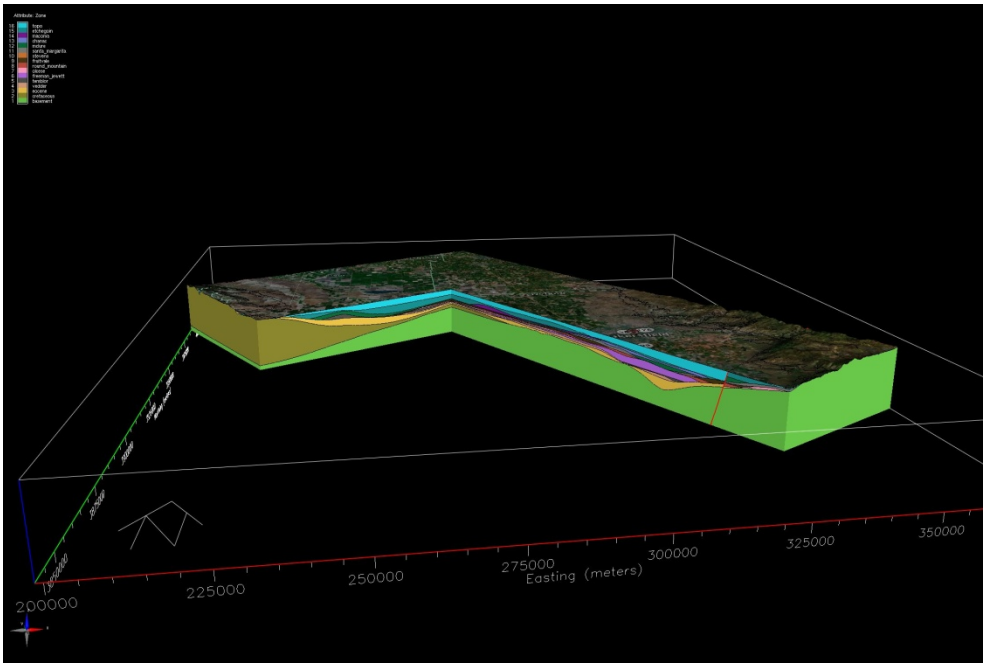

Figure 14: Cut-Away View of the Rotated 103 km by 168 km Regional Model

The faults are shown as subvertical red lines (4x vertical exaggeration).

Figure 15 shows the spatial extent of the Vedder formation projected onto the rotated 103 km by 168 km regional model. Figure 16 shows a similar projection for the Stevens formation. The Vedder and the Stevens formations have been selected in this study to host hypothetical carbon sequestration projects. Figure 17 shows the sequence of all formations in several lateral sections across the basin. One can see that the Vedder formation is a steeply dipping formation that extends over much of the center and eastern side of the basin. The Stevens formation is smaller in spatial extent and located to the southwest of the Vedder, with little spatial overlap. The Stevens formation is quite thick and less dipping than the Vedder. It appears in two distinct spatial lobes, with the eastern portion almost separated from the western portion.

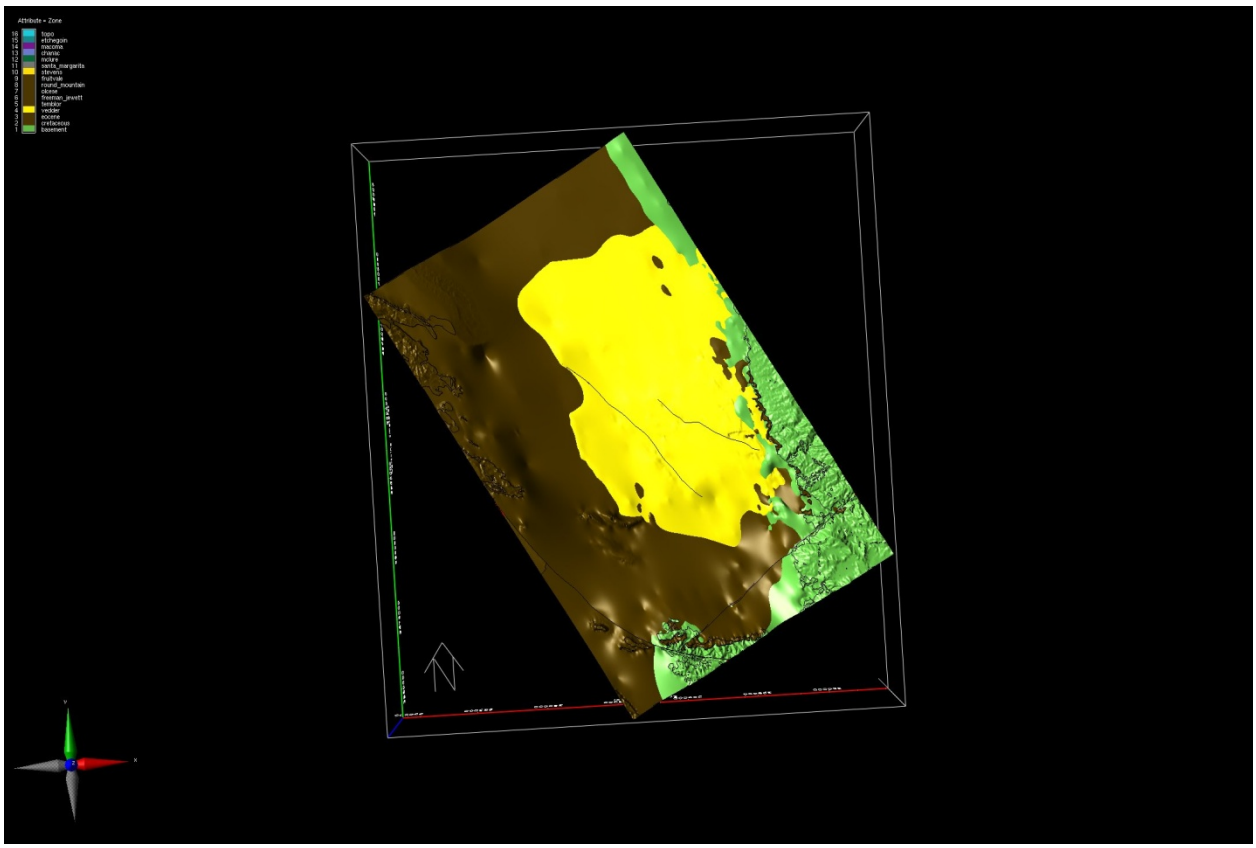

Figure 15: Projection of the Extent of the Vedder Formation (in Yellow) on Top of the Underlying Formations (in Brown)

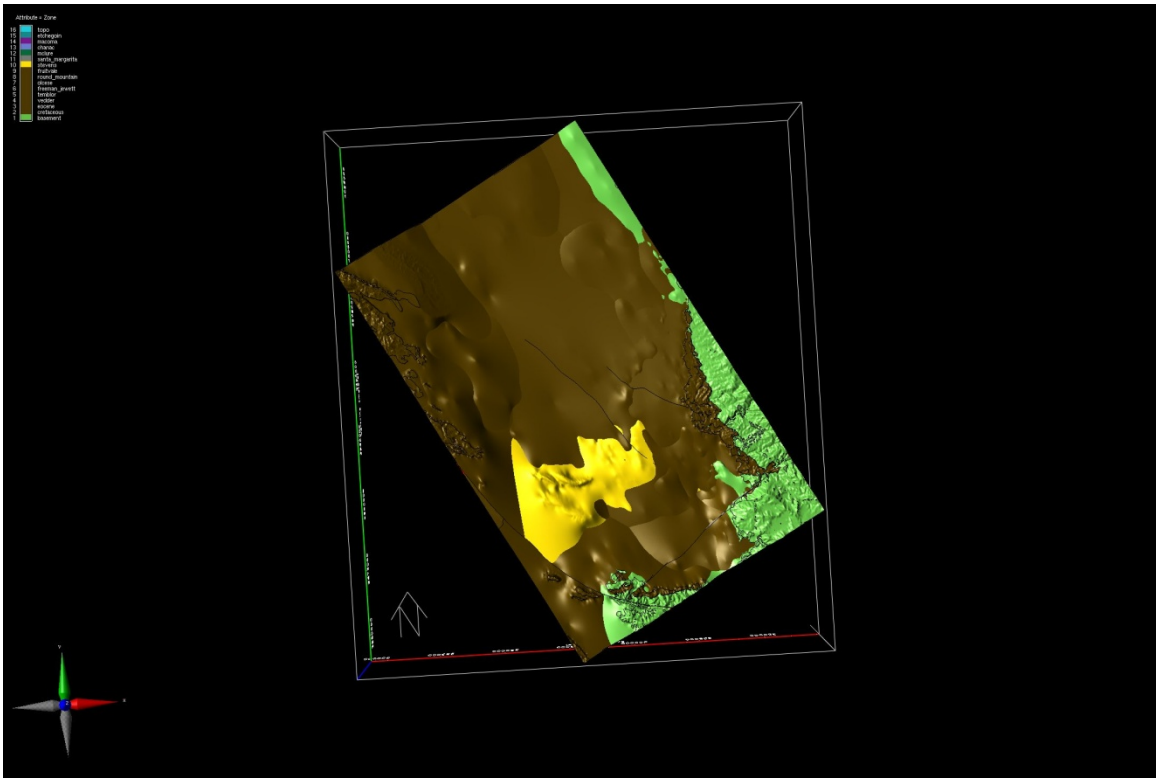

Figure 16: Projection of the Extent of the Stevens Formation (in Yellow) on Top of the Underlying Formations (in Brown)

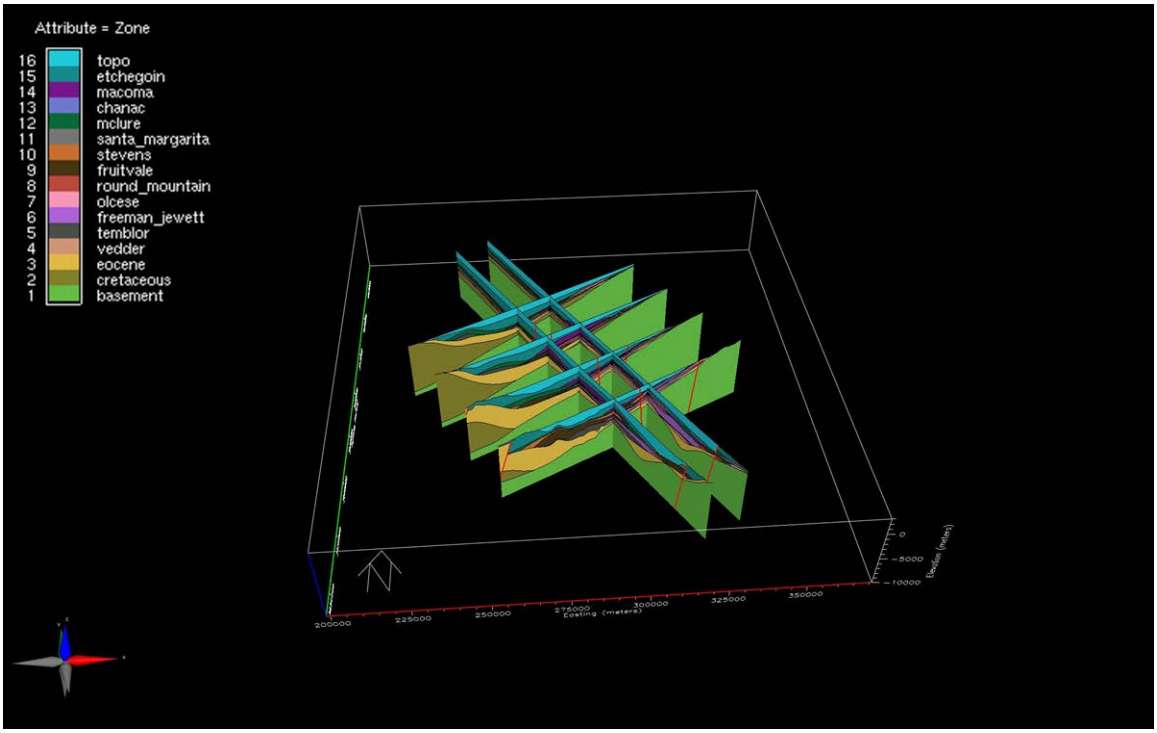

Figure 17: Various Cross-Sections of the Geological Model in a Fence Diagram

CHAPTER 4:
The Deep Basin Reservoir Simulation Model

The "Deep Basin Reservoir Simulation Model" for the Southern Joaquin Basin accurately simulates the multiphase processes of CO_2 and brine flow occurring in response to industrial-scale injection of CO_2 into the deep Vedder formation. This model honors the observed geology at a large number of geologic logs in the model domain and incorporates all salient deep structural features, such as explicit representation of fault zones and the complex sand/shale interbedding within the injection reservoir. The model was initially developed to better understand CO_2 sequestration options in a deep formation that is compartmentalized by faults and affected by sand-shale interbedding (Birkholzer et al., 2011).

In this study, we apply the model to evaluate the potential impact of CO_2 sequestration on shallow groundwater resources. Therefore, more focus was placed on evaluating the response in shallow layers, and a new simulation capability was added to estimate pressure-driven land surface uplift. The model is expected to provide reasonable estimates of shallow pressure changes and land-surface impacts of CO_2 injection, but it does not account for the complex water stresses important for shallow water resources and groundwater management—and does not model any dynamic trends except those induced by CO_2 sequestration. We use the "Deep Basin Reservoir Simulation Model" in this study to ensure that the simplified modeling of CO_2 injection in the "Shallow Water Resources Impact Simulation Model" is reasonable. Also, we apply the "Deep Basin Reservoir Simulation Model" to conduct uncertainty quantification regarding the hydrogeological parameters affecting CO_2 injection and storage.

Consistent with the previous use of the "Deep Basin Reservoir Simulation Model" (Birkholzer et al., 2011), our simulations assume that CO_2 injection is conducted near the Kimberlina site in the center of the domain into the permeable portion of the Vedder formation (Vedder Sand), which is considered to be a viable storage target in this region. In a hypothetical scenario, we assume industrial-scale injection at a constant rate of 5 million tons of CO_2 per year for a period of 50 years. The simulation time includes the injection period of 50 years, and a post-injection period of 150 years. The annual rate of CO_2 represents the captured and compressed emissions from a medium to large coal-fired power plant.

4.1 Model Description

4.1.1 Model Domain and Setup

The reservoir-scale CO_2 migration model is based on the geomodel described in Section 3. Hydrogeological model properties were obtained from many oil fields in the region (Birkholzer et al., 2011; Zhou et al., 2011; Zhou and Birkholzer, 2011). Analysis of these hydrogeologic properties suggested that some units of the geomodel could be combined into a single hydrogeologic unit. The result of this analysis is shown in Table 1, which describes the hydrogeologic model parameters for twelve discontinuous or continuous (stacked) hydrogeologic formations.

Table 1: Hydrogeologic Properties Assigned to Each Formation: k_h and k_v are Horizontal and Vertical Permeability, Φ is Porosity, β_p is Pore Compressibility, α is the Van Genuchten Parameter for Entry Capillary Pressure, and m is the Van Genuchten Parameter for Pore-Size Distribution

Formations	k_h [mDarcy]	k_v [mDarcy]	Φ [-]	β_p [10^{-10} Pa^{-1}]	α [10^{-5} Pa^{-1}]	m [-]
Non-Fault Zones						
Above Etchegoin	3000	3000	0.35	15.5	5.0	0.457
Etchegoin	1200	1200	0.32	15.5	5.0	0.457
Macoma-Chanac	1900	1900	0.31	10.5	5.0	0.457
Santa Margarita-McLure	2000	2000	0.275	10.5	5.0	0.457
Stevens Sand	240	48	0.22	10.5	5.0	0.457
Fruitvale-Round Mountain	0.002	0.001	0.338	14.5	0.42	0.457
Olcese Sand	170	34	0.336	4.9	5.0	0.457
Temblor-Freeman	0.002	0.001	0.338	14.5	0.42	0.457
Vedder Sand (sand layers)	303*	60.6*	0.264*	4.9	13.0	0.457
Vedder Sand (shale layers)	0.1	0.05	0.32	14.5	0.42	0.457
Tumey-Eocence	0.07	0.07	0.07	14.5	0.42	0.457
Baserock	0.0001	0.0001	0.01	22.7	0.5	0.457

* The values are given at the injection points. Depth-dependent permeability and porosity values are assigned to the Vedder Sand (Figure 19).

As mentioned above, we consider a hypothetical CO_2 storage scenario with injection into the Vedder formation. The Vedder formation is a large, permeable sandstone formation, the areal extent of which is shown in black in Figure 18a. The formation pinches out to the far south, west, and north of the injection site, and outcrops are located along the eastern boundary. It has variable *thickness* (Figure 18b) and dips towards the western boundary, at an average slope of about seven degrees (Figure 18c). At the (assumed) injection site in the center of the domain, the Vedder formation is about 400 m thick, and its top elevation is about 2,750 m below the ground surface. Based on well logs, we distinguish six alternating sand/shale layers within the Vedder formation—Vedder Sand and Vedder Shale. These internal facies are considered laterally continuous in our study. The overlying Temblor-Freeman Shale is a suitable caprock formation for stratigraphic containment of the injected supercritical CO_2. At the injection site, the Vedder Sand is 400 m thick, and its top elevation is -2,751 m. The caprock (the Freeman Shale) is about 200 m thick.

Figure 18a also shows the trace of several faults in the area. Fault-zone hydraulic properties are quite uncertain; however, there are qualitative observations that most fault zones are less conductive than the adjacent sandstone formations (Birkholzer et al., 2011): (1) oil and gas trapping is observed under *in situ* effective stress conditions, (2) water-level observations in the Pond-Poso-Creek fault zone east of the hypothetical injection location suggest a partial

groundwater barrier in shallow units, and (3) oil and gas fields are partially compartmentalized, as evidenced by pumping tests. While acting as partial barriers, the fault offsets are in all cases significantly smaller than the thickness of the Vedder formation; thus, some lateral hydraulic connectivity across the faults is expected. For the purpose of this study, we assume a fault scenario representing partial compartmentalization, where the lateral permeability of major faults is reduced by a factor of 100 compared to the adjacent formation permeability. In the model, we explicitly account for the three most prominent faults in the numerical grid (Figure 18a): the Greeley fault west of the injection location, and the Pond-Poso-Creek fault zone as well as the New Hope fault zone east of the injection location. Note that in this study, faults are assumed nonconductive in shale formations; i.e., the potential for leakage of CO_2 and/or brine through permeable faults is not a concern. Also, the potential for fault reactivation is not addressed.

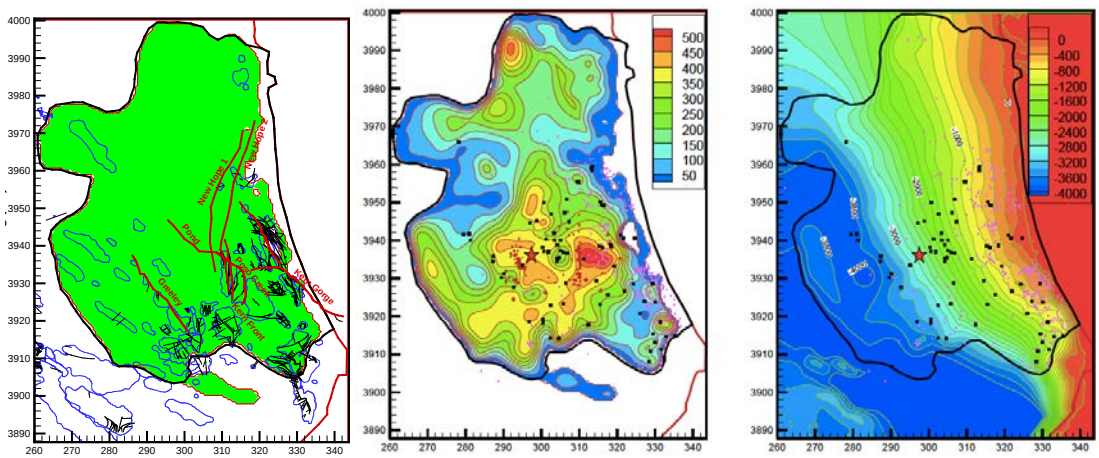

(a) (b) (c)

Figure 18: Vedder Sandstone Reservoir: (a) Areal Extent and Faults, (b) Thickness (in m), and (c) Top Elevation (in m)

The black line shows the areal extent of the Vedder. Red star shows assumed CO_2 injection location near Kimberlina. Coordinate system is given in km.

For the Vedder Sand permeability and porosity, we estimated the depth-dependent parameter values and their uncertainty ranges using the available datasets, as shown in Figure 19. The equations for the fitted trend are given in Wainwright et al. (2013). Except for the Vedder Sand permeability and porosity, we assume that all properties are uniform in each formation.

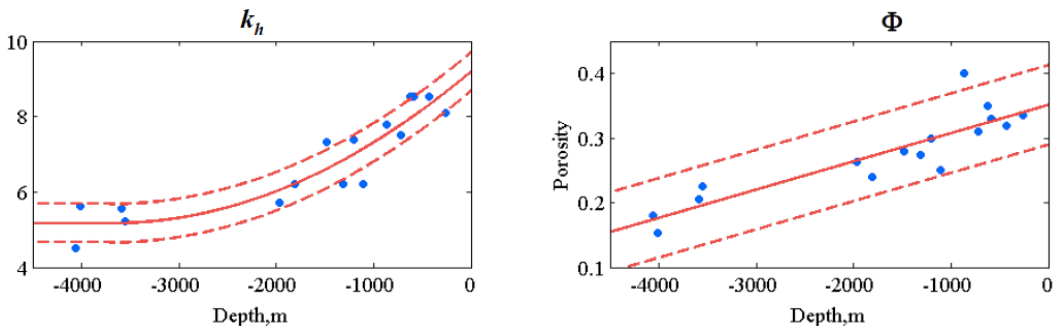

(a) (b)

Figure 19: Estimated Depth-Dependent (a) V Sand Permeability and (b) V Sand Porosity

The blue dots are the data values, the solid red line is the estimated parameter value, and the dotted read lines are the uncertainty bounds (± two standard deviations).

4.1.2 Numerical Model

We used the massively parallel multiphase simulator TOUGH2-MP (Zhang et al., 2008) with the ECO2N module to simulate injection and migration of supercritical CO_2 in the brine reservoir. The ECO2N module describes the thermodynamics and thermophysical properties of H_2O-NaCl-CO_2 mixtures, including phase transitions and dissolutions (Pruess, 2005). It also accounts for the effect of variable brine and CO_2 density in the system, which is considered to have an impact on the pressure responses.

A 3D mesh of 64,214 elements was generated representing the 11 formations from the crystalline base rock to the top shallow aquifer (Figure 20). As mentioned before, the storage formation (the Vedder sandstone) was divided into three sand model layers and three alternating shale layers (Vedder Sand and Vedder Shale). The mesh design was such that we can accommodate a large number of simulations while accurately accounting for the CO_2 plume behavior in the storage formation. The TOUGH2 simulator handles unstructured gridding, which was used to provide adequate mesh refinement to the areas near the injection wells and also allows for model layers to conform to the steeply dipping formations in the deep sediments of the southern San Joaquin River basin. Significant mesh refinement can be seen in the center of the domain, where multiphase processes and strong pressure buildup can be expected in response to CO_2 injection. Major faults are explicitly represented.

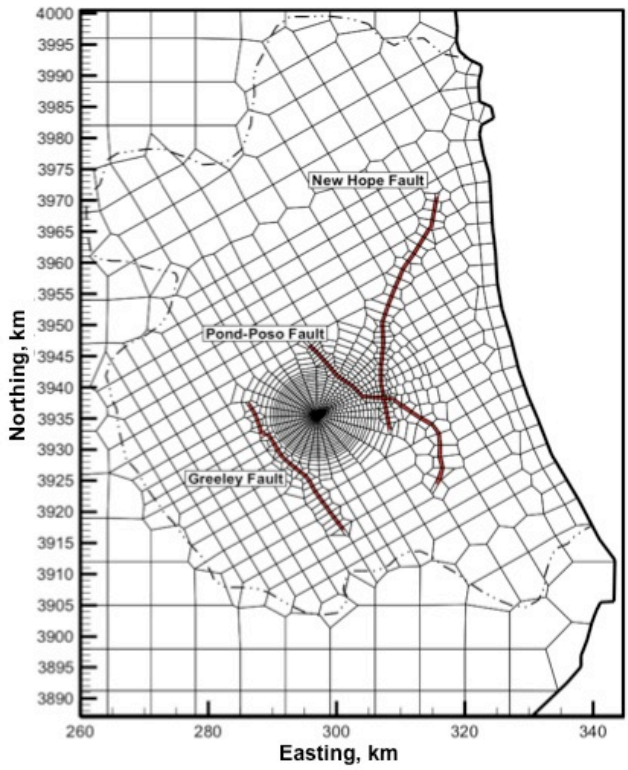

Figure 20: 2D Plan View of Simulation Mesh

The injection location is in the center where the mesh has very small elements sizes. The dash-dotted line shows the presence of the Vedder Formation. Red lines represent major faults that are explicitly represented in the mesh.

4.1.3 System Responses of Interest

In this study, we are mainly interested in the possible impact of deep CO_2 storage on the shallow water resources. Assuming that there are no local high-permeability flow paths such as permeable faults or leaky wells, such impact may be evaluated based on these three system responses:

(1) Pressure response in the shallowest part of the model domain

As is discussed in Section 1.1, the pressure increase from the CO_2 injection is known to reach a larger area beyond the CO_2 plume footprint, and possibly to affect shallow water resources. In this model, the overpressure resulting from deep CO_2 injection may propagate from the injection point to the aquifer layers in two pathways. One is the direct vertical direction through various overlying layers, though many of these have low permeability. The other is in the updip direction of the reservoir towards the east side of the basin. Since the Vedder formation is updipping and reaches the surface on the eastern boundary of the domain, the pressure could propagate through the reservoir and reach a shallow aquifer if hydraulic connection exists. Note that the pressure changes calculated here are only due to the injection of CO_2. All other external forces on the hydrogeologic system are neglected in

the TOUGH2 simulation, as the starting point for the model runs is a hydrostatic system. As mentioned before, the "Deep Basin Reservoir Simulation Model" does not account for the complex water stresses important for shallow water resources and groundwater management and does not model any dynamic trends in surface or groundwater conditions and land-surface uplift, except those induced by CO_2 sequestration.

(2) Brine leakage from the reservoir to the shallow aquifer

Brine leakage could be expected in this domain near the outcrop area at the eastern boundary, where the Vedder Formation reaches the ground surface. We compute both the brine flux and migration distance as caused by CO_2 injection to determine whether the brine leakage could create a significant impact on the shallow aquifer.

(3) Land surface deformation

As opposed to the model used in Section 5, the TOUGH2 simulator used here has no geomechanical module for direct calculation of land surface deformation. Therefore, the surface deformation is calculated here as a post-processing task, by adding the vertical volumetric change in each formation from the impervious bottom boundary to the ground surface. For a homogeneous and laterally infinite aquifer, the vertical change near the injection zone can be calculated from the simulated pressure response as follows (Fjær et al., 2008):

$$\frac{b}{B} = \alpha \frac{(1+v)(1-2v)}{(1-v)E} \Delta P$$

where b is the vertical expansion of the aquifer, B is the thickness of the aquifer, α is Biot's coefficient, v is Poisson's ratio, E is Young's modulus, and ΔP is the change in aquifer pressure. For a semi-pervious aquitard, the total vertical change can be calculated similarly by integrating the pressure changes along the vertical direction. This method provides a rough approximation of actual surface deformation, because it assumes that (1) the formation deformation occurs only in the vertical direction, with negligible lateral deformation, (2) the vertical volumetric deformation in each formation has no interactions with its neighboring formations, and (3) the effective stress varies only with pressure changes, without any change in the total stress from *in situ* conditions. It has been shown that this approximate method is sufficient to provide a reasonable estimate of a few-centimeter uplift observed at the In Salah CO_2 injection site (Rutqvist, 2012). Jung et al., (2013) used this approximation to simulated uplift induced by pressure buildup in a two-aquifer-one-aquitard storage system.

The geomechanical parameters (E and v) used in the deformation calculation are related to the pore compressibility used in TOUGH2 simulation, as follows (Jaeger et al., 2007):

$$\beta_p = [\frac{3(1-2v)}{E} - (1+\phi)\beta_m] \Big/ \phi$$

where β_P is pore compressibility, β_m (typically 2.5×10^{-11} Pa^{-1}) is the rock matrix compressibility or grain compressibility, and ϕ is porosity.

The surface uplift is caused by the pressure increase and subsequent geomechanical expansion in the reservoir and overlying formations. Following Jung et al. (2013), we approximate the surface uplift by adding the vertical volumetric change in each formation. The vertical volumetric change in one formation is given as:

$$\frac{b}{B} = \alpha \frac{(1+v)(1-2v)}{(1-v)E} \Delta P$$

where b is the vertical expansion of the formation, B is the formation thickness, α is Biot's coefficient, v is Poisson's ratio, E is Young's modulus, and ΔP is the pressure change, respectively.

As pointed out earlier, all other external forces on the hydrogeologic system are neglected in the TOUGH2 simulations, meaning that the surface deformation calculated here is only due to the injection of CO_2, neglecting many other sources of strong surface deformation in the area.

4.2 Base-Case Results

Our base-case simulations use the geological model and the hydrogeological properties described in Section 4.1 As explained earlier, we assume industrial-scale injection to be conducted near the Kimberlina site at a constant rate of 5 million tons of CO_2 per year for a period of 50 years.

4.2.1 Deep Injection Reservoir

First, we look at the system responses in the deep injection layer (Vedder formation). Figure 21 shows the evolution of the separate CO_2 phase and the pressure buildup in the uppermost reservoir layer just below the caprock. Note that the depth of the reservoir-caprock interface increases from west to east, as shown in Figure 18. In the top four plots of Figure 21, the pressure response to CO_2 injection increases with injection time and eventually affects a large region close to all the boundaries. At the end of injection, the highest pressure occurs towards the Pond fault (the fault on the eastern side of the injection location), where a thick column of supercritical CO_2 exists, causing additional pressure buildup due to buoyancy. The maximum pressure increase of about 1 MPa (or 10 bar), observed at the end of injection period, is moderate and is not expected to create geomechanical damage or seismicity. During the post-injection period, the pressure dissipates quickly and returns to hydrostatic within decades. The semi-permeable faults clearly affect the pressure response by confining the pressure buildup to the region between the two major faults.

In the bottom four figures of Figure 21, CO_2 plume migration is a much slower process than pressure propagation. At the end of injection, the CO_2 plume remains within a 5 km radius from the injection point. After injection ends, the plume continues migrating eastward in the updip direction driven by buoyancy, until it arrives at the fault around 100 years and is stopped there from further migration. Without local permeable pathways (i.e., permeable faults or leaky wells), the injected CO_2 is effectively trapped by the faults, meaning that there is no endangerment of potable groundwater resources by CO_2 leakage.

4.2.2 Shallow Groundwater Resources

Figure 22 shows the predicted pressure buildup in the shallow aquifer for the same time steps as those depicted in Figure 21. Note that the color scale has changed drastically, and that overall the pressure impact on shallow groundwater is very small. The maximum pressure increase is less than 1000 Pa (equivalent to less than 0.1 m head change), which would not have any noticeable impact on the shallow groundwater aquifer. Note that the region of slightly increasing pressure is not above the CO_2 injection location (which would be expected if it was caused by a vertical pressure propagation through the multiple geological units between the deep and the shallow layers), but rather appears along the eastern and southeastern boundaries. This suggests that the vertical pressure propagation is sufficiently blocked by the caprock and other intervening low-permeability layers. This pressure increase along the boundary is caused by the earlier mentioned direct hydraulic connection between the Vedder formation and the shallow groundwater aquifer at the eastern and southeastern boundary, where the Vedder formation reaches the surface due to the updip structure. The pressure change is generally the largest at the end of the injection period (50 years), and decreases back to hydrostatic pressure during the post-injection period.

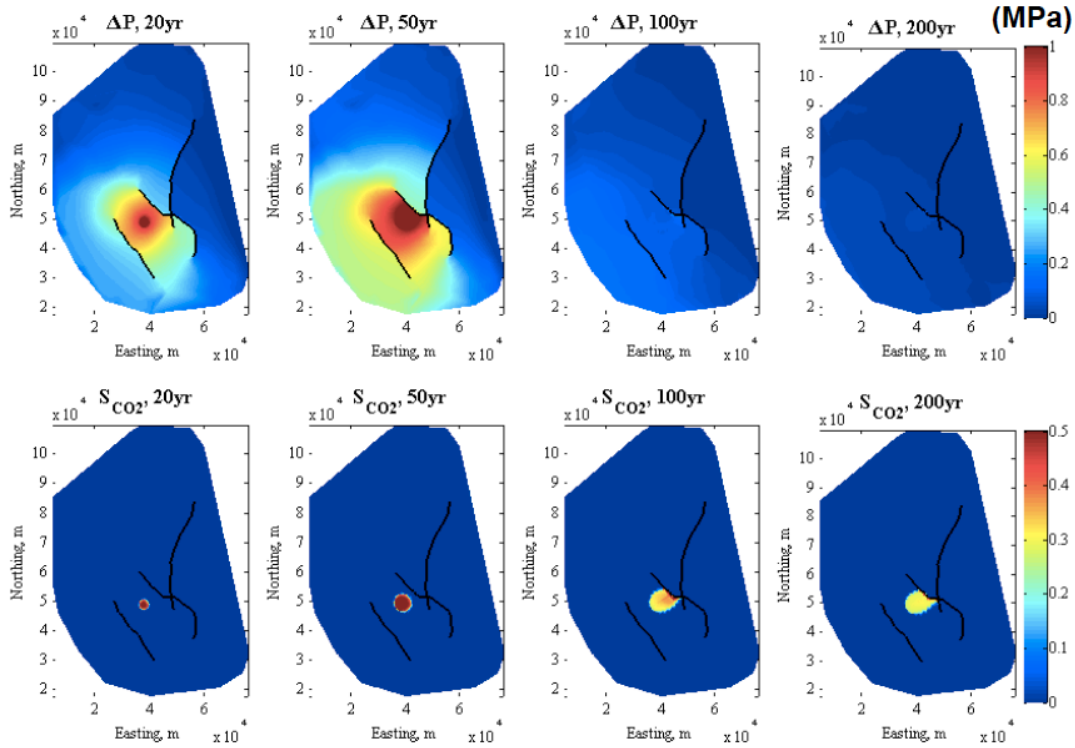

Figure 21: Evolution of Pressure Buildup (Top Row in MPa) and CO_2 Saturation (Bottom Row) at 20, 50, 100 and 200 yr after Start of CO_2 Injection (Left to Right Columns)

The solid thick black lines are fault locations.

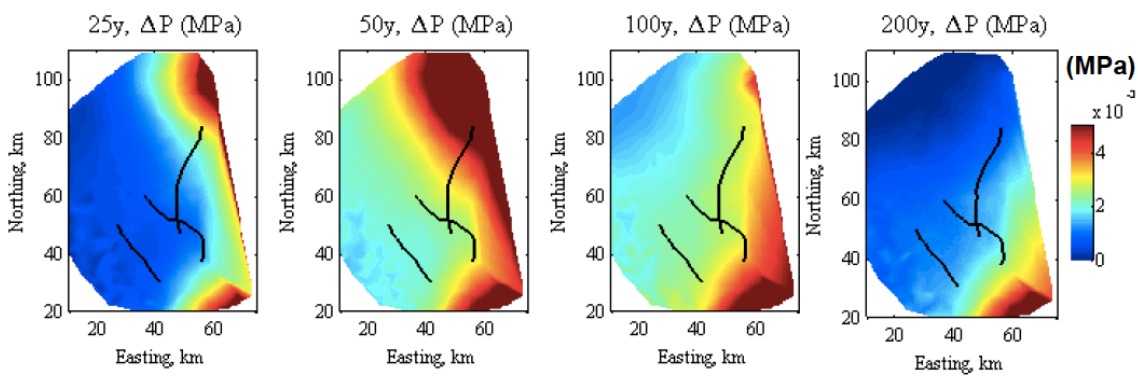

Figure 22: Evolution of Pressure Buildup (in 10^{-3} MPa) in the Shallow Aquifer at 25, 50, 100 and 200 Years from Left to Right

Note that the contour scale is different from Figure 22, by three orders of magnitude.

4.2.3 Land Surface Uplift

Figure 23 shows the time evolution of land surface deformation generated by the injection of CO_2. As mentioned earlier, the calculated surface deformation is based on a simplified evaluation method that is based on vertical integration of pressure-induced porosity changes. This leaves out the effect of overburden stiffness, which means that the predictions of uplift are on the conservative side. We stress again that the calculated surface deformation is only due to

injection of CO_2, neglecting many other sources of strong surface deformation in the area. The total expected land surface deformation from all sources, including groundwater pumping, is calculated in Section 5.

Land-surface deformation starts initially in the center of the domain, which corresponds to the injection location. The extent and the magnitude of uplift increase during the 50 years of injection. Spatially, the area affected by uplift is mostly confined to the region between the two main faults. As to the spatial distribution, we found that the magnitude of the surface uplift depends mainly on the pressurization of deep layers but also on the layer thickness. For example, the Vedder formation layer thickness is quite heterogeneous as shown in Figure 18, which explains some of the spatial patterns seen in Figure 23. At all locations, the surface uplift assumes the maximum values at the end of the injection period, and decreases quickly in the post injection period. The maximum land surface uplift of about 0.25 m is observed after 50 years of injection near the injection location.

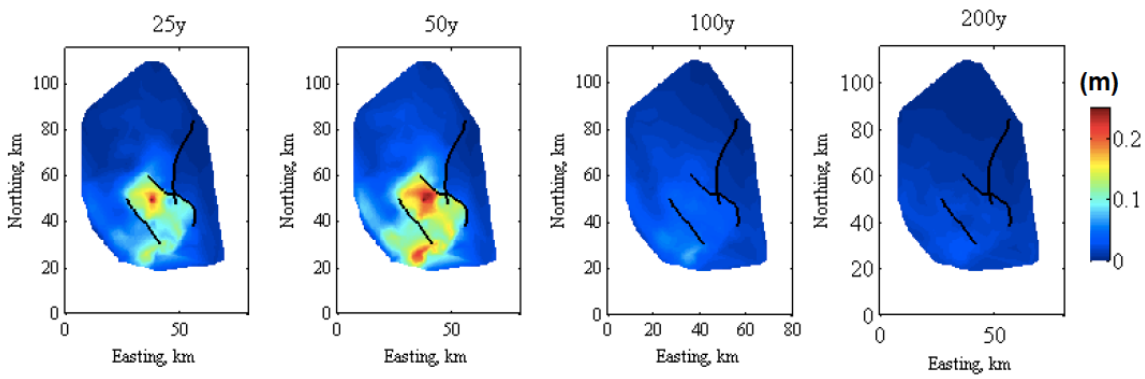

Figure 23: Surface Uplift at 25, 50, 100, and 200 Years from Left to Right

4.3 Uncertainty Quantification

Geological and hydrogeological properties can be associated with large uncertainties. In this section, we evaluate how such uncertainties can affect the above-mentioned system responses. In particular, we are interested in cases that could potentially increase the system responses related to hydrogeological impacts.

4.3.1 Parameter Range and Distribution

To evaluate the impact of the uncertainty in the model parameters (Table 4.1), we systematically varied relevant hydrological parameters in three relevant geological units, the Vedder Sand, the Vedder Shale, and the Temblor-Freeman. We did not change the properties of other overlying formations, because these three layers drive most of the relevant system responses. We changed five properties in each of the three formations: permeability, porosity, compressibility, and two properties related to the multiphase behavior of the CO_2-water system (the van Genuchten α and m parameters), shown in Table 4.1.

We assumed an independent normal distribution for each parameter with the mean equal to the reference value shown in Table 1. The permeability anisotropy ratio was not changed in this study. The standard deviation of the distribution is half-order-of-magnitude in permeability, factor-of-2.5 in pore compressibility, and 15 percent in porosity, respectively. These ranges are based on local data and, in some cases, on experience with other representative formations. For the depth-dependent Vedder Sand permeability and porosity shown in Figure 19, we simply shift the curves up and down by values sampled from the parameter, which leaves the basic trends represented in the polynomial curves unchanged. We used the Latin Hypercube sampling method to sample each parameter from the distribution specified above. A total of 300 parameter sets were sampled. We confirmed that 300 realizations were sufficient to get convergence in the mean and confidence interval.

4.3.2 Pressure Profiles

Figure 24 shows the vertical profile of the pressure increase near the injection location. During the injection period, the pressure increases significantly within the storage formation. The increase is quite variable such that the maximum possible pressure change is one order of magnitude larger than the minimum value. Wainwright et al. (2013) found in the sensitivity study that the pressure response near the injection well is largely impacted by the Vedder Sand permeability. The pressure increase is particularly large when the reservoir permeability is low.

None of the simulation cases shows significant pressure increase above the caprock (Temblor Freeman formation). This suggests that the main confining unit above the injection reservoir has sufficiently low permeability to prevent vertical pressure propagation from the reservoir, for all the 300 uncertainty cases studied. As shown in Figure 22, the small pressure impact on the shallow aquifer occurs not as a result of direct vertical connectivity, but rather through the hydrological connection at the eastern boundary due to the updip of the Vedder formation.

After injection ends, the pressure quickly dissipates in the reservoir, whereas pressure remains elevated in the caprock and in the shale layers for a while (up to 100 years), due to its low permeability. This also suggests that the main pressure dissipation in this system happens mainly in the horizontal direction (along the updipping layer) in the reservoir.

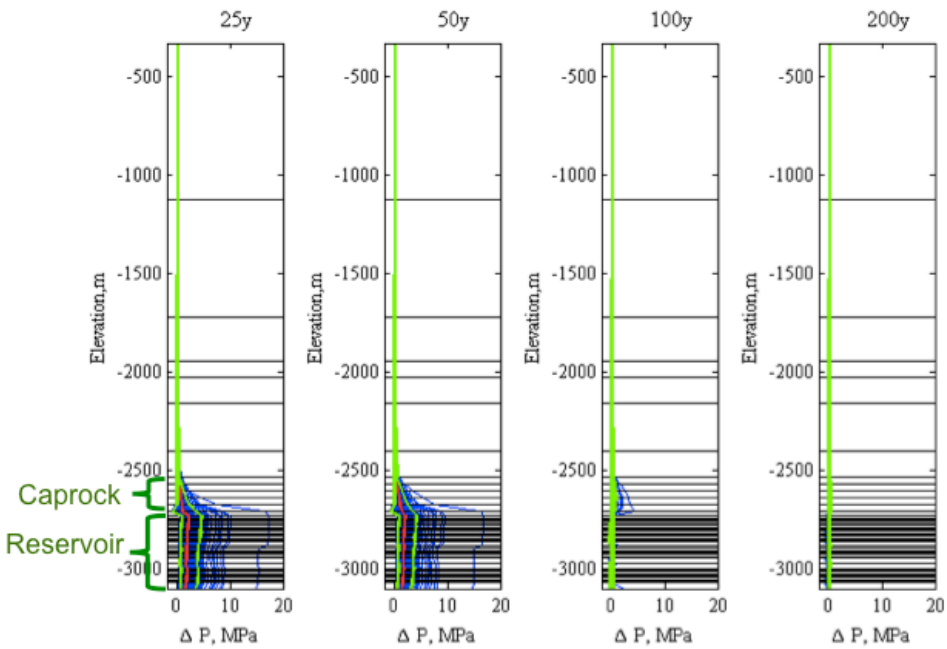

Figure 24: Pressure Increase along a Vertical Column at the Location Adjacent to the Injection Location

The times shown are 25, 50, 100 and 200 years from left to right. The blue curves represent individual profiles from uncertainty quantification simulations. The red and green curves are their mean and 90-percent confidence intervals, respectively.

4.3.3 Fluxes at Eastern Boundary

Figure 25 shows the injection-induced changes in groundwater flux and migration distance along a selected point at the eastern boundary, where the Vedder formation reaches the ground surface and may connect with other shallow groundwater resources. (Note that the migration distance is calculated by dividing the flux value by the porosity value). Both the flux and the migration distance increase during injection period, and decrease quickly in the post-injection period. The variability between individual runs is not significant compared to the reservoir pressure; i.e., the difference between the minimum and maximum values is less than the factor of two. The variability is also the largest at the end of the injection period.

The mean flux and migration distance at the eastern boundary are about 2.5 m/yr and 7 m/yr, respectively, while the 90-percentile values are 3m/yr and 8m/yr. Compared to the typical shallow groundwater velocities, these flux values are considered too small to cause a detrimental impact on groundwater resources. We may use the migration distance as an indicator for the possible displacement of the brine-freshwater interface within the injection reservoir. A maximum migration distance of 8 m/yr is not a concern in this regard.

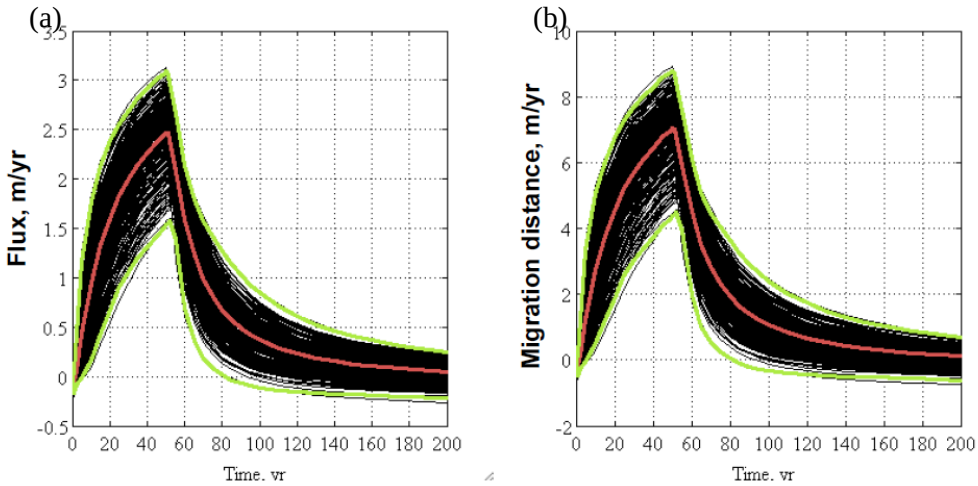

Figure 25: (a) Flux and (b) Migration Distance at the Eastern Boundary in the Updipping Vedder Formation

The black curves represent the individual runs. The red and green curves are their mean and 90% confidence intervals, respectively.

4.3.4 Land-Surface Uplift

Figure 26 shows the uncertainty-analysis results for land-surface uplift in the vicinity of the injection point, where the maximum value was observed (Figure 23). While the general behavior is similar (the surface uplift increases during the injection period and rapid decreases quickly afterwards), we observe a large variability between the simulation cases, similar to the pressure buildup in the reservoir (Figure 24). This results from the vertical expansion of each layer being linearly correlated to the pressure increase, as shown in Section 4.1.3.

Most realizations are limited to surface deformations of less than 1 m, but there are some outliers of up to 5 m. Such uplift values could certainly be a concern for the area, starting with impact on water resources and but also infrastructure. We note that the cases with very high uplift are typically correlated to very low reservoir permeability, which causes (in turn) local pressure in the reservoir to be very high, perhaps higher than realistically achievable. We caution that the relevant model parameters used in the uncertainty quantification need to be better constrained.

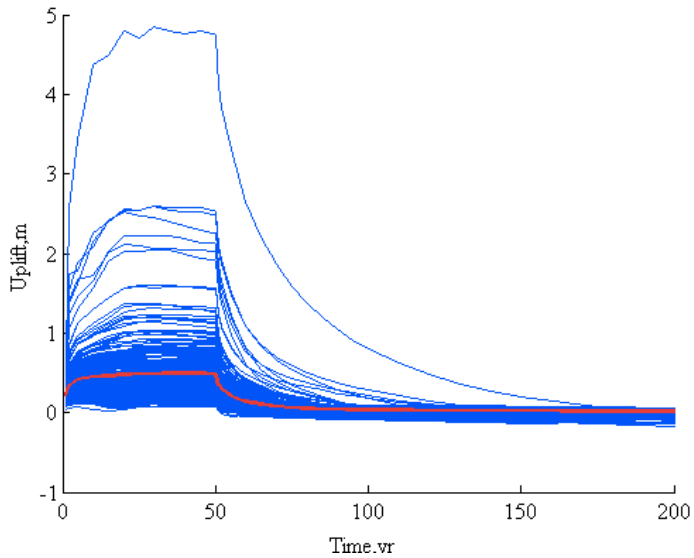

Figure 26: Land-Surface Uplift above the Injection Point

The blue lines represent individual runs. The red and green curves are their mean and 90% confidence intervals, respectively.

4.4 Compartmentalized Reservoir

Zhou et al. (2008) introduced a categorization of CO_2 storage reservoirs with respect to pressure impacts (Figure 27). The first category comprises "open" systems, which are large sedimentary formations from which the displaced brine can easily escape laterally. On the other hand, a storage basin may be composed of a number of compartmentalized reservoirs laterally separated by low-permeability zones, forming a second category referred to as "closed" systems. Zhou et al. (2008) demonstrated that the pressure response to injection and storage in "closed" systems is different from that in "open" systems. In closed systems, additional fluid volumes can only be accommodated by compressibility and diffuse pressure bleed-off. As a result, the pressure buildup caused by continuous industrial-scale CO_2 injection may be much larger, which in turn could cause a strong increase in land surface uplift.

Review of Figure 21 suggests that the Vedder Formation responds to the injection of CO_2 as a mostly open system. While pressure mitigation is limited in eastern and western direction due the fault presence, the pressure propagation and brine migration find open "boundaries" to the north and south, helping to limit the pressure increase in the reservoir. The reservoir is quite large, and the pressure response does not extend to the formation boundaries. However, while this is true for the Vedder Formation, it is well known that many deep formations in the Southern Central Valley are compartmentalized due to the presence of sealing faults, and could in fact act as "closed" systems. In this section, we investigate the potential impact of injecting large volumes of CO_2 into a closed reservoir system by creating a hypothetical closed reservoir based on the original Vedder Formation. As is shown in Figure 28, we limit the extent of the reservoir to the region between the two major faults, and we assume that the properties outside this region are similar to low-permeability caprock.

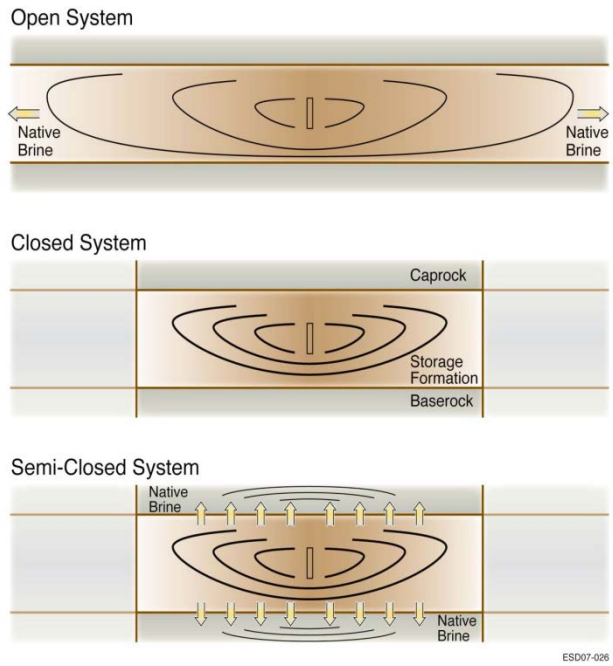

Figure 27: CO_2 Storage Scenarios for Different Systems; Open, Closed and Semi-Closed System from the Top

A semi-closed system is essentially a closed system that allows for diffuse pressure bleed-off into over- and underlying formations.

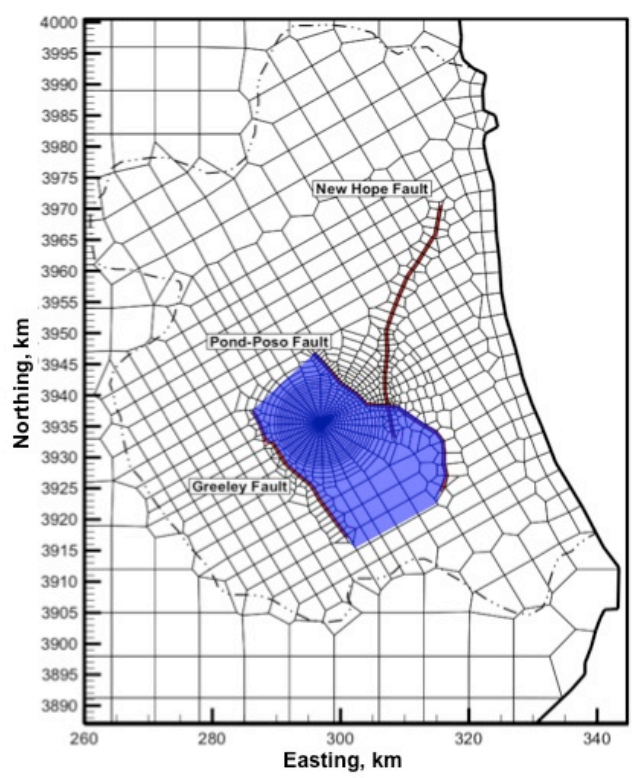

Figure 28: Domain for the Compartmentalized (closed) System

4.4.1 Deep Injection Reservoir

We first show the system responses in the storage formation, for better understanding of the difference between the open and closed reservoirs. Figure 29 shows the time evolution of pressure buildup and CO_2 saturation in the uppermost layer of the reservoir, just below the caprock, in the same format as Figure 21. Compared to the original reservoir, the pressure buildup is much higher than in the "open" case, although it is confined to the region between the two faults. This is because the pressure dissipation is limited and hindered by the low-permeability outside of the region between the two faults. The pressure also remains elevated for a much longer period of time because brines cannot easily be displaced from the confined reservoir. At 200 years, the pressure buildup is still above 2 MPa, and the pressure does not return back to hydrostatic during the simulation period.

In contrast, the CO_2 plume migration is much less affected by the change in the reservoir extent, and thus the migration pattern very similar to Figure 21. The plume moves eastward in the updip direction until it arrives at the fault. This is because (a) the pressure gradient is not significantly affected by the reservoir extent, and (b) the plume was also driven by buoyancy. There is no CO_2 leakage from the reservoir during the simulation period.

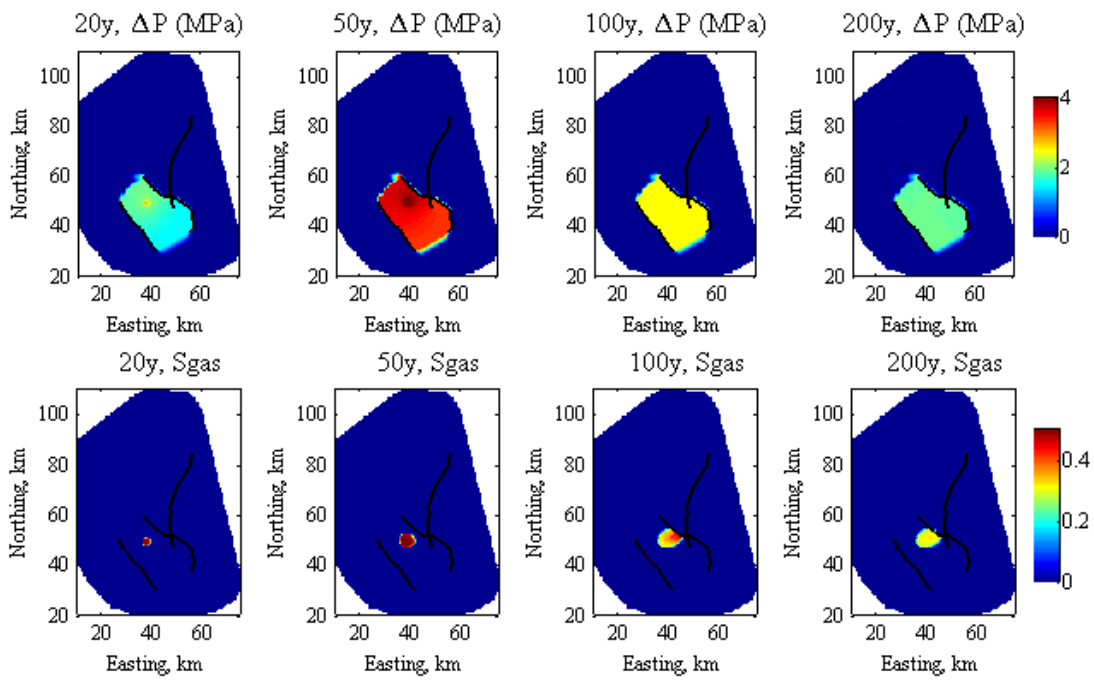

Figure 29: Evolution of Pressure Buildup (Top Row in MPa) and CO_2 Saturation (Bottom Row) at 20, 50, 100 and 200 yr after Start of CO_2 Injection (Left to Right Columns) for the Compartmentalized Reservoir

The solid thick black lines are fault locations.

Figure 30 shows the vertical profile of the pressure increase at the location adjacent to the injection location, in the same format as Figure 24. Similar to the original open reservoir, there is no significant pressure increase in any formation above the main caprock. Although the

pressure within the reservoir is higher on average compared to the open-reservoir case (Figure 24), the maximum pressure is around 20 MPa at 50 years, which is not significantly different due to one outlier in Figure 24. The outlier in the open-reservoir case is a case with very low reservoir permeability. While the reservoir permeability has a large impact on the pressure dissipation in the open reservoir (i.e., by allowing brine to be displaced laterally into distant reservoir regions), it does not affect the closed reservoir significantly, because the pressure dissipation in the closed reservoir is mainly through compressibility and diffusive pressure bleed-off into the caprock.

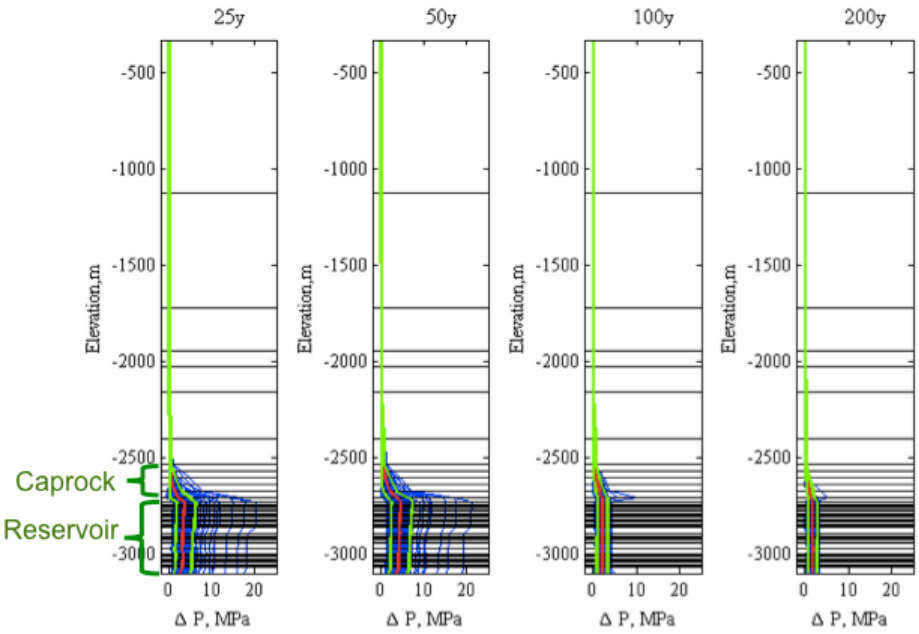

Figure 30: Pressure Increase along the Vertical Columns at the Location Adjacent to the Injection Location for the Compartmentalized Reservoir

The times are 25, 50, 100 and 200 years from left to right. The blue curves represent individual profiles from uncertainty quantification simulations. The red and green curves are their mean and 90-percent confidence intervals, respectively.

4.4.2 Land Surface Uplift

Figures 29 and 30 suggest that there is no significant pressure impact on the shallow aquifer. We did not observe any noticeable brine migration at the eastern boundary, either. These observations suggest that the surface uplift would be the only major concern in the compartmentalized-reservoir scenario.

Figure 31 shows the evolution of the surface uplift in the closed reservoir system in the same format as Figure 23. Compared to Figure 23, we find the magnitude of the surface uplift to be much higher than the original open reservoir case, although the surface uplift is limited to the smaller region above the closed reservoir. At the end of the injection period (50 years), the land-surface uplift is up to 1.0 m near the injection location, which is four times larger than the original open-reservoir case. In the post-injection period, the uplift continues for a longer time

period compared to the open-reservoir case. This is mainly due to the slower pressure dissipation in the compartmentalized reservoir unit, as shown in Figure 29 and 30.

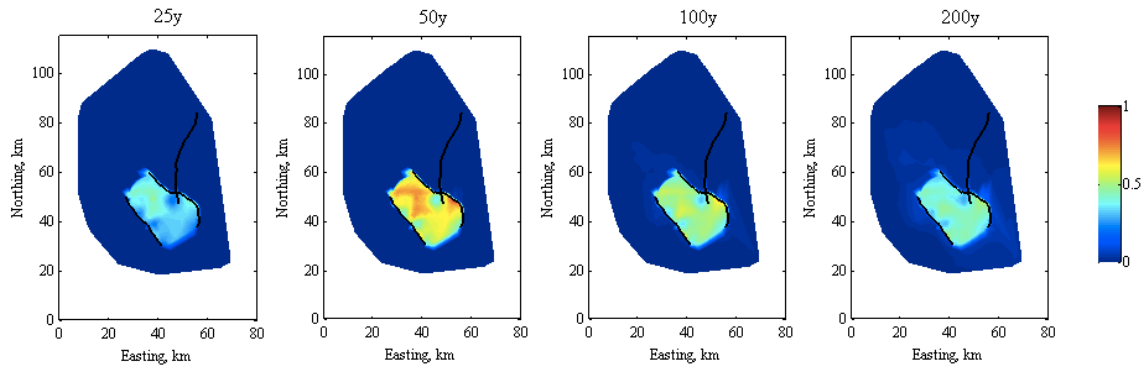

Figure 31: Base Case Results: Land-Surface Uplift in Top Model Layer in the Compartmentalized Reservoir.

Figure 31 shows the uncertainty quantification result for the surface uplift above the injection point, where the maximum value was observed. For the compartmentalized reservoir, the land surface uplift on average can be higher than the one in the original open reservoir (Figure 26), but the uncertainty range seems less affected. This is because the pressure buildup in the deeper units has less variability than the open-reservoir case, as is shown in Figure 30. Note that the maximum uplift of any uncertainty case in Figure 32 is about 5 m, which is similar to the range predicted in the open-reservoir case.

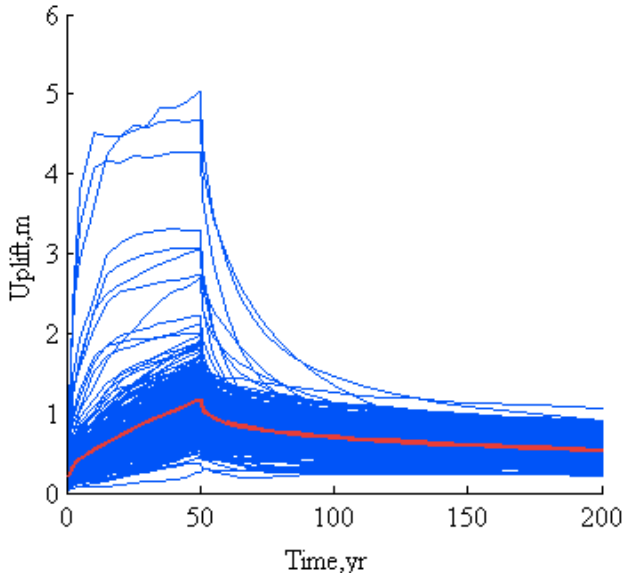

Figure 32: Land Surface Uplift above Injection Point for the Compartmentalized Reservoir

The blue lines represent individual runs. The red curve is the mean.

4.5 Summary Results from Deep Basin Reservoir Simulation Model

In this section, we investigated the potential impacts of deep CO_2 storage on shallow groundwater resources, using the multiphase flow simulator TOUGH2-MP/ECO2N. The developed numerical model takes into account complex multiphase fluid dynamics associated with injecting supercritical CO_2, such as two-phase flow and variable density effects. The simulation model was based on a realistic geological model with detailed representation of geological features, such as the internal Vedder Formation structure and the presence of major faults. To evaluate potential hydrological impacts, we considered the pressure increase in the shallow aquifer, the brine flux along the eastern boundary, and the ground-surface deformation as the main responses of interest.

Our results show that the caprock above the CO_2 storage reservoir effectively limits pressure and brine migration in the vertical direction. Given that there are several additional low-permeability formations between the Vedder Formation from the reservoir and shallow layers, it is clear that a direct hydrological impact of large-scale CO_2 sequestration via vertical interaction can be effectively ruled out. In our model, the main conduit for pressure and brine migration is along the updipping reservoir that reaches shallow groundwater resources, near the outcrop area along the eastern boundary. The large reservoir extent and the large distance, however, reduce the magnitude of the pressure increase and brine flux there to small values that should not endanger groundwater resources. These findings were confirmed over the possible range of the parameters through an uncertainty quantification study.

In addition, we conducted a hypothetical study to consider a closed (or compartmentalized) injection reservoir to explore possible scenarios that might result in higher reservoir pressure. This was done by changing the Vedder Formation extent in the original model. We found that even though the reservoir pressure becomes higher than the original case, the overpressure does not propagate into shallow units within this simulation period due to the low permeability of the overlying units. We may conclude that in the absence of localized flow paths (such as leaky faults or fractures), the potential for pressure changes or brine migration to affect shallow water resources is extremely low.

Our results, however, suggests that the CCS-induced land surface uplift may possibly affect land use and shallow water resources. The uncertainty analysis showed that the uplift near the injection site could be more than one meter in some cases. These expected deformations need to be considered in the context of ongoing subsidence in the Southern Central Valley. Further analysis on the simultaneous effect of surface uplift from CO_2 storage and subsidence from groundwater pumping and other effects is provided in Section 5, using the Shallow Water Resources Impact Simulation Model.

We note that this study does not look into the potential for and the impact of leakage of CO_2 and/or brine in localized pathways, such as improperly abandoned wells or undetected permeable faults. Another topic not addressed in this study is the potential for pressure-induced fault activation, or "induced seismicity"; however, the simulation conducted in this study can provide a starting point for evaluation of induced seismicity potential.

CHAPTER 5:
The Shallow Water Resources Impact Simulation Model

The purpose of the "Shallow Water Resources Impact Simulation Model" is to approximate the potential impact of deep CO_2 sequestration on a stressed water system. In this study, we use as a starting point an accurate and well-calibrated simulation tool for surface water and groundwater resources in the Central Valley (see Section 5.1). This model is then modified to (a) focus on the region of interest in the southern San Joaquin Valley, and (2) to allow for modeling the injection of CO_2 into deep geological formations underlying the current model domain (Section 5.2). The latter requires extension of the existing model to include several deep sand and shale layers. Since the selected simulation tool does not allow for representation of multiphase processes, the latter also requires approximation of the two-phase behavior of CO_2 and brine as a single-phase process that represents CO_2 injection as equivalent-volume water injection. Single-phase models have been shown to give reasonable estimates for the pressure behavior in deep CO_2 storage reservoirs (Cihan et al., 2013).

As described below, the modified and expanded surface water and groundwater resources model can evaluate the impact from geologic carbon sequestration in the area, in the context of the long-term groundwater and subsidence trends occurring as a result of other water stresses (e.g., pumping and irrigation). In other words, the model can be used to (1) to evaluate the future water level changes in the freshwater aquifers from ongoing water management with or without CO_2 sequestration, and (2) to evaluate similar trends for land-surface deformation with and without CO_2 sequestration. The model is applied to the same hypothetical CO_2 injection scenario as considered with the "Deep Basin Reservoir Simulation Model." Injection is conducted at a constant rate of 5 million tons of CO_2 per year for a period of 50 years near the Kimberlina site into the deep Vedder formation. In addition, we evaluate a two-project injection scenario, where in addition to the Kimberlina site another injection project is conducted in a different formation in the area (the Stevens formation).

5.1 Selection of Suitable Shallow Simulation Model

As previously noted in Chapter 1, the development of the candidate C2VSIM and CVHM models occurred simultaneously with cooperation between groundwater hydrologists in both DWR and the USGS. Data resources that were used to parameterize and obtain time series input data for both models were common and largely shared. The main distinctions between the two models are in the assumptions made in estimating source and sink terms that affect groundwater hydrologic balance, and in the model parameterizations to make these estimates. Distinction should be made between the model codes and the model applications.

The model application C2VSIM (Brush et al., 2011) *http://baydeltaoffice.water.ca.gov/modeling/hydrology/C2VSim/index_C2VSIM.cfm* is built upon a relatively new model code named IWFM (Integrated Water Flow Model), *http://baydeltaoffice.water.ca.gov/modeling/hydrology/IWFM/index.cfm* developed by Dr. Can Dogrul within the California

Department of Water Resources (Dogrul et al., 2011). The IWFM code is an outgrowth of the Integrated Groundwater Simulation Model (IGSM) originally developed by Dr. Young Yoon (Boyle Engineering Consulting Engineers Inc., 1990). The IGSM code introduced a land and water use pre-processor which made it relatively easy to estimate irrigation hydrology inputs based on parameters such as land use, irrigation diversions, irrigation efficiency, evapotranspiration (ET), and drainage return flow. Most models, up until this time, estimated aquifer recharge outside the model simulation. This land- and water-use pre-processor has been replaced by a more comprehensive code referred to as the Integrated Flow Model Demand Calculator (IDC):

http://baydeltaoffice.water.ca.gov/modeling/ hydrology/IWFM/ IDC/index_IDC.cfm.

The model application CVHM (Faunt et al., 2009c) was developed using the USGS modeling code MODFLOW 2000 (MF2K) combined with the Farm Process (FMP) model (Schmid and Hanson, 2009), and has been used to determine the groundwater and surface water components of the hydrologic cycle in a similar manner to DWR's IDC model. The FMP is a more detailed and comprehensive pre-processor than the IDC, although not as well documented and more difficult to use. The FMP code is still relatively recent, and new versions of the pre-processor have been released in the past six months. The current version of MODFLOW-FMP utilizes MODFLOW 2005 and the FMP 3.0 pre-processsor. Figure 33 is a flow diagram that describes the essential hydrologic components of MODFLOW-FMP. These components will be contrasted with IWFM and the IDC in the discussion below. This discussion is provided to document the basis for the decision to opt for the CVHM model application using MODFLOW-FMP as the shallow simulation model in this project. Although the C2VSIM and CVHM-FMP model applications were developed in a collaborative manner utilizing many of the same state-level well-log, cropping, irrigation diversion and soil survey data sets, it will become clear to the reader from the analysis below that the CVHM-FMP model permits a more rigorous simulation of the combined shallow and deep geologic system. Expansion of CVHM-FMP with MODFLOW-FMP to include deeper formations provides a tool that links CO_2 storage in suitable geological formations with surface and near-surface processes affecting surface water deliveries, groundwater conjunctive use, and irrigation agriculture.

5.1.1 Model Mesh

The IWFM model uses a finite element mesh where calculations are performed at the model nodes. In contrast, MODFLOW-FMP is limited to a regular finite difference mesh, where the centroid of the cell represents the properties of each cell. Finite element grids allow unstructured gridding and are superior at representing areas where gradients are changing rapidly and for depicting complex hydrographic features. The same resolution can be achieved using telescoping finite difference models, but with more computational overhead. However, for the model application C2VSIM, the finite element grid resolution is much coarser than the structured grid for CVHM using MODFLOW-FMP, making it more difficult to precisely place the injection site in the model domain for both single well and multiple well scenarios.

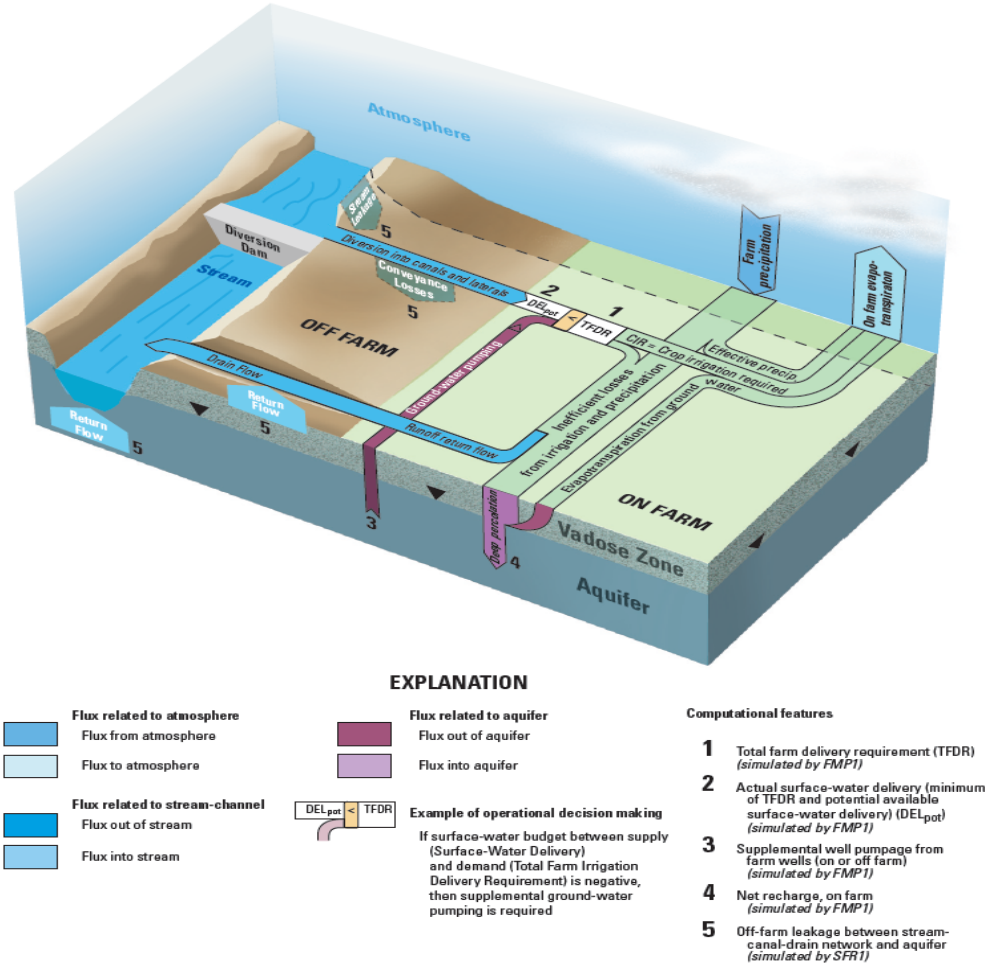

Figure 33: Conceptual Water Flow Diagram Showing the Relative Fluxes Related to Atmosphere, aquifer and Stream Channels Components in the MODFLOW-FMP Pre-Processor (Schmid et al., 2006; http://water.usgs.gov/nrp/gwsoftware/mf2k-fmp/tm6A17.pdf).

5.1.2 Stream-Aquifer Interactions

A significant potential strength of the finite element method is to be able to refine the mesh along rivers and streams to improve the representation of groundwater head and hence estimation of groundwater fluxes. However, in the case of the C2VSIM model, although the mesh triangulation more closely follows the river flowpath, the relative size of the model elements is in fact larger than for CVHM-FMP, nullifying any potential advantage. One strength of CVHM-FMP is that the length of each stream reach within a cell can be user specified whereas in C2VSIM the river length is automatically assumed to be the length between two adjacent stream nodes. In the current application, however, the Friant-Kern Canal, the Cross-Valley Canal, and the Kern River (see Figure 7) are the only surface water conveyance facilities of consequence. None of these is highly sinuous and the advantage of the MODFLOW methodology is not expected to be significant.

5.1.3 Evapotranspiration

The two models produce significantly different estimates of evapotranspiration, which is typically the most critical hydrological parameter in basin-scale models of agricultural watersheds. In CV2SIM, cropping is defined at the watershed or subregion level and the crop-mix is defined uniformly over the entire subregion. The DWR performs land use surveys of crops every 5 – 7 years (although with remote sensing they are striving to improve the frequency of these surveys) and these data were utilized by both models during their development. In C2VSIM, crop evapotranspiration is determined using estimates of potential evapotranspiration for each month of the year, multiplied by the crop-specific crop coefficient obtained from tabular values. In areas where crop distribution is not uniform, this can lead to subregional bias. In the case of CVHM-FMP, each cell is assigned to the dominant crop and there is no attempt to recognize crop distribution. However, since the CVHM cells are much smaller than the subregions defined in C2VSIM the introduced bias is likely to be less and the model should be better able to deal with geographic differences in crop distribution. In C2VSIM, bare soil evaporation is set to approximately 50 percent of potential ET (ET_P). However the model does not account for changing vegetative cover over the growing season. CVHM-FMP in contrast does make this adjustment – a time series of vegetative area for each crop is a required model input.

5.1.4 Deficit Irrigation

Given the reduction in water deliveries from the Friant Division to Kern County via the Friant Kern Canal, previously described in Section 2.1, the practice of deficit irrigation, whereby a crop is provided less than the optimal irrigation application for maximum yield, is likely to increase provided returns still exceed the costs of production. Deficit irrigation results in an increase in effective irrigation efficiency and will reduce annual recharge to regional water tables. CVHM-FMP has more flexibility than C2VSIM in recognizing deficit irrigation. C2VSIM makes the assumption that irrigation demand will be met by other sources such as increased groundwater pumping.

Both models have the capability of estimating groundwater pumping as a residual after matching water requirements with surface water supply. Specified agricultural demand is calculated in C2VSIM as the potential evaporation, multiplied by a monthly crop coefficient—there is no capability in the model to recognize reductions in crop evapotranspiration due to anoxia or deliberate deficit irrigation. CVHM-FMP, on the other hand, has the capability of simulating both. Given the likelihood of irrigation deficit irrigation practices in the Basin at the present time and into the future--this is a serious potential limitation in the use of C2VSIM to simulate realistic impacts the carbon dioxide injection scenarios contemplated in this study.

5.1.5 Simulation of Ggroundwater Wells

One limitation of the MODFLOW-FMP model is that only one well can be simulated within any one model cell, whereas C2VSIM allows multiple wells to be assigned to any given element. This limitation can be overcome by adding the pumping volumes expressed within pumping stress period for each production well. MODFLOW-FMP is generally more flexible than C2VSIM and has the capability of turning wells on and off when well water levels in a model

cell reach a certain pre-defined levels. Both CVHM-FMP and C2VSIM are able to distribute pumping in proportion to the agricultural area within model cell or element. The models treat well screens differently with respect to groundwater pumping. In CVHM-FMP the distribution of pumpage across multiple model layers is pre-determined, and the volume of pumpage is a function of aquifer horizontal and vertical permeability within each layer. In C2VSIM, the model determines which layers are pumped based on the layers intersected by the vertical well bore. CVHM-FMP has the ability to simulate interbore flow within each well—although this feature is often turned off, since it can result in long simulation times and create model instability. This is a potential source of pressure loss in a CO_2 injection well and should not be ignored in the current project.

5.1.6 Subsidence

For groundwater subsidence modeling, MODFLOW provides the best documented and most versatile code; this has been an active area of USGS research for the past 50 years. Both models calculate vertical displacement of the land surface due to permanent compaction of permeable clay beds (subsidence) and are based on Terzaghi and Peck (1948) theory which tracks changes in the pre-consolidation head (lowest water level experienced by the reservoir system). The pre-consolidation head controls the initiation of subsidence. CVHM-FMP also has the ability to simulate clay interbeds within time-delayed subsidence (found in thick clay beds such as the Corcoran Clay) as well as non-time delayed subsidence (more common in thinner clay beds). This is an important new development and supercedes code that has been utilized in MODFLOW for more than 20 years. The C2VSIM model only simulates instantaneous compaction of beds and uses the previous MODFLOW subsidence algorithms (although beds can be subdivided in the current IWFM code).

5.2. Description of CVHM-FMP Attributes

As explained above, we decided to use (in this study) the existing CVHM-FMP regional groundwater model as the starting point for modeling the impact of CO_2 storage on shallow water systems. To be used for this purpose, we made several modifications to this application model, for example selecting a submodel domain that focuses on the Southern Joaquin basin area (the Kern sub-basin) and adding the various geological units of the deeper reservoir system (see Section 5.3 below). The simulator used for CVHM-FMP is MODFLOW-FMP, albeit in a new version that contains a more sophisticated treatment of pressure build-up and dissipation within confining layers. Dr. Randy Hanson, one of the developers of the MODFLOW-FMP code and a project collaborator, provided prototype code updates during the course of the project, namely MODFLOW-FMP2 and more recently MODFLOW-FMP3. The MODFLOW-FMP3 code splits deformation into elastic and inelastic components, assigned separately according to the texture model that underpins the assignment of hydraulic properties in the regional groundwater model and the deep reservoir model. An additional innovation has been the formulation of deformable mesh capability that renders calculated deformation estimates in 3-D space. This is significant for visualization of deformation as a result of deep reservoir CO_2 injection (uplift) and shallow aquifer pumping in excess of safe yield that lowers the pressure below the unconsolidated pressure head (inelastic subsidence).

In this section, we shall briefly introduce some of the salient model features and inputs before discussing the CVHM-FMP modification made for the CO_2 project. The discussion focuses on the southern portion of the CVHM-FMP regional groundwater model, the Kern sub-Basin. Six major types of data were compiled for the current CVHM model application. These include (1) hydrologic data that such as precipitation (PRISM), well water levels, and streamflow; (2) land-use data including crop type; (3) surface-water deliveries and diversions; (4) water-use data from previous studies; (5) borehole lithologic data including texture information; and (6) subsidence and compaction data from extensometers (Faunt et al., 2009c). The previous CV-RASA model (Williamson et al., 1989) and the current Central Valley modeling effort by the California Department of Water Resources were the source of current and historic hydrology, water delivery, and groundwater well log data.

5.2.1 Hydrologic and Land Use Data Inputs

The estimated effective precipitation (i.e., the precipitation that infiltrates the soil) is shown in Figure 34. The Farm Process (FMP3) module of CVHM dynamically allocates groundwater recharge and groundwater pumpage on the basis of crop water demand, surface-water deliveries, and depth to the water table (Schmid and Hanson, 2009). The farm irrigation diversion requirement is calculated from consumptive use, effective precipitation, groundwater uptake by plants, and on-farm efficiency. Figure 35 shows the estimated crop water requirements for the mix of crops being grown in the Kern sub-basin. Figure 36 shows the total acreage under irrigation for the time period 1970 through 2010 and Figure 37 shows the distribution of major crops within the region during 2010. The California Department of Water Resources annual cropping database that used to be updated every 5-7 years is now updated more regularly with the goal of annual data availability. These data were directly parsed into the model after re-configuring several of the crop categories (lumped categories based on crop water demand.

The Streamflow Routing Package (SFR1) is linked to facilitate the simulated conveyance of surface-water deliveries (Schmid and Hanson, 2009). If surface-water deliveries do not meet the farm delivery requirement, the FMP invokes simulated groundwater pumping to meet the irrigation demand. Based on this demand, the FMP uses specified irrigation efficiencies to calculate irrigation return flows. Figure 38 shows the estimated groundwater pumping by the Kern County Water Agency for the region. These estimates have been used by the USGS in calibration of the current CVHM-FMP3 model (Faunt et al., 2009c).

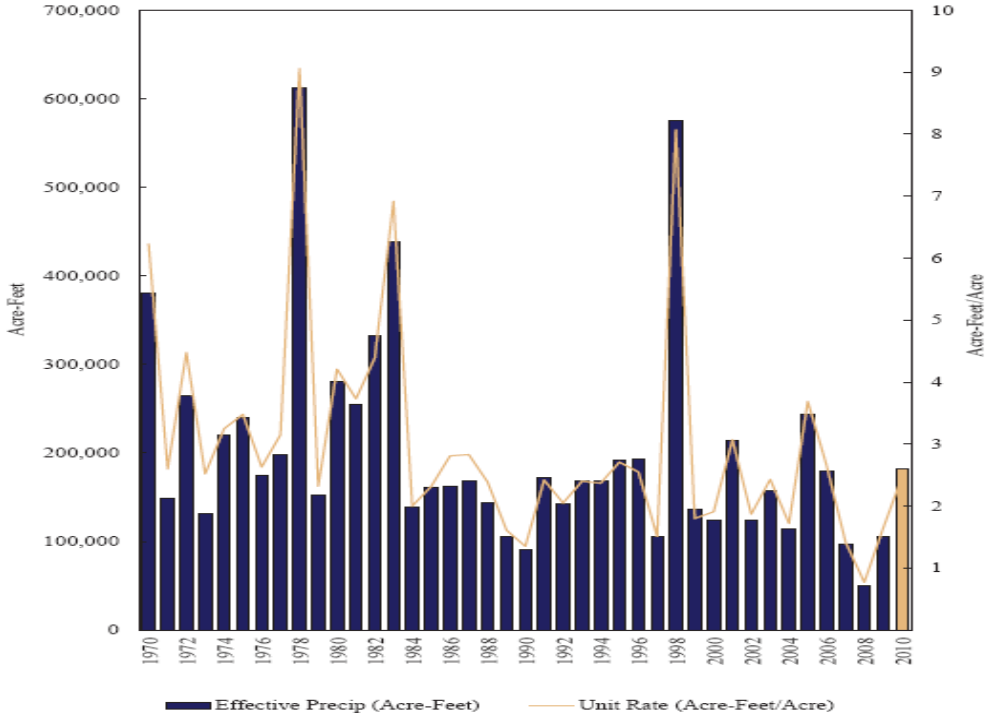

Figure 34: Historical Effective Precipitation for the Kern Sub-Basin Model through 2010 Estimated by the Kern County Water Agency (KCWA, 2013)

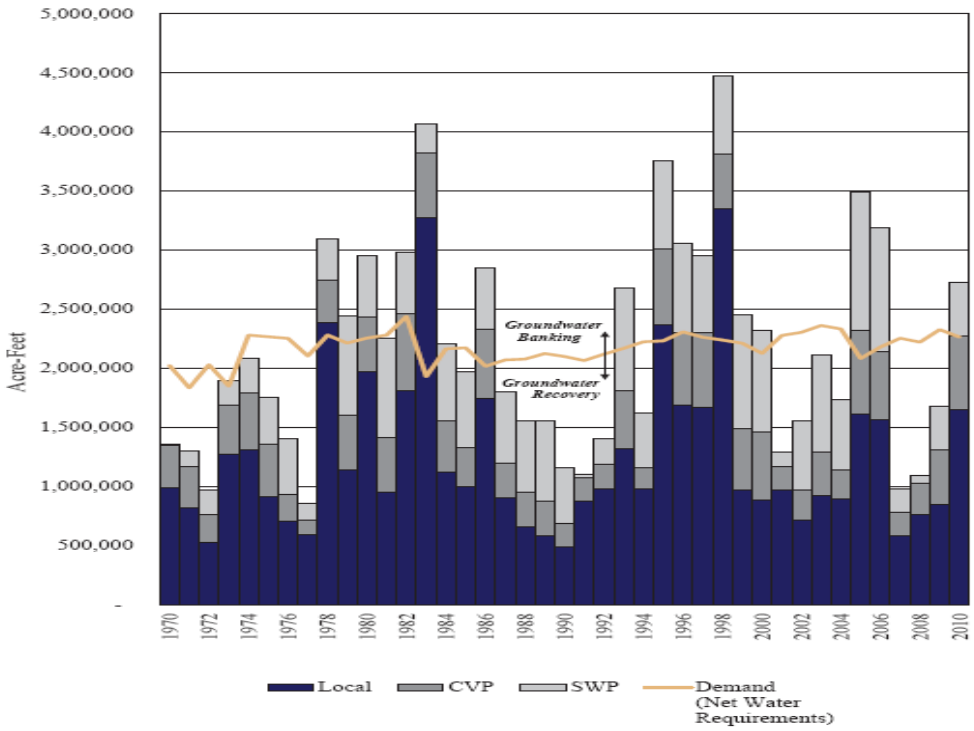

Figure 35: Gross Water Supplies and Net Crop Water Requirements within the Kern Sub-Basin Estimated by the Kern County Water Agency (KCWA, 2013)

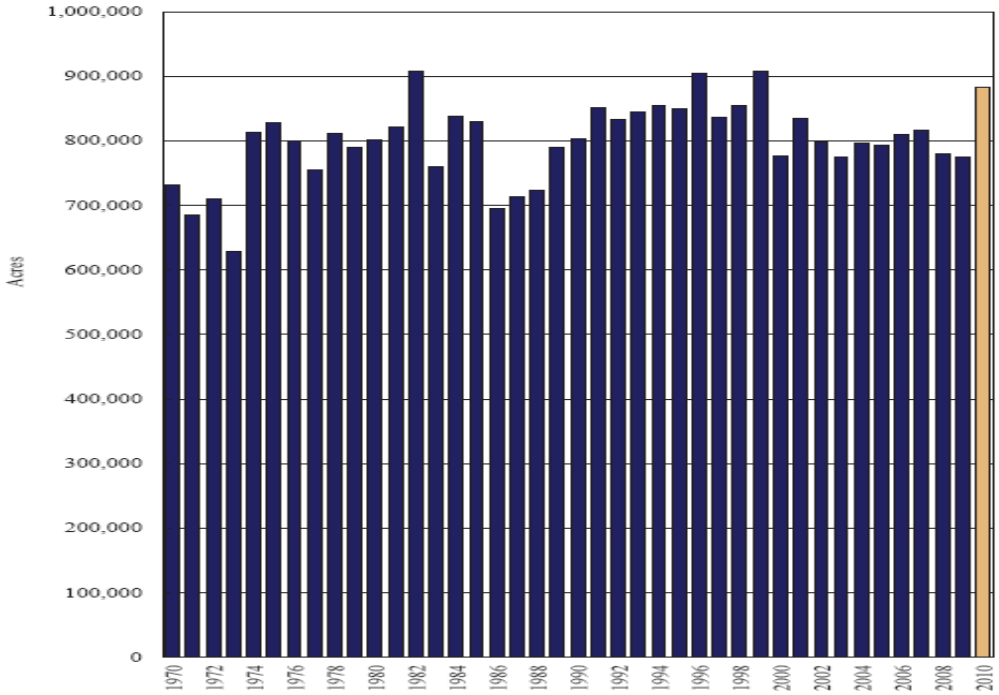

Figure 36: Irrigated Acreage Estimated by the Kern County Water Agency – the Major Water Purveyor for the Region Covered by the Kern Sub-Basin Model (KCWA, 2013)

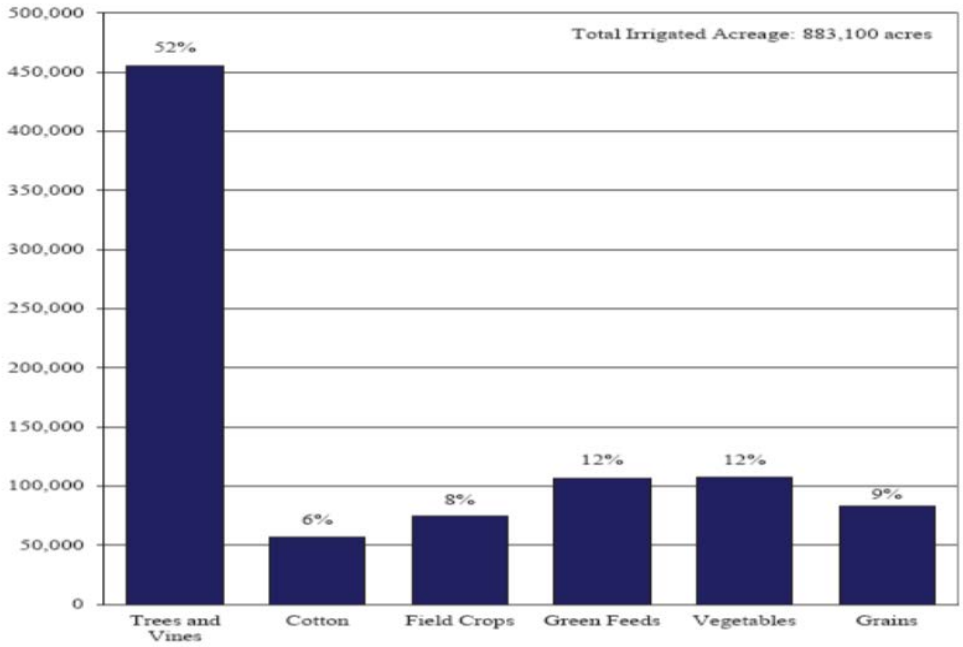

Figure 37: Main Crop Distribution for 2010 within the Kern Sub-Basin (KCWA, 2013)

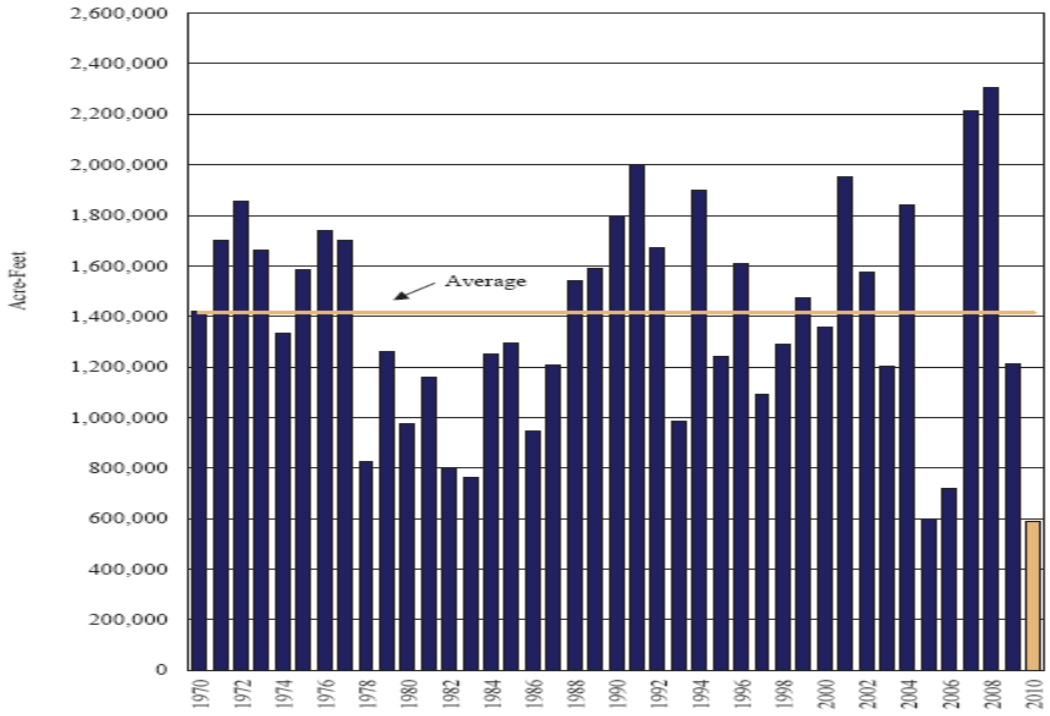

Figure 38: Groundwater Pumping Estimated by the Kern County Water Agency for the Kern Sub-Basin (KCWA, 2013)

5.2.2 Lithologic Data Inputs and CVHM-FMP3 Model Topology

The numerical grid of the CVHM-FMP3 model was chosen to be relevant to water management decisions for irrigated agriculture in the Central Valley aquifer system, which was discretized horizontally into 20,000 model cells of a square mile extent, and vertically into 10 layers ranging in thickness from 50 to 1,800 ft (Faunt et al., 2009c) (see Figure 39).

A texture model was used to estimate hydraulic conductivity for every cell in the CVHM-FMP3 model based on a methodology developed earlier work by Page (1986), Laudon and Belitz (1991) and Phillips and Belitz (1991). The textural analysis was based on the percentage of coarse-grained texture, compiled from driller's logs of wells and boreholes provide by the California Department of Water Resources for wells completed in the Central Valley (Figure 39). The texture analysis was completed in two stages. First, the texture was estimated for each 50 ft thick layers in the model. In a second step, the resulting estimates of texture were aggregated vertically into 10 model layers. Each lithologic log interval was classified using a discrete binary texture classification of either "coarse grained" or "fine grained" on the basis of the description in the log (Faunt et al., 2009b). The textural distribution was then used to define the vertical and lateral hydraulic conductivity and storage property distributions for the CVHM-FMP3 model.

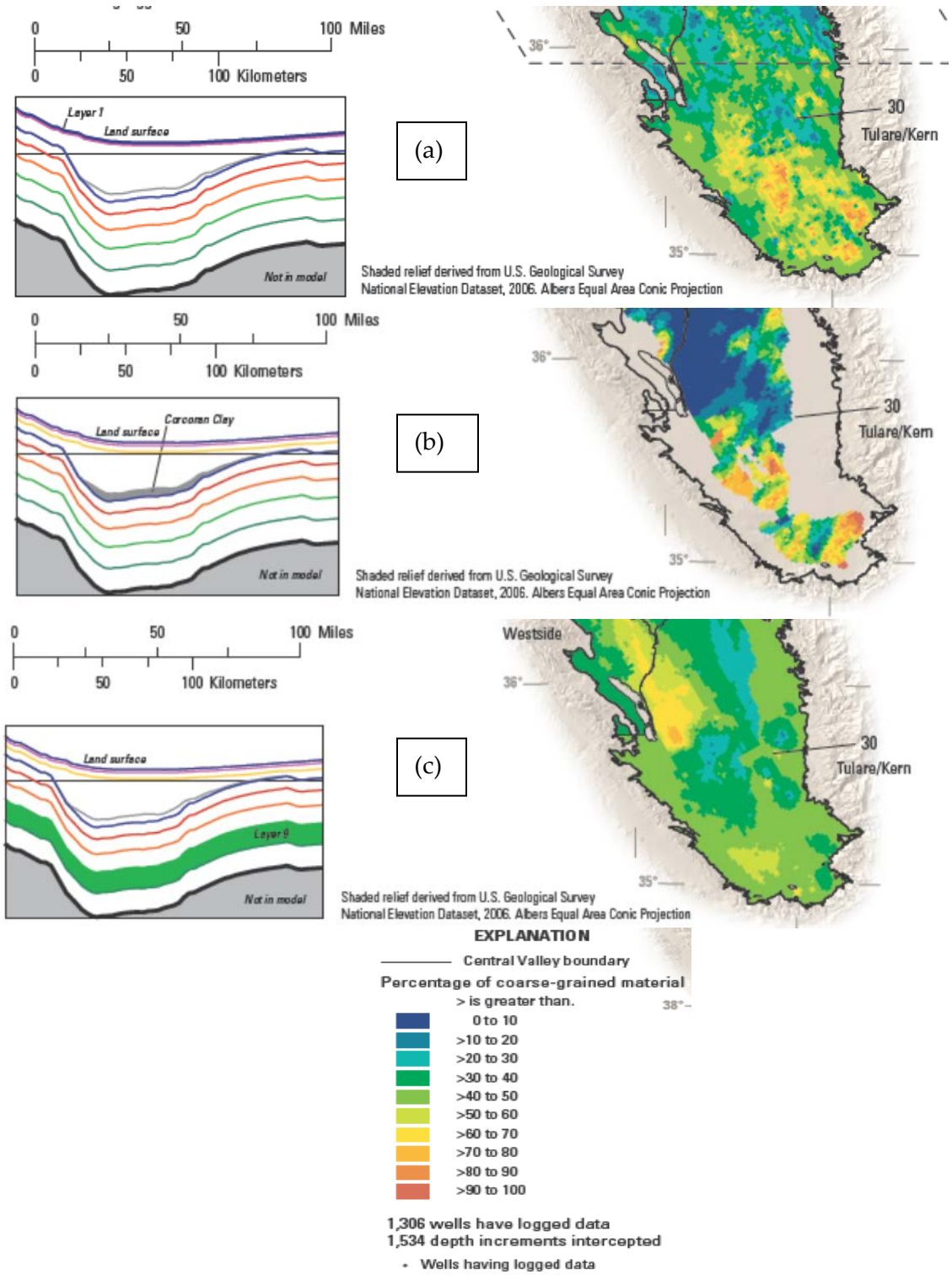

Figure 39: Texture Distributions for Three Layers within the 10 Layer CVHM-FMP3 Model for the Kern Sub-Basin. (a) Model Top 50 ft Layer; (b) Corcoran Clay Aquitard Layer; (c) Model Layer 6.

The key opposite shows the color legend associated with each coarse grained fraction (Faunt et al., 2009b).

5.2.3 Shallow Model Subsidence Simulation

The Kern sub-Basin has been developed extensively for agriculture and petroleum extraction over the past 100 years. Land subsidence is an important consequence of intense groundwater pumpage in susceptible aquifer systems, especially in the southern San Joaquin Valley, where the demand for water exceeds supply (Figure 40). Increasing urbanization in the Kern sub-Basin has further stressed the current groundwater reservoir.

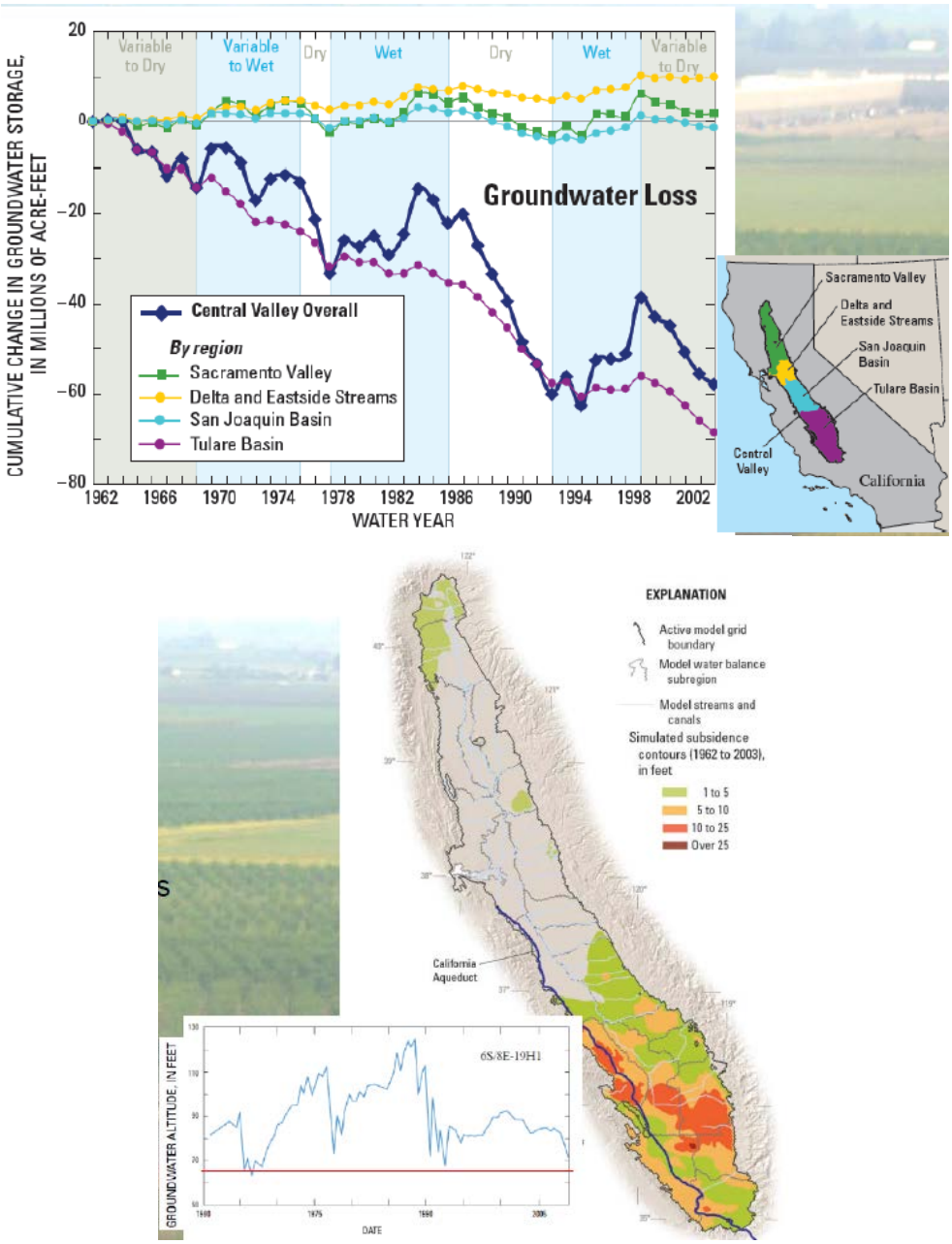

Figure 40: Map of Subsidence in the Central Valley Showing the Concentration of Problems in the Kern Sub-Basin Simulated by the CVHM-FMP3 Model.

Permanent (inelastic) subsidence occurs when groundwater levels fall below the pre-consolidation head value (Faunt et al., 2009b).

The CVHM-FMP3 model subsidence module (SUB) has been calibrated against available extensometer data. As previously described, CVHM-FMP3 simulates elastic and inelastic deformation separately—allowing better representation of the deformation properties of the aquifer and underlying layers. The MNW package within CVHM-FMP3 is capable of simulating intra-borehole flow which can be an important mechanism for taking account of vertical flow within and between hydro-geologic units such as across the Corcoran Clay. Deep wells that penetrate both above Corcoran and below Corcoran formations are sometimes imperfectly sealed, leading to significant induced flow between the upper and lower layers of the model. Figure 41 shows the major land subsidence areas with land surface deformation of greater than 1 foot (green polygons) in the Kern sub-Basin caused primarily by a decline in water levels. Model simulated contours plots of land subsidence show small subareas north of Bakersfield and in the north-west corner of the Kern sub-Basin where subsidence is greatest and expected to exceed 10 feet.

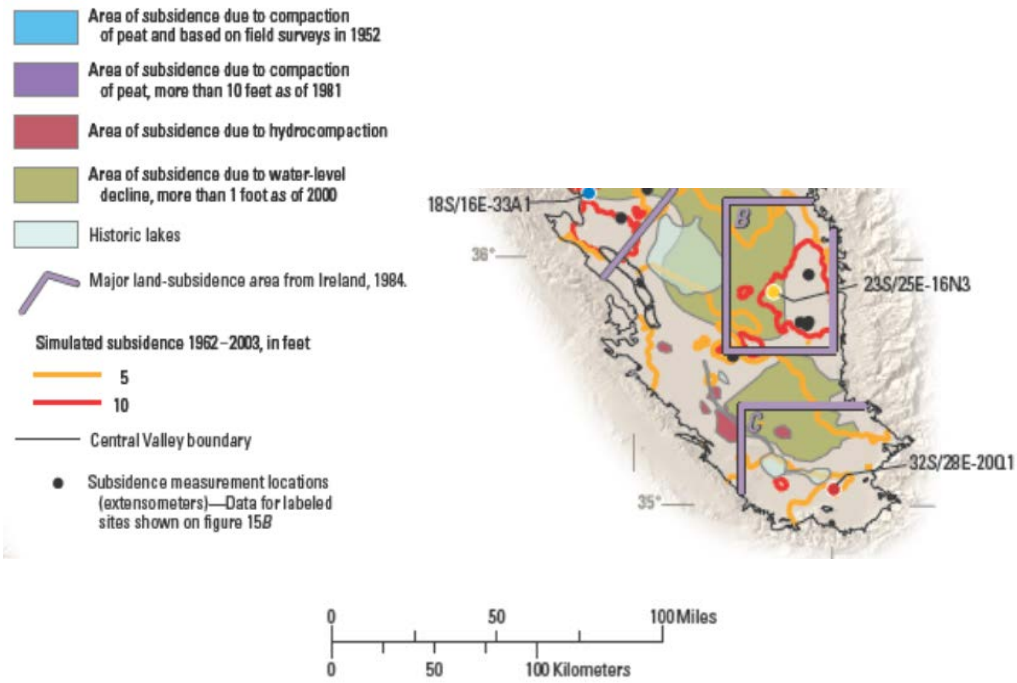

Figure 41: Major Land Subsidence Areas in the Kern Sub-Basin Mostly Due to Water Level Declines over Time.

Affected areas cover a significant portion (in green) of the sub-Basin (Faunt et al., 2009c).

5.2.4 Water Budget Analysis

One of the most useful tools that result from the development of a groundwater simulation model like CVHM-FMP3 is the ability to construct separate water budgets for different regions and within subregions such as the Kern sub-Basin. In Figure 42, these subarea budgets show the high level of groundwater overdraft in western Kern County (subarea 19) and also exhibit the relatively small amount of additional water storage contained in the shallow unconfined aquifer (specific yield) and, via elastic and inelastic storage, in the deeper confined aquifer layers. Of interest is the fact that the model results suggest that there is a positive flux of water from

outside the subarea in the case of subarea 19 and a negative flux out of each subarea in the case of subareas 20 and 21.

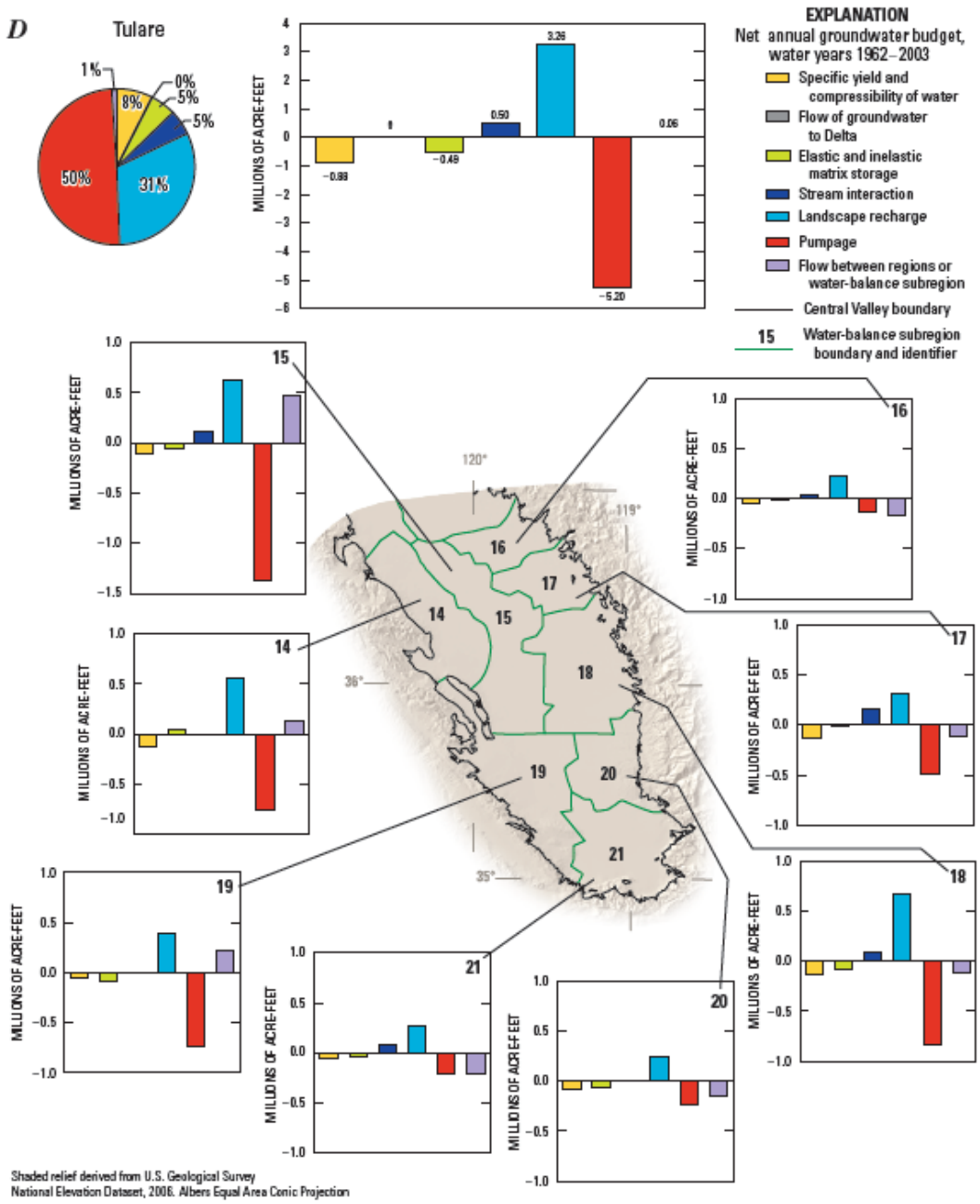

Figure 42: Water Budgets for Component Subareas within the Kern Sub-Basin.

The model subareas (virtual farms) of consequence are labeled 19, 20 and 21. The hypothetical CO_2 injection sites fall in the south of subarea 20 and in the north of subarea 21 (Faunt et al., 2009b).

5.2.5 Model Calibration against Monitoring Well Data

The CVHM-FMP3 model was calibrated using the optimization tool PEST, (Doherty, 2010) which performs error minimization analysis on the parameters shown to affect the model

simulation most. Hydrographs of shallow groundwater level and piezometric head data at selected monitoring wells is typically used by PEST to perform the calibration. Figure 43 shows the depth to water table in an area south of Bakersfield and another in an area northwest of Bakersfield. In both areas contours depict areas between 5 and 20 feet below land surface at 5-foot contour intervals. The occurrence of clay lenses above the Corcoran Clay can impede deep percolation of irrigation water and lead to localized shallow groundwater tables. These clay lenses coincide with the location of ancient lakes that acted as depositional areas for fine-grained sediments, leading to clay lenses of low permeability.

Groundwater quality declines as one moves east to west across the Basin, as shown in the contours of electrical conductivity in Figure 44. This is reasonable to expect, since shallow aquifer recharge from the east is from the snowmelt in the Sierra. Water infiltrating the granitic geologic parent material dissolves little in the way of soluble ions, resulting in high quality aquifer recharge. The western half of the basin is bounded by the Coast Range Mountains that are younger in geologic origin and were once an ancient seabed uplifted by tectonic forces. Water percolating through these marine layers is typically rich in dissolved ions as a result of solubilization of salts precipitated in various sedimentary formations. Groundwater pumping tends to be greatest in areas with low salinity and declines when salinity exceeds 2,000 ppm, as shown in the blue contoured areas.

Depth to groundwater in the unconfined (above-Corcoran) aquifer is shown in Figure 45. Except for the incidence of localized shallow groundwater table in old lakebeds (shown in Figure 43), the depth to groundwater over most of the Kern sub-Basin is between 100 and 250 ft below ground surface. The declining average water level over time for the Kern sub-Basin that was shown in Figure 40 suggests a long-term problem of aquifer overdraft, which could lead to continued inelastic subsidence.

The CVHM-FMP3 model simulations of the Kern sub-Basin suggest that more than 1/3 of the area of the sub-Basin will experience long-term land subsidence which can potentially impact the surface delivery canal network by slowing and possibly reversing flow along certain canal segments. The SFR module in CVHM-FMP3 has the ability to simulate canal and stream flow hydrodynamically – allowing rudimentary assessment of the potential long-term implications of land subsidence in the Kern sub-Basin.

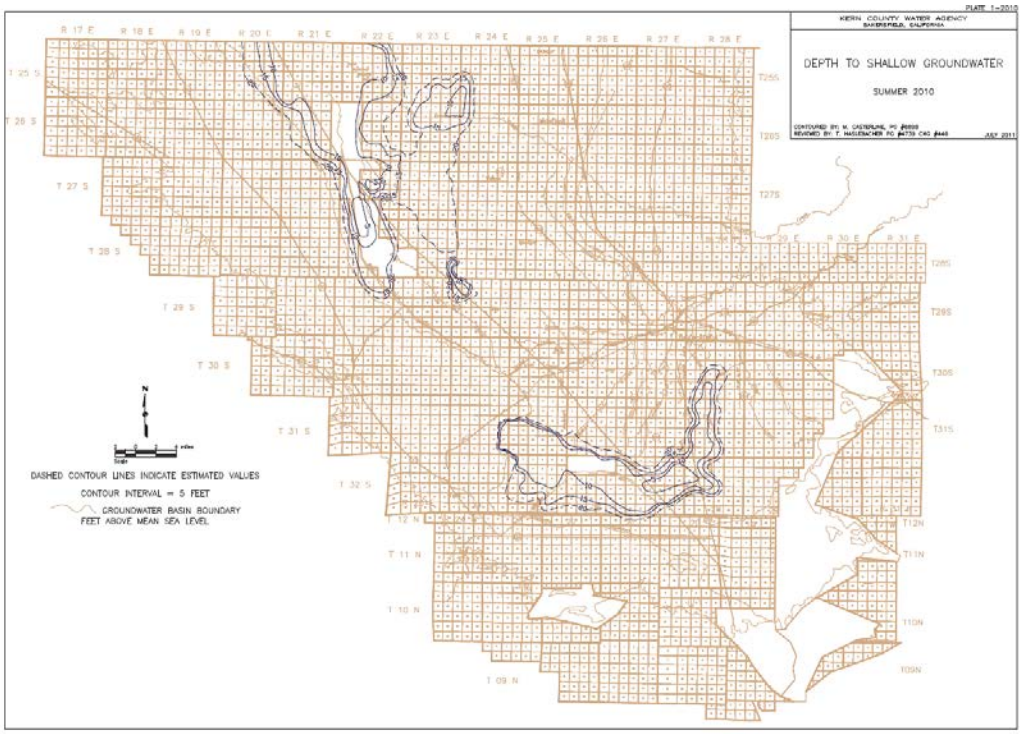

Figure 43: Depth to Shallow Groundwater in the Kern Sub-Basin (KCWA, 2013)

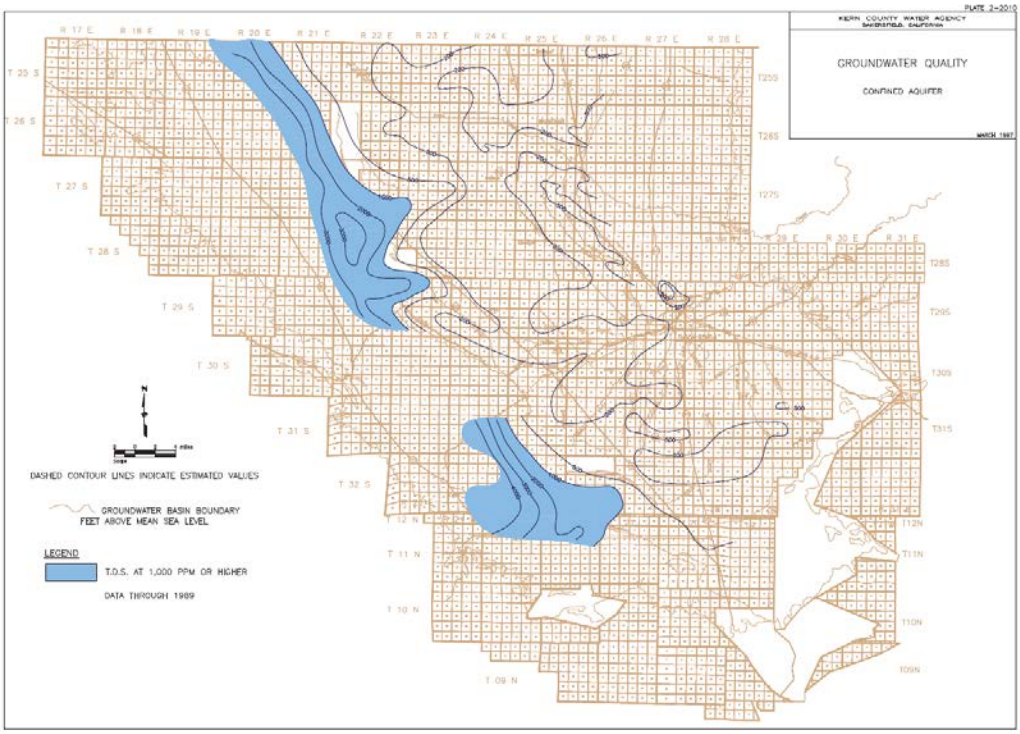

Figure 44: Groundwater Quality in the Confined Aquifer below the Corcoran Clay in the Model Kern Sub-Basin

Optimal areas for groundwater conjunctive use (KCWA, 2013).

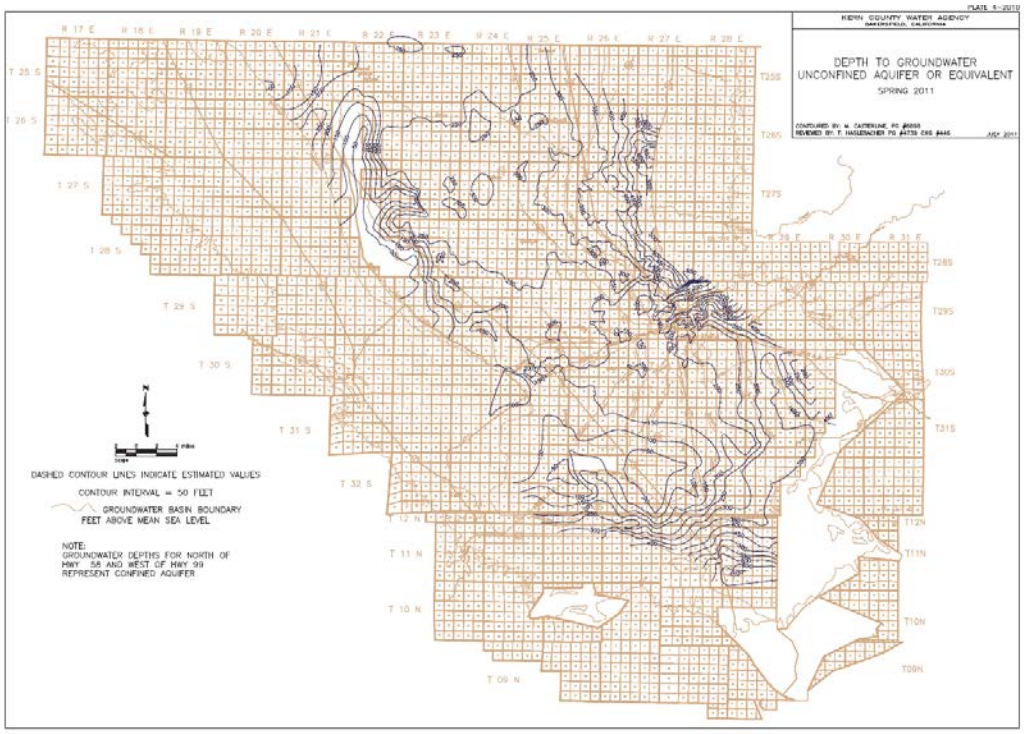

Figure 45: Depth to Groundwater in the Unconfined (above Corcoran) Aquifer (KCWA, 2013)

5.3 Modification of CVHM-FMP to Build Shallow Water Resources Impact Simulation Model

5.3.1 Development of Kern Sub-Basin Model

For the purpose of this project, we chose to extract the southern portion of the CVHM-FMP regional groundwater model to form the so-called Kern sub-basin model. This name is chosen because it covers the three southern subareas of the San Joaquin Basin, overlying a large portion of Kern County (namely subareas 19, 20 and 21 in Figure 42). The smaller model is close in spatial coverage to the TOUGH2 reservoir simulation model discussed in Section 4. As explained below, the Kern sub-basin model was then extended vertically, adding to the existing layers of the Central Valley groundwater simulation model CVHM-FMP(3) a suitable number of deeper model layers representing the geologic units down to the basement rocks. In other words, geologic formations were added to support a program of CO_2 sequestration at suitable injection well sites. The main objective of developing the model was to create a simulation tool that could be used to assess potential long-term impacts to the shallow aquifer, notably groundwater levels (which can affect crop growth and the cost of conjunctive groundwater pumping), and evaluate the potential for damage to the surface water distribution system that relies on gravity flow to provide water supply to Kern Basin agriculture. The economic importance of this agricultural resource to the state and nation has already been discussed.

Since creating a submodel from an existing regional finite element or finite difference model can be tedious, many modelers choose to recreate a model mesh from scratch rather than attempt to develop a “child” model from a “parent” model. Creating a submodel not only requires

developing a new set of boundary conditions along the external boundaries that the new model shares with its parent, but also involves considerable file manipulation, specifically to pare down the number of model cells to recognize only those in the new model. The most problematic issue with finite element models such as IWFM is that it requires the renumbering of the model nodes and sometimes also the model elements. This can create considerable opportunity for error, which can significantly delay the development of a new working model. With CVHM-FMP, the structure of MODFLOW somewhat facilitated the creation of the Kern sub-basin model. A new boundary was created that ran along the northern boundary of farms 19 and 20 (which correspond to the same subareas in C2VSIM). Using GIS, the Kern sub-basin model mesh was separated from CVHM-FMP, and a time-series head dependent boundary was established with heads from the parent model. Other changes were necessary in each of the MODFLOW packages where watershed features, such as steam and canal networks, are described by the row and column labels of the grid cell within which they fall. CVHM-FMP has been designed to allow the time-series boundary-condition file to be updated to easily recognize different parent-model scenarios and future assumptions.

5.3.2 Vertical Extension of Kern Sub-Basin Model

The existing ten-layer CVHM-FMP3 MODFLOW model, previously described in Section 5.2 and illustrated in Figure 39, was configured by the model developers to conform to both the topology of the land surface and the underlying Corcoran Clay layer. The Corcoran Clay (Layer 3 in CVHM-FMP3) is the most important geologic unit in the groundwater flow system which controls the rate of vertical groundwater flow. One of the challenges in developing an extended reservoir model with additional deep formations was reconciling the existing CVHM-FMP3 model with the topology of the geologic units below. A total number of 21 additional layers were inserted between the bottom of the existing CVHM-FMP3 model and the basement rock layer that defines to bottom boundary. In plan-view, the grid structure of the deeper geologic model layers was made identical to the existing 10-layer model. The lowest layers of the geologic model below the injection zones were sloped to conform to the basement geologic boundary. Model layering above the zone of pumping was represented by layers of uniform thickness. Refined layering was created in the vicinity of the CO_2 injection wells in the Vedder formation to improve simulation accuracy. Different views of the mesh and the layering of the vertically expanded model are given in Figures 46, 47 and 48.

The next task of the vertical extension of the CVHM-FMP3 model was the assignment of geologic layers to the added model layers. The 3-D geomodel described in Section 3 was used to intersect the top and bottom of each geological formation with the extended numerical grid below the original 10-layer model of CVHM-FMP3. Based on the geological model assignment, the model properties of the deeper layers were then taken from Table 4.1 to be consistent with the Deep Basin Reservoir Simulation Model. The model properties of the upper 10 layers were left unchanged from the original CVHM-FMP3 model, which had undergone significant calibration using many thousands of groundwater wells made available through a confidential interagency agreement between the USGS and the California Department of Water Resources. Aquifer hydraulic properties for the ten layer CVHM-FMP3 model (such as horizontal and

vertical hydraulic conductivity and storativity) were established using the texture model described earlier developed from well log data.

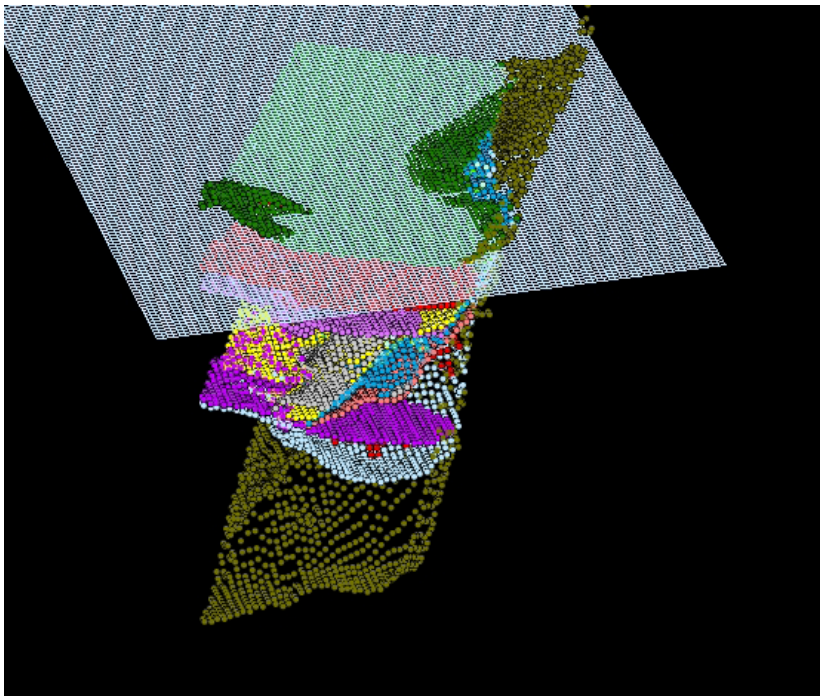

Figure 46: 3-D View Showing the 15 Vertical Formations of the Deep Geomodel Mapped to CVHM-FMP3

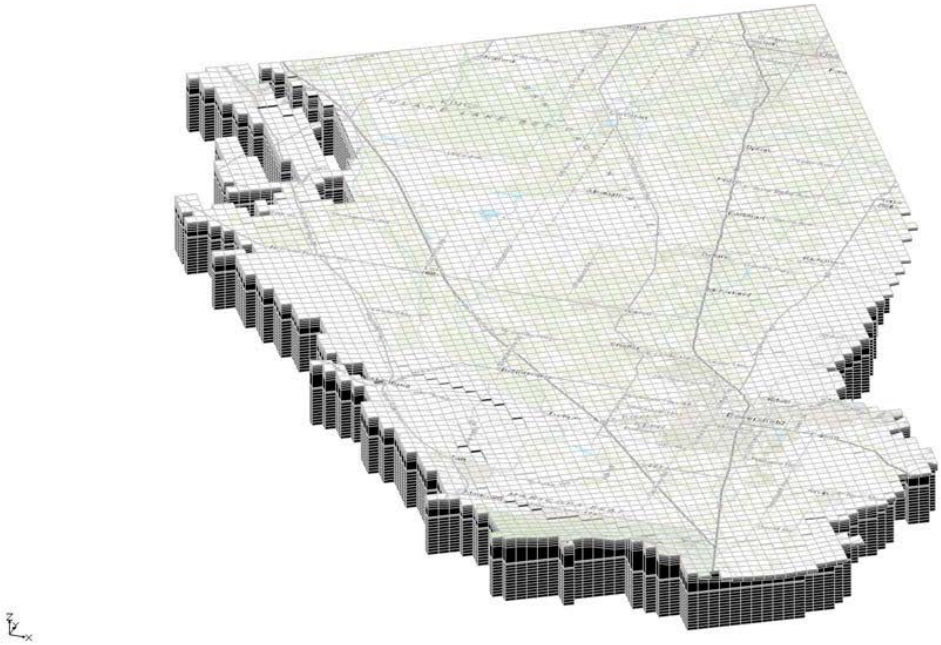

Figure 47: 3-D Rendering of the CVHM-FMP3 Model Showing Surface Features with an Overlay of the Model Rectangular 1 Mile by 1 Mile Mesh

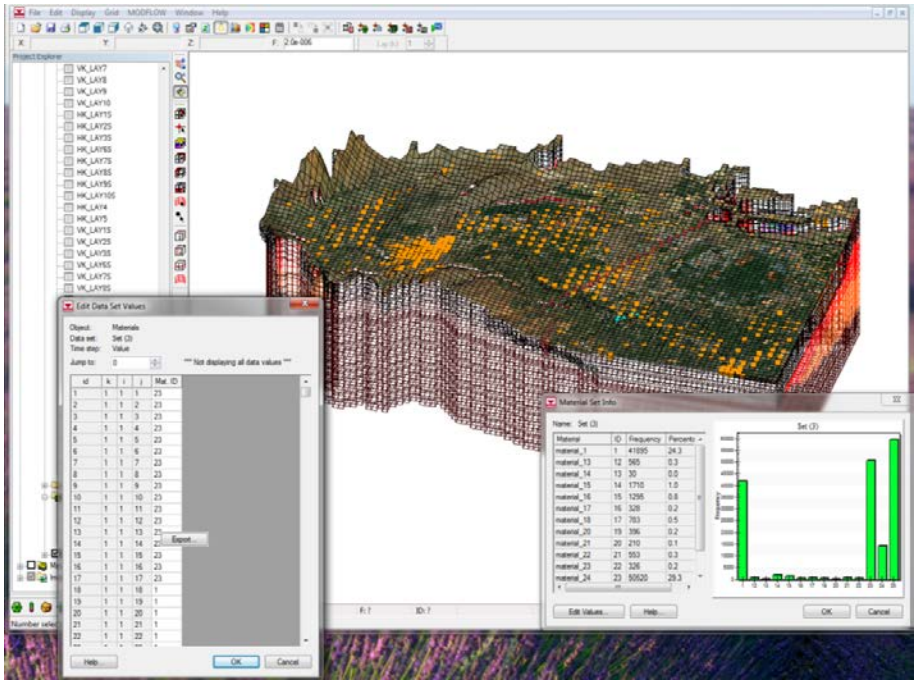

Figure 48: CVHM-FMP3 Model Imported into GMS

5.4 Model Results

5.4.1 CO_2 Injection Scenario

Two CO_2 injection scenarios were simulated by the model. The first scenario is the same as the one considered in the previous section, with injection into the Vedder formation. The second scenario has two injection projects: the Vedder injection and an injection into the Stevens formation. This second scenario is investigated (1) to evaluate the cumulative impact of multiple injections in the same region and (2) to analyze for possible project interference. Both of these scenarios were compared to a base simulation in which the same level of groundwater extraction continues in the upper formations (upper 10 layers simulated by the CVHM-FMP3 model), but there is no CO_2 injection. Injection rates were set equivalent to 5 million tons of CO_2 at the Vedder and Stevens formation locations (see Figure 49 for injection locations). This is roughly equivalent to half the CO_2 at a 90 percent capture rate from local CO_2 generating sources - sources that emitted more than 200,000 tons during the most recently available inventory year. Using the same injection rate for both injection simulations allows a direct comparison of effects, particularly any cumulative effects, from adding a second injection not far away in a different geologic unit. Volumetric CO_2 injection rates were set equivalent to 7,200,000 m^3/yr per injection project. The MODFLOW code does not simulate multi-phase flow (Harbaugh, 2005) (unlike TOUGH2) – hence we make the assumption in these simulations that the injected volume of supercritical or dense-phase CO_2 displaces an equivalent volume of fluid in the formation. The CO_2 equivalent is injected at a constant rate for the duration of the simulation. This typically results in near-field pressures that can increase significantly over time if the formation is confined. Pressure leakage from the formation can occur if the caprock is

discontinuous, or when internal pressure is sufficient for the injected CO_2 to find a flow path into a more permeable formation.

5.4.2 Observation Locations

When analyzing the output from a simulation model such as CVHM-FMP3 it is useful to examine not only the response at the injection site (i.e., in the grid cell where injection takes place), but also at strategically located observation points, to provide a window on how the fluid pressure is changing in different parts of the same geologic formation or in adjacent formations. Two observation locations were chosen for each CO_2 injection well (see Figures 50 and 51): (a) a hydrologic monitoring location "Vedder hydro," about 6 km updip of the Vedder formation injection location to the east; (b) a location "Vedder geo" updip of that point to the east, where the Vedder formation is in contact with the base of the shallow mesh (about 23 km east of the injection location); (c) a hydrologic monitoring location "Stevens hydro" about 5 km west of the Stevens formation injection location; and (d) a location "Stevens geo" about 6 km northeast of the Stevens formation injection well, where the Stevens formation overlies a portion of the Vedder formation. It is possible that the pressure response from both injection wells reaches this fourth location, in which case we would expect to observe a small additive effect on head change and uplift.

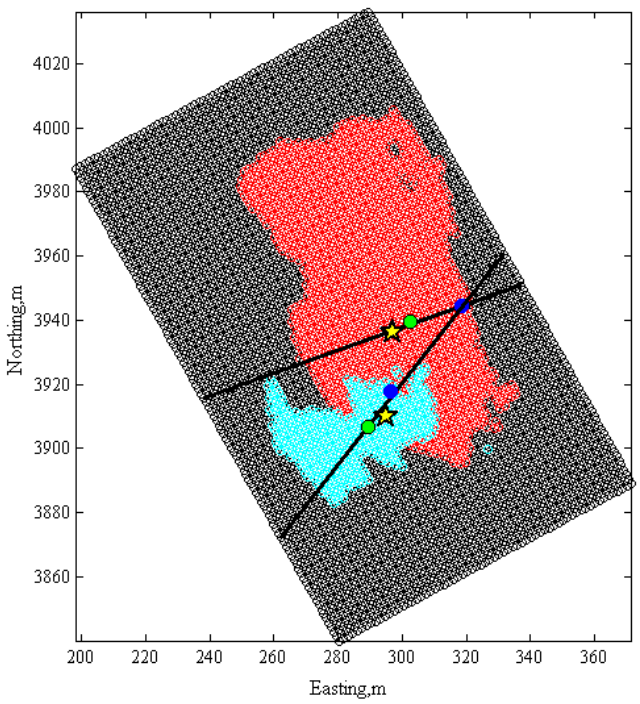

Figure 49: Plan View of Injection Locations and Observation Locations

Yellow stars indicate injection locations in the Vedder formation (red) and the Stevens formation (turquoise). Green circles are the "hydro" observation locations; blue circles show the "geo" observation locations. Black lines show location of cross sections in Figures 50 and 51. The northern cross section is shown in Figure 50; the diagonal one is shown in Figure 51.

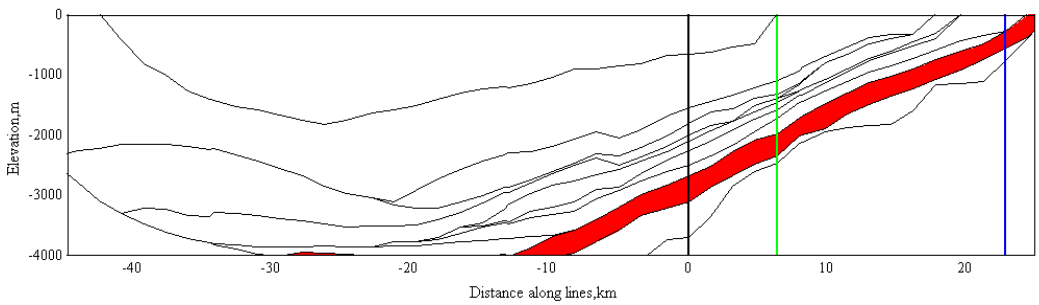

Figure 50: East-West Cross Section Showing Vedder Formation in Red, with Vedder Injection Well as Vertical Black Line.

The Vedder "hydro" location is indicated in green, the Vedder "geo" in blue.

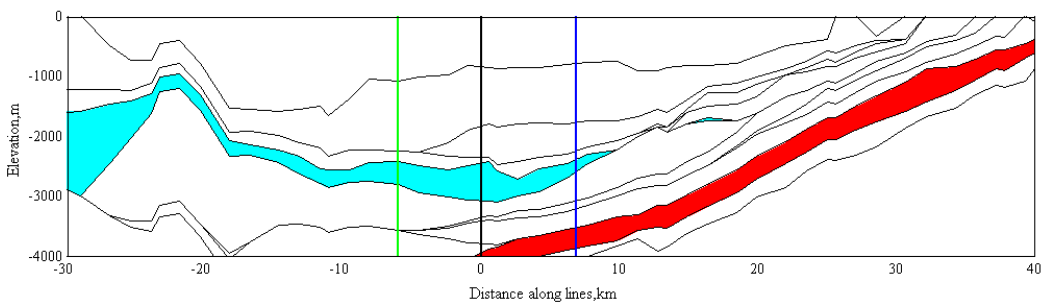

Figure 51: Diagonal Cross Section Showing Stevens Formation in Turquoise and Vedder Formation in Red, with Stevens Injection Well as Vertical Black Line

The Stevens "hydro" location is indicated in green, the Stevens "geo" in blue.

Note that like many groundwater flow models, MODFLOW solves for hydraulic head, not pressure. We therefore provide hydraulic head results in this section, which need to be compared with the pressure results in Section 4. A change in pressure of 1 MPa converts to a hydraulic head change of about 100 m.

5.4.3 Vertical Profiles of Head and Displacement Response at Vedder Injection Location

We start discussing model results with vertical profiles of head distribution at years 0.1, 10, 25, and 50 during CO_2 injection into the Vedder and Stevens formations (Figure 52). The profiles are shown at the injection location in the Vedder formation; injection occurs into Layers 26 and 27. The strong head-buildup response to the injection is clearly centered initially within the injection formation. With time, the head buildup increases in amplitude, dominated by injection into the Vedder layers. However, the profile appears to become bi-modal by year 10, suggesting perhaps some small influence from the injection at the shallower Stevens location. As expected, the profile reaches its maximum amplitude by year 50, the time when CO_2 injection stops.

Of equal interest is what appears to be happening in the shallow formations—notably the layers affected by groundwater pumping—most of which occurs in the shallow layers of the CVHM-FMP3 model. Dewatering of these zones at current rates of extraction appears to lead to a significant loss in groundwater head, which will lead to continued land subsidence as pressure heads are further reduced below the pre-consolidation heads associated with the onset of

inelastic deformation. This, of course, is a water-resources impact due to pumping mostly for agricultural purposes, and has nothing to do with deeper CO_2 injection.

In both injection and pumping instances, as the head response increases in amplitude it also migrates upward and downward into adjacent layers. This is a slow process, however, due to the low permeability of intervening shale formations, and the overall propagation distance is not very large. In the deeper layers, injection is felt in an upward direction up to about Layer 20 at the end of 50 years but only migrates downward to Layer 28 in the same time interval. In the shallow layers, the Corcoran Clay appears to prevent the pressure response to pumping from moving much higher than Layer 5 and much lower than Layer 12. The Corcoran Clay is a significant hydraulic barrier: the FMP3 code simulates drainage of this thick aquitard, which is more realistic than an algorithm that equalizes head in a single time step. It becomes clear that the impacts of deep injection and shallow pumping are largely independent of each other, each constrained to a smaller vertical distance without much interaction.

The vertical profiles from the CVHM-FMP3 model can be checked for consistency with the same injection scenario modeled with the Deep Basin Reservoir Simulation Model (Figure 24). The head increase in the injection layer seen in Figure 52 is approximately 100 m at the end of injection. In Figure 24, we see a head change of about 130 m (converted from pressure change in MPa) at the end of injection for the base case, and we obtain a range from about 60 m to about 300 m as the 90 percent confidence interval of the uncertainty simulations. That the head increase in Figure 52 is less than the TOUGH2 base case results from Section 4 is to be expected, since (a) the TOUGH2 numerical grid is much more refined near the injection wells, (b) the partially compartmentalized nature of the Vedder formation is better represented in the TOUGH2 numerical grid which explicitly accounts for major faults, and (c) the TOUGH2 simulations account for buoyancy pressure of free-phase CO_2. We also see consistency between the two models with regards to the strong effect of over- and underlying shale units on retarding the vertical pressure propagation is similar in both simulation results. Overall we can conclude that the simulation results from the Shallow Water Resources Simulation Model provide a sufficiently accurate representation of pressure perturbation in the deep formations. What is different between the two models is the simulated behavior in the shallow layers. We recall that the Deep Basin Reservoir Simulation Model does not consider any effects of shallow water management and thus shows no pressure changes except for those caused by the deep injection of CO_2.

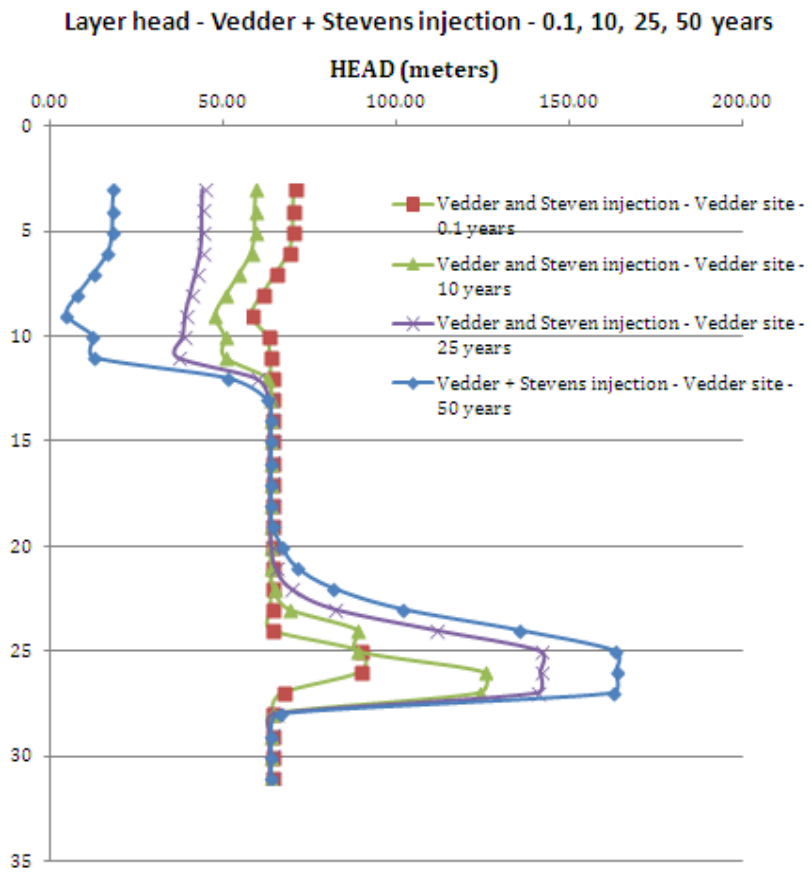

Figure 52: Head Profiles for the Vedder and Stevens Formation Injection Simulation Observed at the Vedder Site for 0.1, 10, 25 and 50 Year Simulations

Depth in the vertical axis is represented as "layer number."

Figure 53 shows vertical displacement in the different model layers at the Vedder injection locations. The output shown in these figures has been scaled so that the small upward displacement from CO_2 injection in deeper layers (shown as negative in the bottom graph, owing to the MODFLOW sign convention) can be discerned from the pumping-induced subsidence in shallow layers (shown as positive in the top graph). The injection effects are discerned in Layers 13 through 31, whereas the subsidence impacts are discerned in Layers 6 through 10. The injection into the Vedder and Stevens formations dilates the pores of the geological materials, creating a small upward displacement (up to 10 cm) that causes uplift in the model cells within and above the injection layers. The magnitude of uplift increases within the injection layers (Layers 26 and 27) and also in a few overlying layers (Layers 21 through 25), where head changes occur. No further changes in uplift are seen in Layers 20 through 13. In Layers 6 through 10, the effect of uplift is dwarfed by the much larger subsidence and thus is not obvious in the graph.

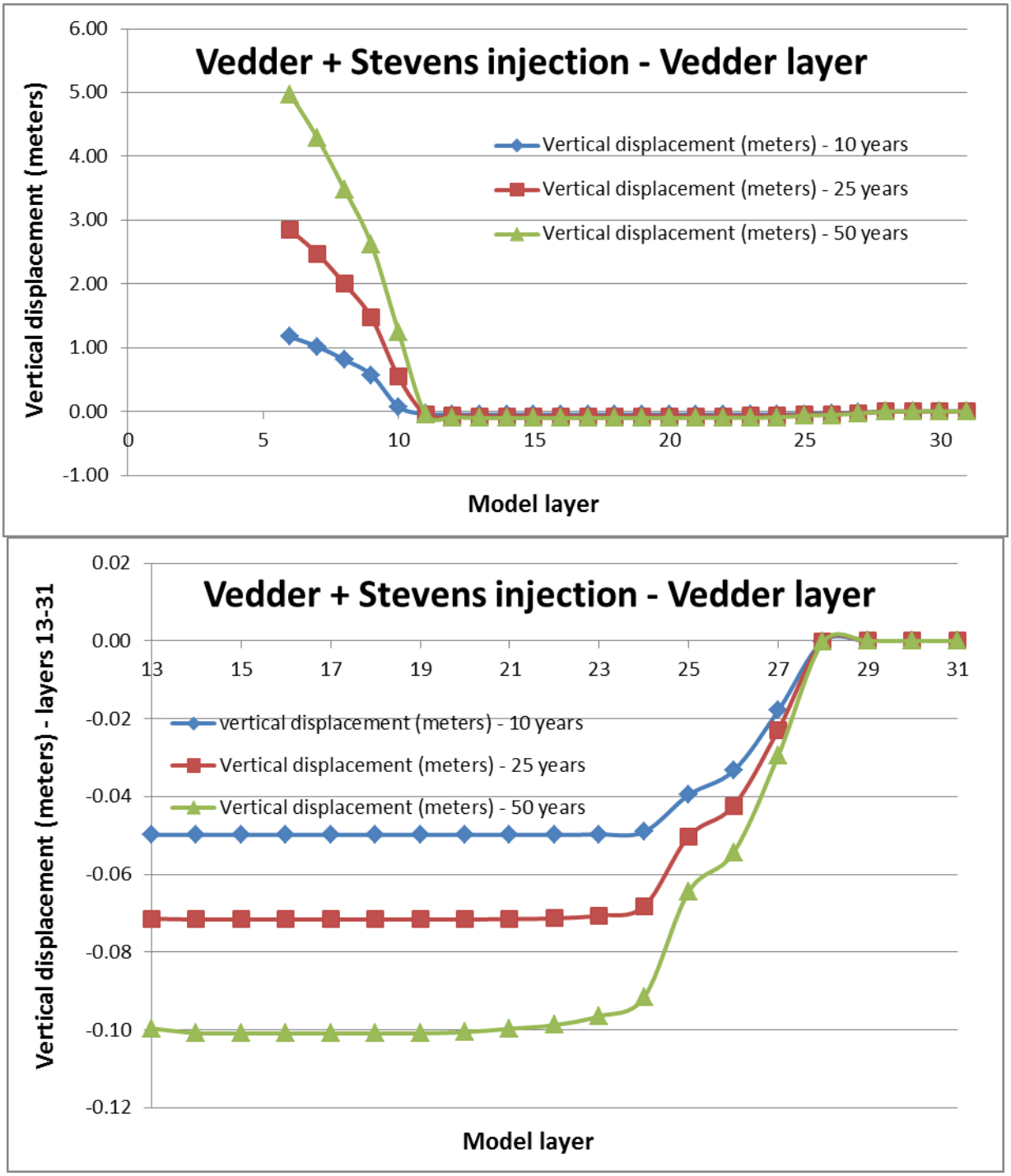

Figure 53: Displacement Profiles for the Vedder and Stevens Formation Injection Simulation Observed at the Vedder Site for 10, 25, and 50-Year Simulations

Positive values indicate subsidence, negative values indicate uplift. Depth in the vertical axis is represented as “layer number.”

5.4.4 Time Evolution of Head and Displacement Response at Vedder Injection Location

To better understand the vertical head and displacement profiles displayed in Figures 52 and 5.21, the same results are displayed as time-series plots. The head and displacement time-series graphs are also taken at the Vedder injection location, at different depth levels. In Figure 54, the head and vertical displacement in Layer 6 (first model layer containing the injection sites with active model cells) are compared across all three scenarios: (a) baseline (no injection); (b) injection in Vedder formation only; and (c) injection in both the Vedder and Stevens formations. Layer 6 is above the major aquifer stresses induced by deep agricultural pumping below the Corcoran Clay layer.

The heads in Layer 6 show the typical annual cycle of pumping-induced aquifer stress where pumping peaks in the period between April and August each year. The trajectory of the head profile is downward, indicating a loss of head in the sub-Corcoran aquifer layers. The vertical displacement of the model layer, which represents combined elastic and inelastic deformation, is shown below. Positive displacement represents subsidence; negative displacement represents uplift. What is immediately obvious is that pumping-induced subsidence is predicted to occur on the order of several meters over 50 years.

All three lines in Figure 54 have the same trajectory and almost fall on top of one another, meaning there appears to be little or no effect in the shallow Layer 6 due to injection at the Vedder formation injection site or the combined Vedder and Stevens formation injections. A very small deviation can be seen between the baseline displacement and those for the CO_2 injection scenarios, with the latter showing slightly less subsidence than the former. This results from the deep injection causing expansion in the Vedder and Stevens formations, which translates to a few centimeters of uplift at the surface, thus slightly reducing the trend of strong subsidence seen in the graphs.

Overall, the head and vertical displacements in shallow Layer 9 (Figure 55) are similar to those in Layer 6, for all three scenarios. However, the heads exhibit a larger amplitude of variation between summer and winter seasons. This is obviously the layer from which the greatest extraction of groundwater pumping occurs. Of interest in the vertical displacement graph below is again a small but distinct separation between the baseline and the two injection scenarios. This shows that by year 10, there is some positive impact of the deep CO_2 injection, although the impact is very slight—less than 10 centimeters by the end of the 50-year simulation. The response to fluid injection in the deep formations is able to offset some of the annual land subsidence induced by over-pumping of the sub-Corcoran aquifer.

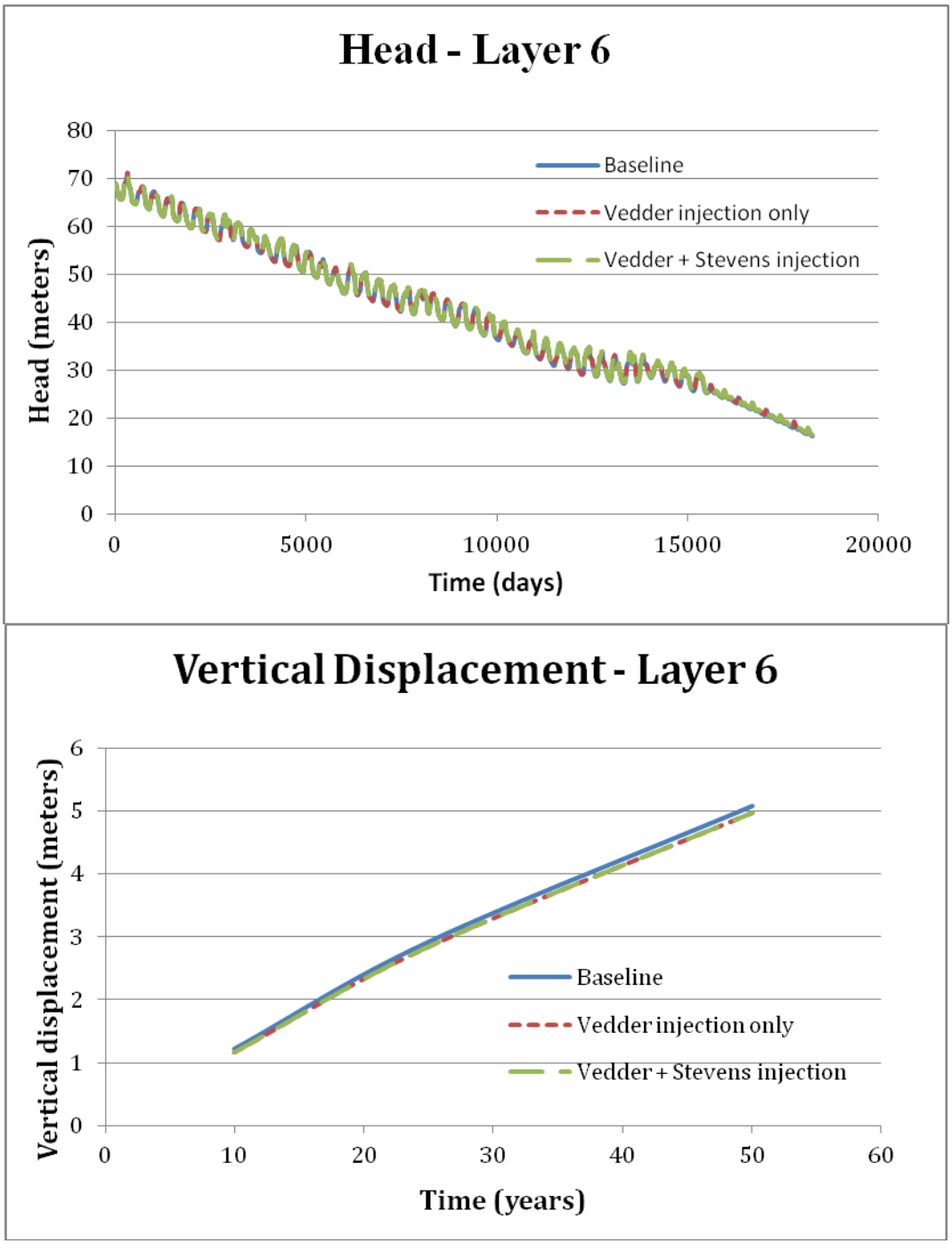

Figure 54: Head and Vertical Displacement in Layer 6 Comparing Vedder Formation and Combined Vedder and Stevens Formation Injection Scenarios with the Base (No Injection) Scenario

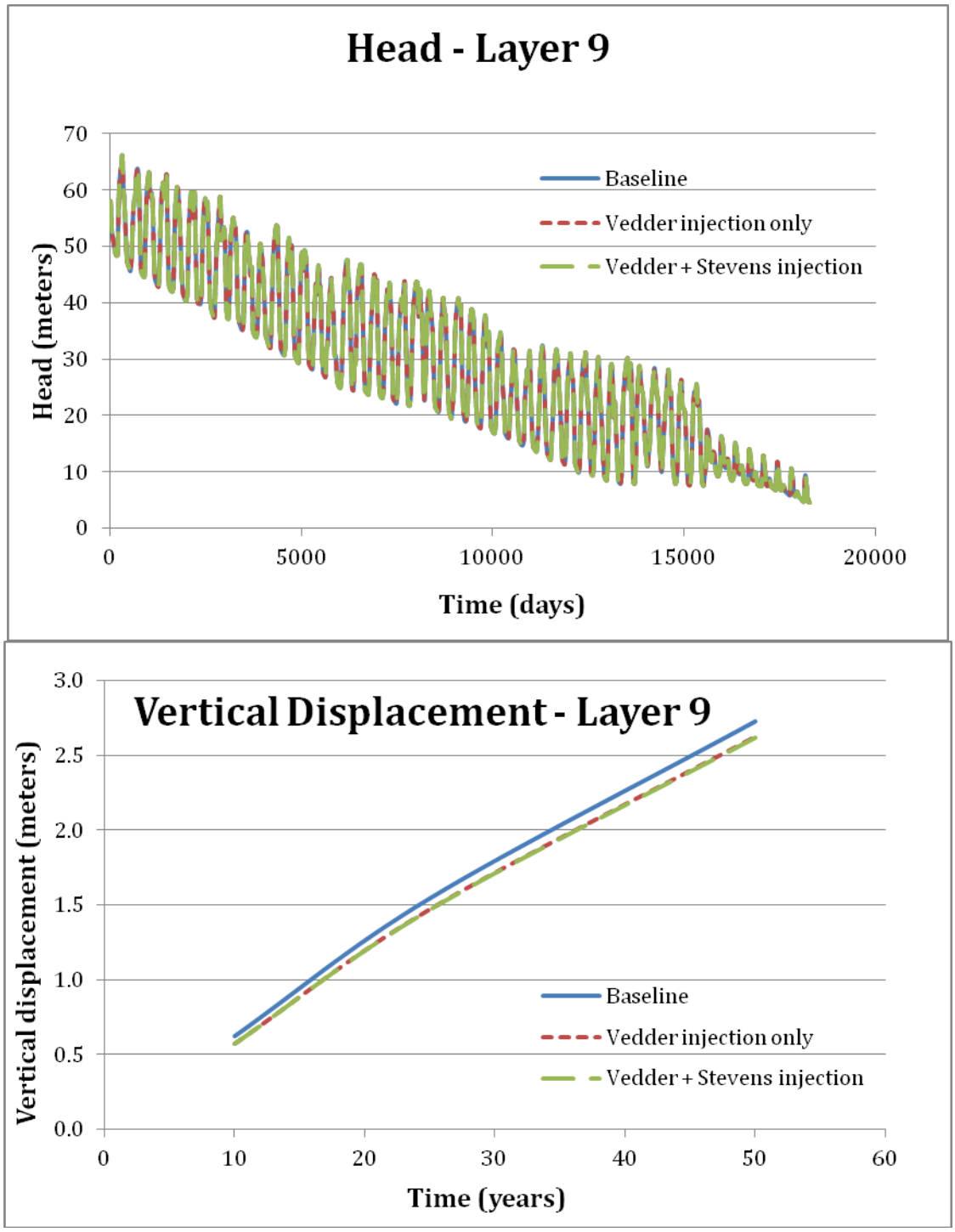

Figure 55: Head and Vertical Displacement in Layer 9 Comparing Vedder Formation and Combined Vedder and Stevens Formation Injection Scenarios with the Base (No Injection) Scenario.

Figures 56, 57 and 58 show the head and displacement evolution in the deeper geologic layers of the combined model. Layer 11 (Figure 56) is the first layer below the boundary between the two models (i.e., the original shallow CVHM-FMP3 model and the deep formation model extension), and it is still mostly influenced by the shallow groundwater system. In this layer, the amplitude of the groundwater extraction from the overlying aquifers diminishes, but we still observe the general downward trajectory of head, similar to the shallower formations. With regard to vertical displacement, the overall values are much smaller than those observed in Layers 6 and 9, on the order of centimeters rather than meters. We observe that the baseline scenario shows a small but still positive trend, suggesting that the pumping in the overlying groundwater aquifers causes minor subsidence. In contrast, the injection scenarios clearly diverge from the baseline scenario, showing initial uplift but later flattening of the signal. In this layer, the subsidence caused by pumping above is on the same order of magnitude as the uplift from CO_2 injection below, which leads to an overall cancelling out of the effect.

As we move vertically through the transition zone directly into the deeper layers near the injection into the Vedder formation (Layers 25, 26 and 27), the head and displacement responses completely change, from a system influenced by shallow pumping of groundwater to a system influenced by deep CO_2 injection. Layer 21 is above the injection horizon (Figure 57) and Layer 26 is one of the injection layers (Figure 58). For both injection scenarios, the head in Layer 26 rises strongly (as expected) to around 160 meters by the end of the 50-year injection period. The increase follows a roughly linear increasing trend after the reservoir volume is pressurized initially. Displacement in Layer 26 represents a modest uplift of about 5 to 6 cm at 50 years. In Layer 21, above the injection horizon, we observe a modest head increase, which represents the influence of deeper injection retarded by the low permeability of the intervening shale layers. The uplift in Layer 21 is larger, though, than in Layer 26. This reflects the fact that the uplift within a vertical column is roughly the cumulative effect of pore expansion in different model layers. The uplift in Layer 21 is roughly equal to the uplift within the injection layer (Layer 26), plus the vertical expansion caused by head increases in Layers 25, 24, 23, and 22.

We also note that the baseline results in both deep layers (Layers 21 and 26) show essentially zero changes over time. In other words, the shallow groundwater pumping causes no measurable response in the deeper layers, another sign that there is no hydraulic communication between them. We furthermore observe that the two injection scenarios show identical response at the Vedder injection location. In other words, the additional injection occurring in the Stevens formation, about 17 km away and separated stratigraphically, does not affect the head and displacement conditions at the Vedder injection location.

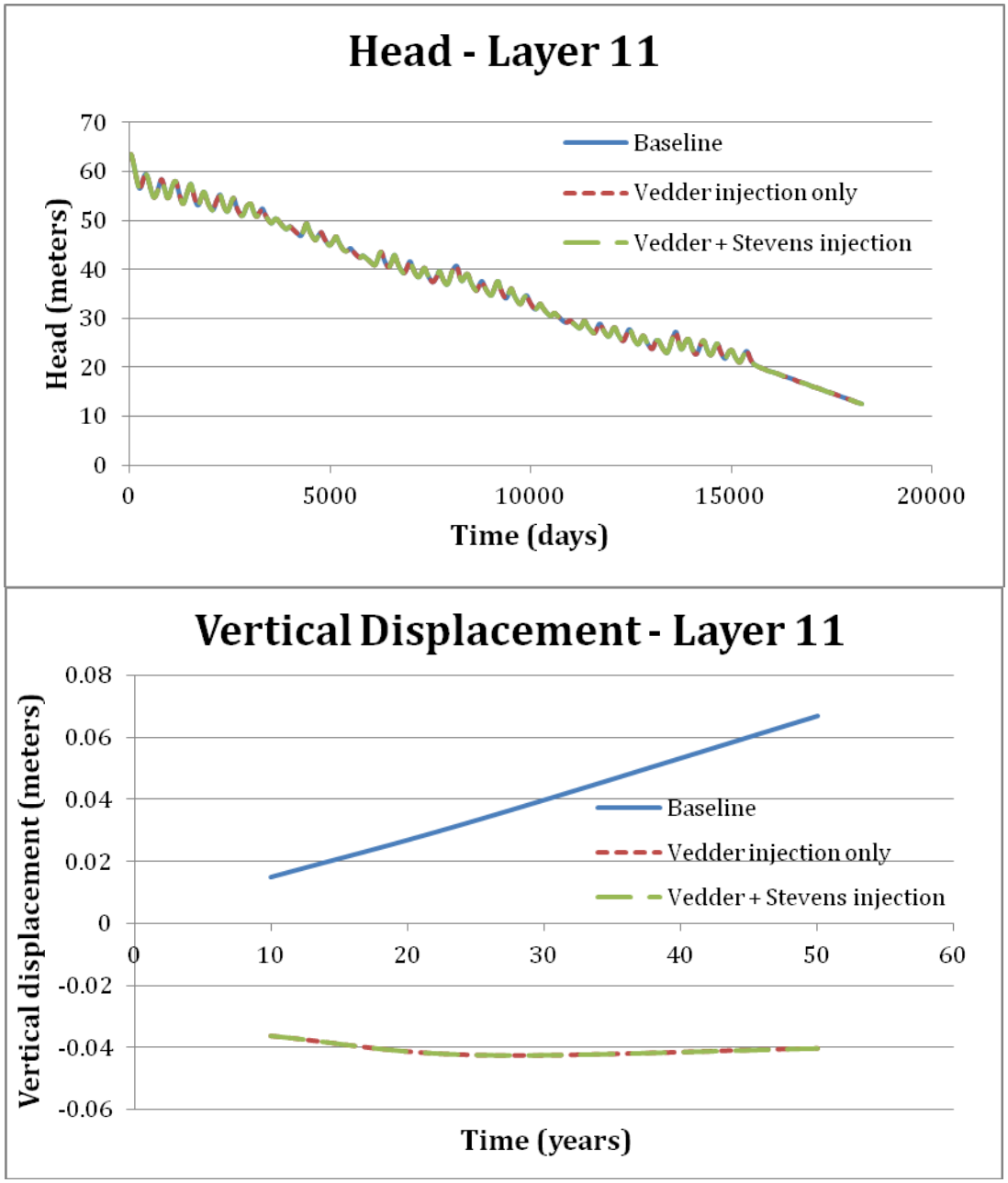

Figure 56: Head and Vertical Displacement in Layer 11 Comparing Vedder Formation and Combined Vedder and Stevens Formation Injection Scenarios with the Base (No Injection) Scenario

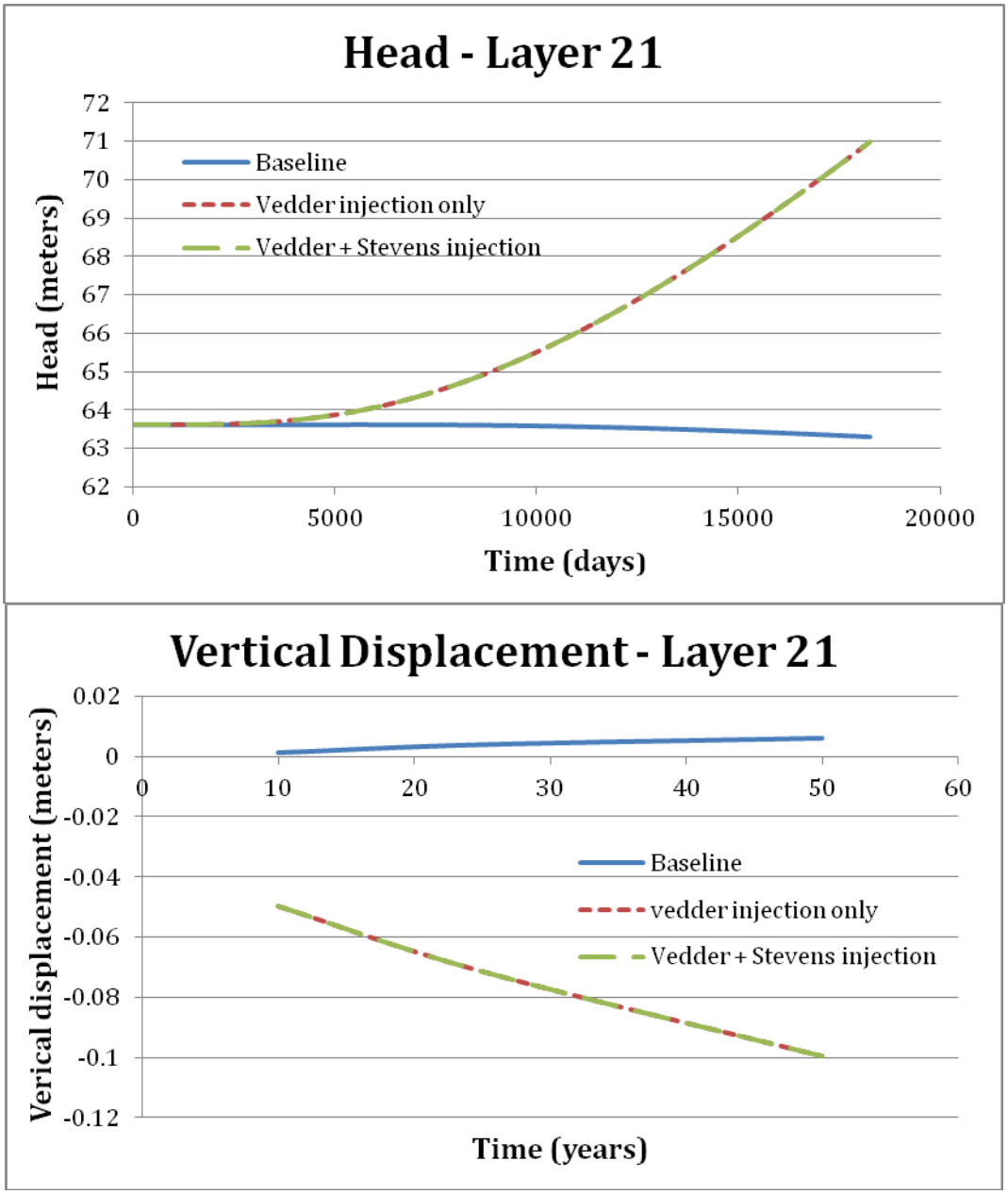

Figure 57: Head and Vertical Displacement in Layer 21 Comparing Vedder Formation and Combined Vedder and Stevens Formation Injection Scenarios with the Base (No Injection) Scenario

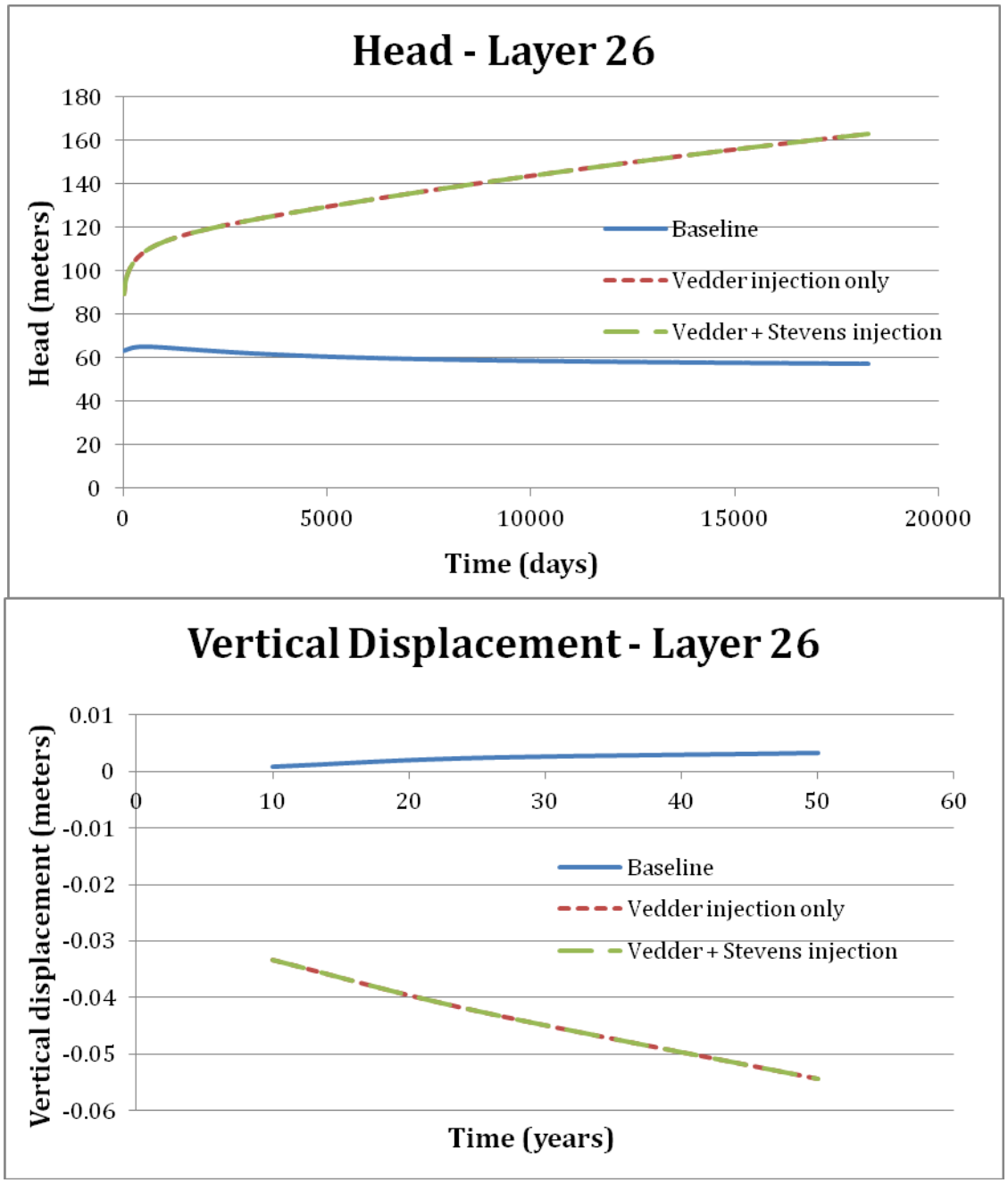

Figure 58: Head and Vertical Displacement in Layer 26 Comparing Vedder Formation and Combined Vedder and Stevens Formation Injection Scenarios with the Base (No Injection) Scenario

Pressure is highest in the injection layer, as expected.

5.4.5 Time Evolution of Head and Displacement Response at Other Locations

We report here on the time evolution of head and displacement at the four observation locations defined in Section 5.4.2. As a reminder, we have defined (1) a hydrologic monitoring location "Vedder hydro" as about 4 km updip of the Vedder formation injection location to the east; (2) a location "Vedder geo" as updip of that point to the east, where the Vedder formation is in contact with the base of the shallow mesh (about 14 km east of the injection location); (3) a hydrologic monitoring location "Stevens hydro" as about 4 km west of the Stevens formation injection location; and (4) a location "Stevens geo" as about 5 km northeast of the Stevens formation injection well, where the Stevens formation overlies a portion of the Vedder formation (Figure 49-10).

The pressure head and vertical displacement results for the observation wells are first provided for Layer 6 (the first active model layer that includes the injection wells) and the two Vedder observation locations (Figures 59 and 60). There is a difference in the amplitude of the response to groundwater pumping between these two observation wells, possibly due to the location of the Vedder "geo" in an area where the Corcoran Clay is less thick, allowing greater transmission of stresses across the aquitard. However, the vertical displacement profile shows almost linear land subsidence with time, and is similar for the "hydro" and "geo" observation wells. As seen earlier, in this layer, there is no clear difference between the baseline and the two injection scenarios. We can see a very small deviation in surface displacement in Figure 59, but essentially zero deviation in Figure 60. This is likely due to the Vedder "geo" location being farther away from the injection, meaning that the injection-induced head changes and uplift are less pronounced.

The observation results at the locations associated with the Stevens formation injection site are shown in Figure 61 and 62 for Layer 6. The results show the same general trends as the Vedder observation wells. Heads in the shallow formation model exhibit a general downward trend as the groundwater aquifer continues to be dewatered and the overlying agricultural land subsides in response. What is more pronounced than in the Vedder locations is the stronger uplift signal seen in the simulation case with CO_2 injection into both formations, with clear deviation of this case from the other simulation cases. This suggests that the injection into the Stevens generates a head and uplift response that is slightly larger than that in the Vedder, which is an expected result because of the smaller formation extent and the more pronounced compartmentalization.

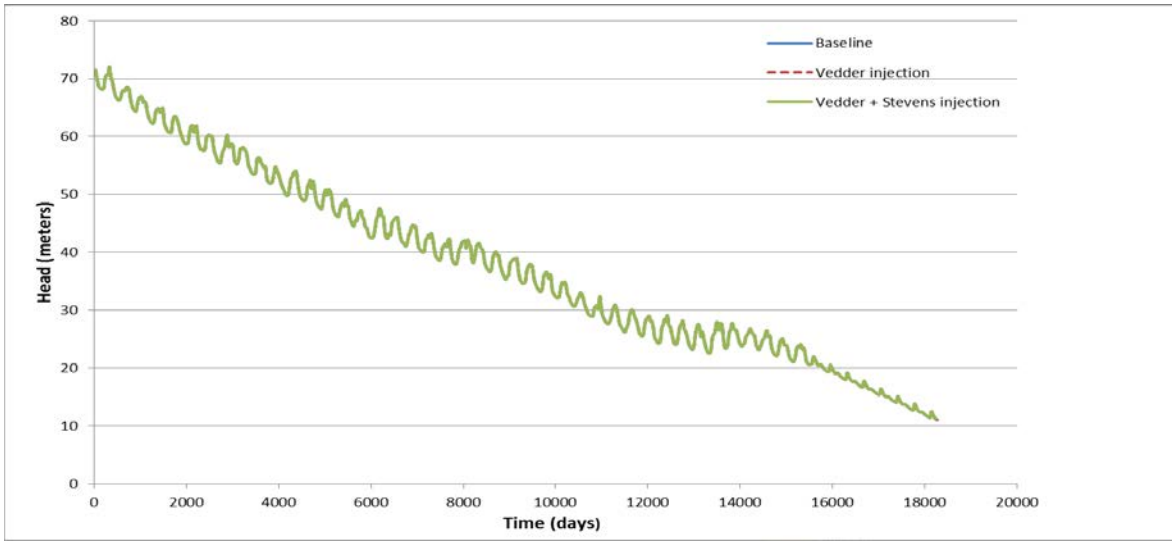

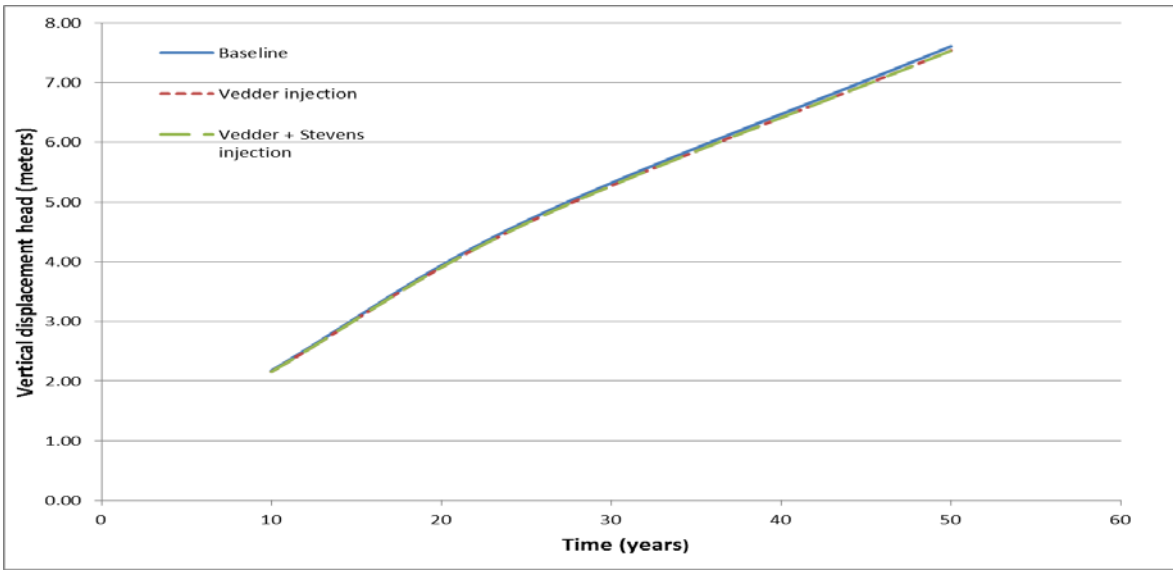

Figure 59: Pressure Head and Vertical Displacement in Layer 6 at the Vedder "Hydro" Observation Location. Vedder "Hydro" is about 4 km Updip of the Vedder Formation Injection to the East

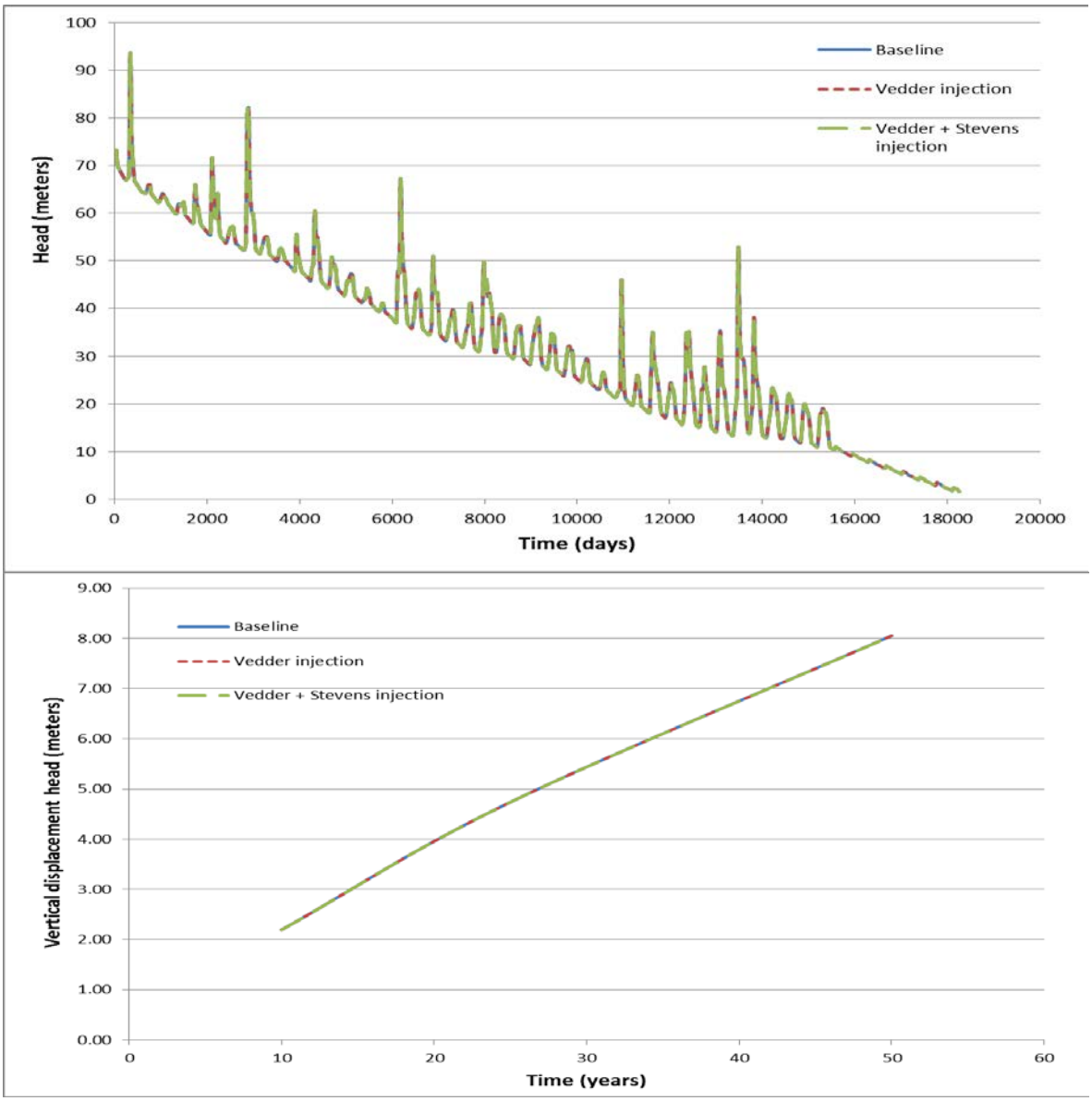

Figure 60: Pressure Head and Vertical Displacement in Layer 6 at the Vedder "Geo" Observation Location. Vedder "Geo" is about 14 km Updip of the Vedder Formation Injection to the East

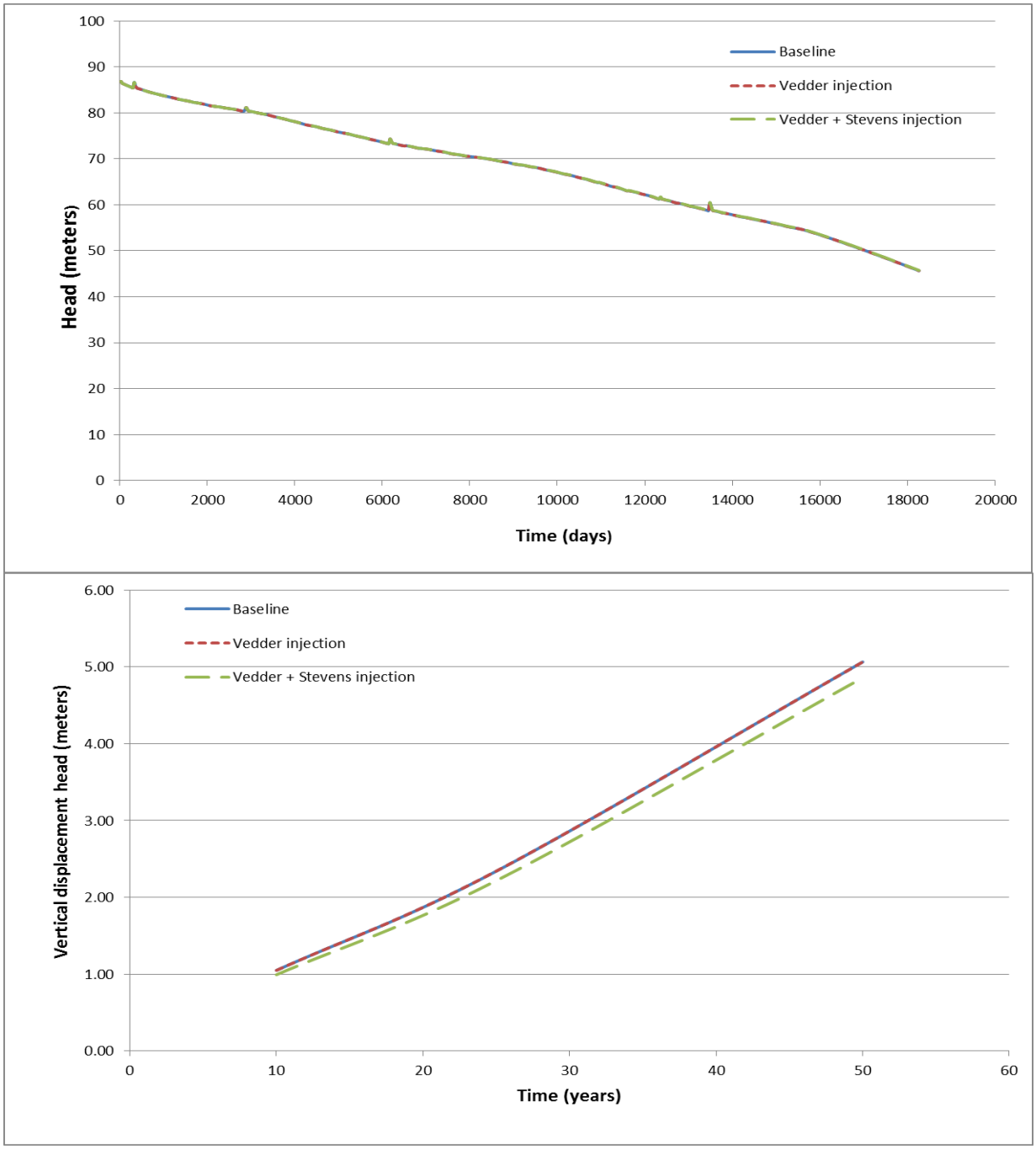

Figure 61: Pressure Head and Vertical Displacement in Layer 6 at the Stevens "Hydro" Observation Location. Stevens "Hydro" is about 4 km West of the Stevens Formation Injection

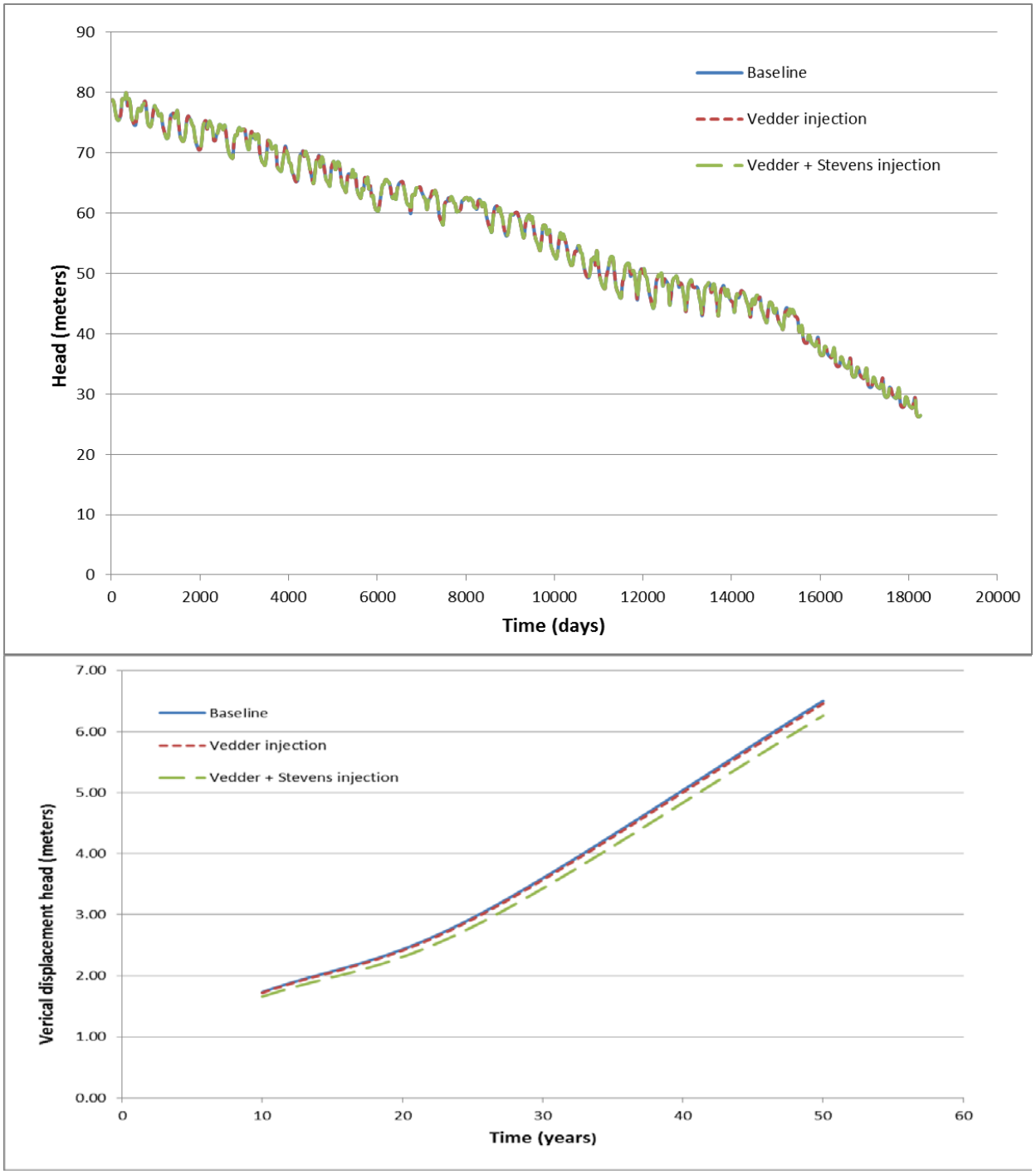

Figure 62: Pressure Head and Vertical Displacement in Layer 6 at the Stevens "Geo" Observation Location

Stevens "geo" is about 5 km northeast of the Stevens formation injection where the Stevens formation overlies a portion of the Vedder formation.

Figure 63 shows results from the Vedder "hydro" observation location. At 4 km distance from the injection well, the head changes from CO_2 injection propagating within the formation are not as strong as at the injection location (lower by about 60 meters from the maximum head), but still significant, with about a 50 m increase. This is to be expected, as the pressure typically decays nonlinearly with distance from the injection point. The uplift is also less than at the injection well, about 1 or 2 cm compared to the maximum value of about 10 cm near the injection. As seen before, there are no differences between the two CO_2 injection scenarios.

The Vedder "geo" location is about 14 km updip of the Vedder injection. At this location, the Vedder is much shallower, as represented by Layer 11 of the model grid, which is near the transition zone between shallow and deep formation models (Figure 64). Although there is a direct hydraulic connection between the deeper Vedder unit at the injection location and the shallower unit at the "geo" location, the effects of CO_2 injection are clearly overwhelmed by the effects of groundwater pumping, both in the head and the displacement trends. For all scenarios (baseline or CO_2 injection), the heads decline due to pumping, and the annual pumping variation between irrigation and nonirrigation seasons is clearly visible. There is a small separation in the vertical displacement of approximately 0.01 meter at 50 years, indicating a minor impact from CO_2 injection partially offsetting the vertical subsidence within this layer.

Figures 65 and 66 show head and vertical displacement at the Stevens "hydro" and the Stevens "geo" observation locations. Results are extracted from Layer 22 and 23, respectively, both within the Stevens formation. We now observe that Scenario 2, with CO_2 injection into the Stevens *and* the Vedder formations, results in a much stronger head and displacement response than in the other scenarios. At both locations, injection into the Stevens formation creates head changes of up to 150 m and displacement of up to16 cm. The smaller spatial extent of the Stevens formations causes the head and displacement perturbations to be stronger than in the Vedder, though the injection volumes are the same. We also note that the baseline results and those from Scenario 1, the Vedder-only injection, are identical for the Stevens "hydro" location, meaning that CO_2 injection into the Vedder has no effect there. This location is about 4 km west of the Stevens injection, away from the influence of the Vedder unit, which is farther east. In contrast, at the Stevens "geo" location, the Vedder-only injection causes uplift of about 4 cm in the Stevens, compared to zero uplift in the baseline simulations and about 16 cm uplift from the combined Vedder and Stevens injections. At this location, the Stevens formation overlies a portion of the Vedder formation and the observed uplift is the cumulative result from both injections.

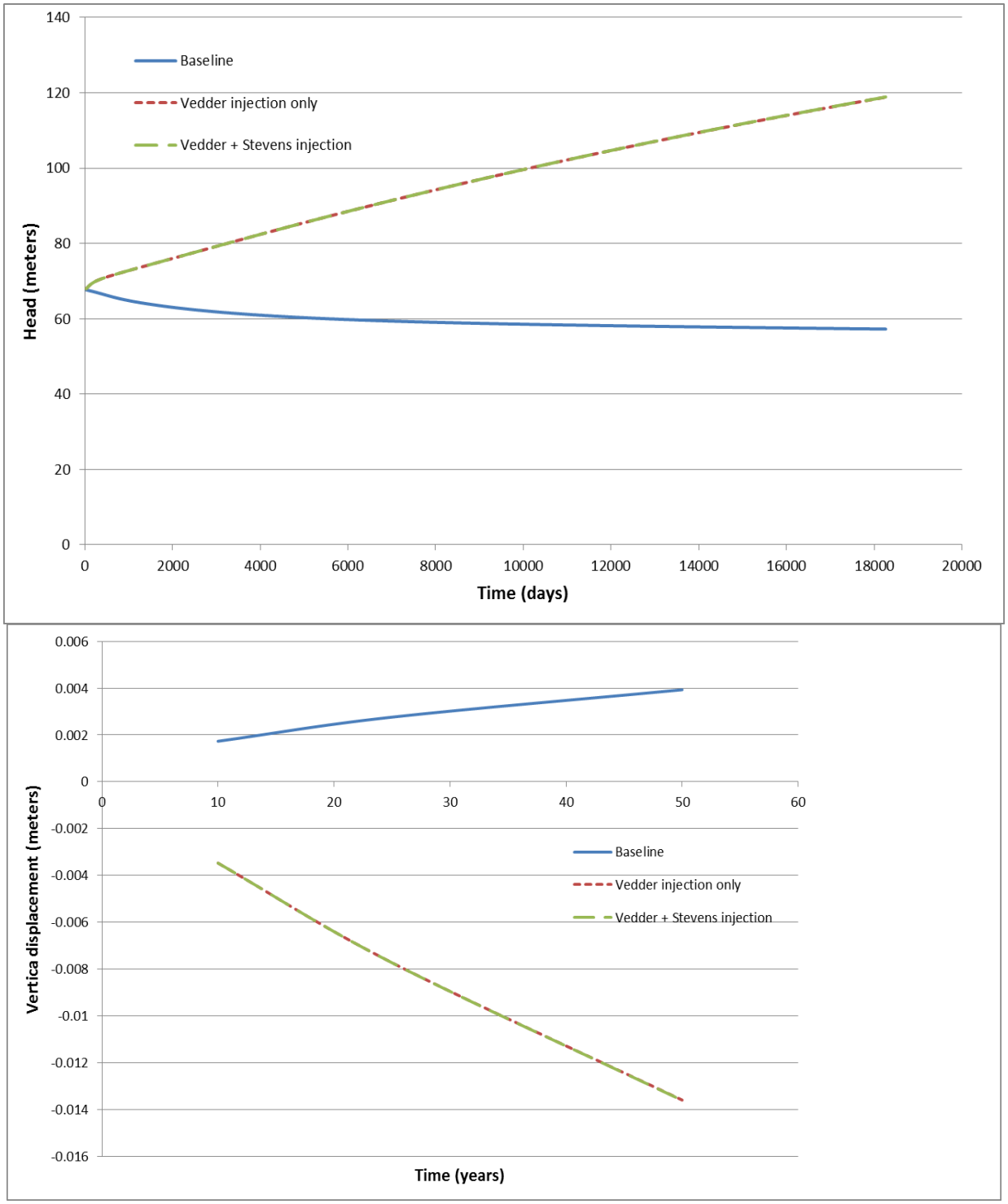

Figure 63: Pressure Head and Vertical Displacement in Layer 21 at the Vedder "Hydro" Observation Location

Vedder "hydro" is about 4 km updip of the Vedder formation injection to the east. At this location, Layer 21 is within the Vedder formation.

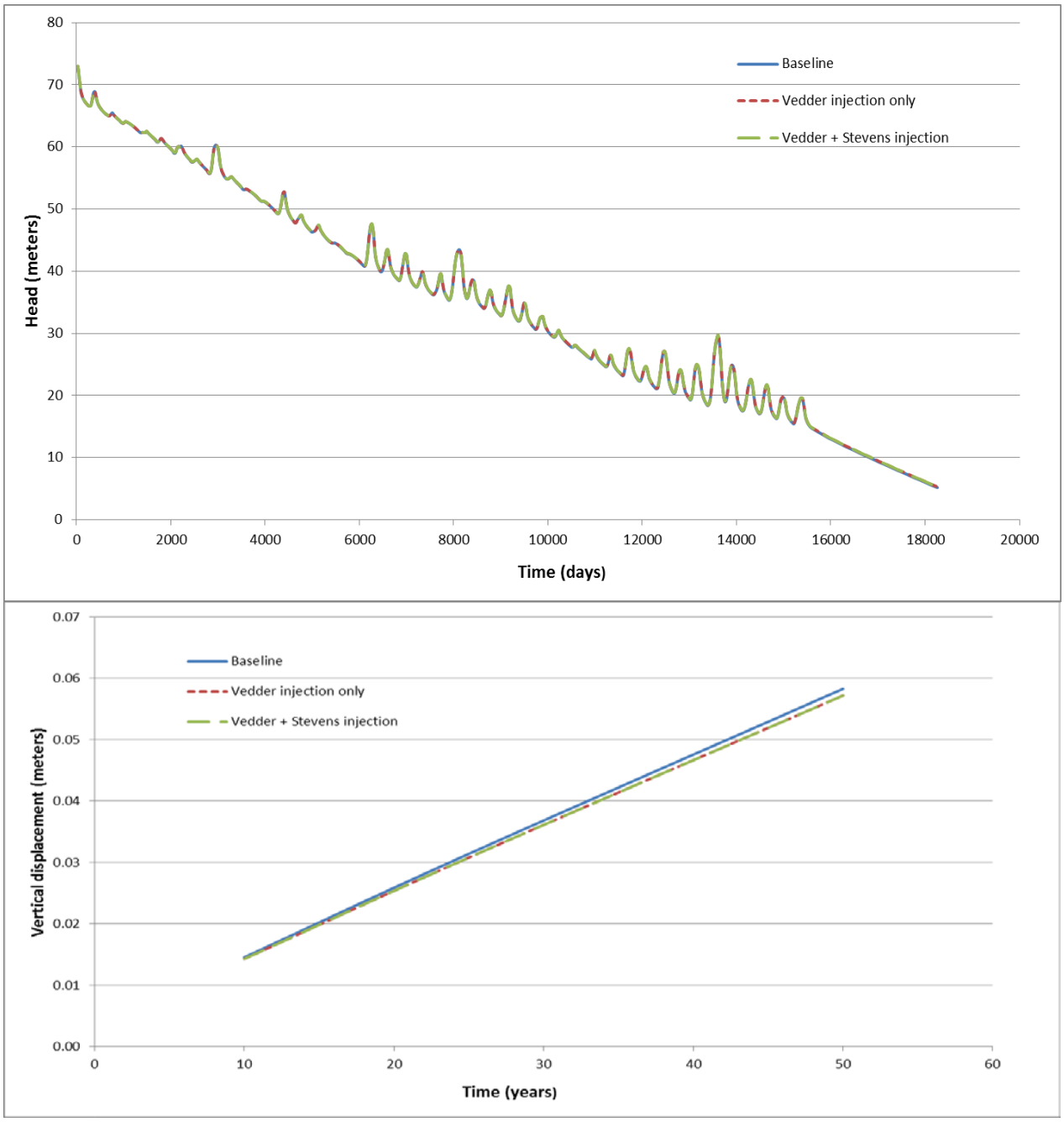

Figure 64: Pressure Head and Vertical Displacement in Layer 11 at the Vedder "Geo" Observation Location

Vedder "geo" is about 14 km updip of the Vedder formation injection to the east. At this location, Layer 11 is within the Vedder formation.

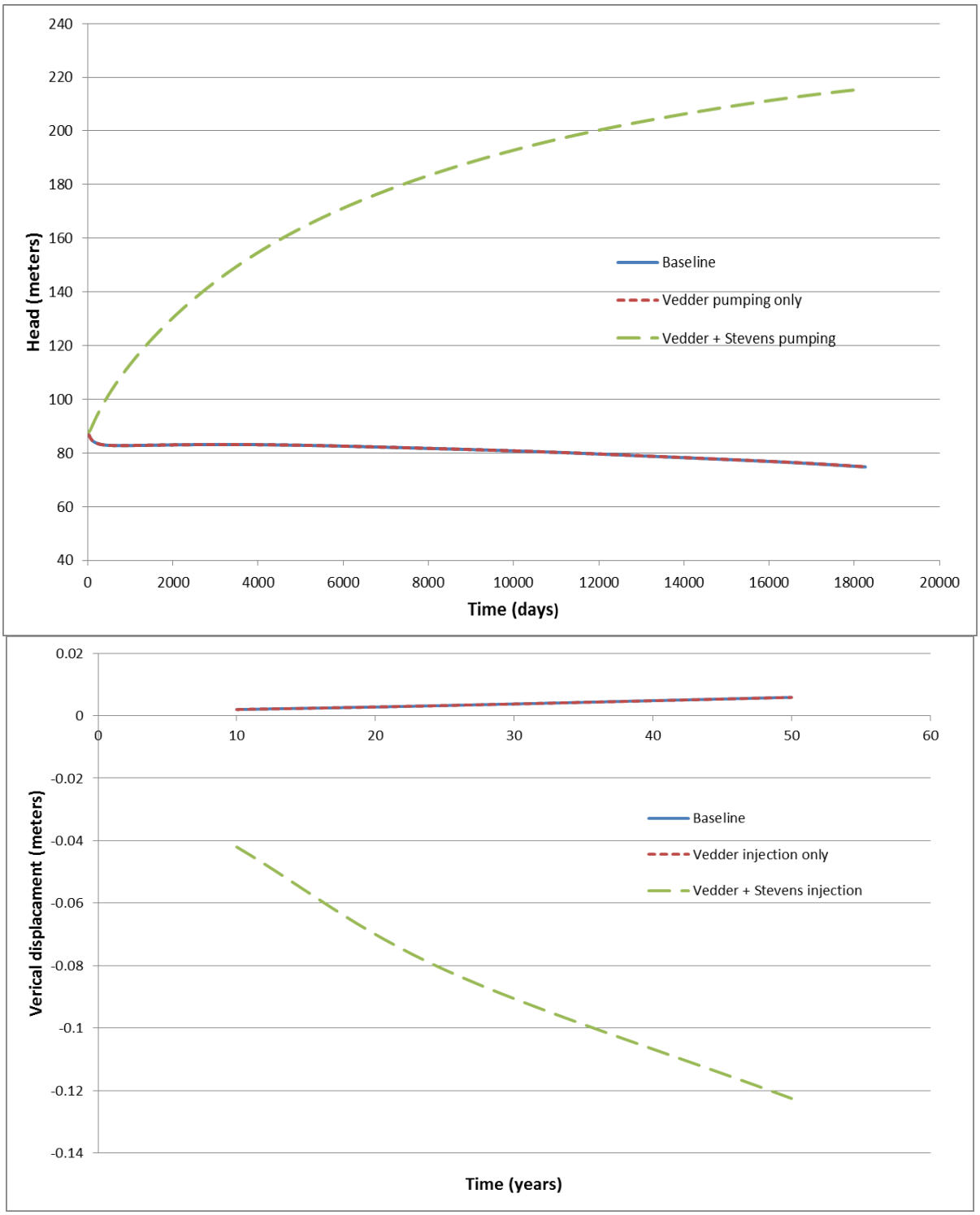

Figure 65: Pressure Head and Vertical Displacement in Layer 22 at the Stevens "Hydro" Observation Location.

Stevens "hydro" is about 4 km west of the Stevens formation injection. At this location, Layer 22 is within the Stevens formation.

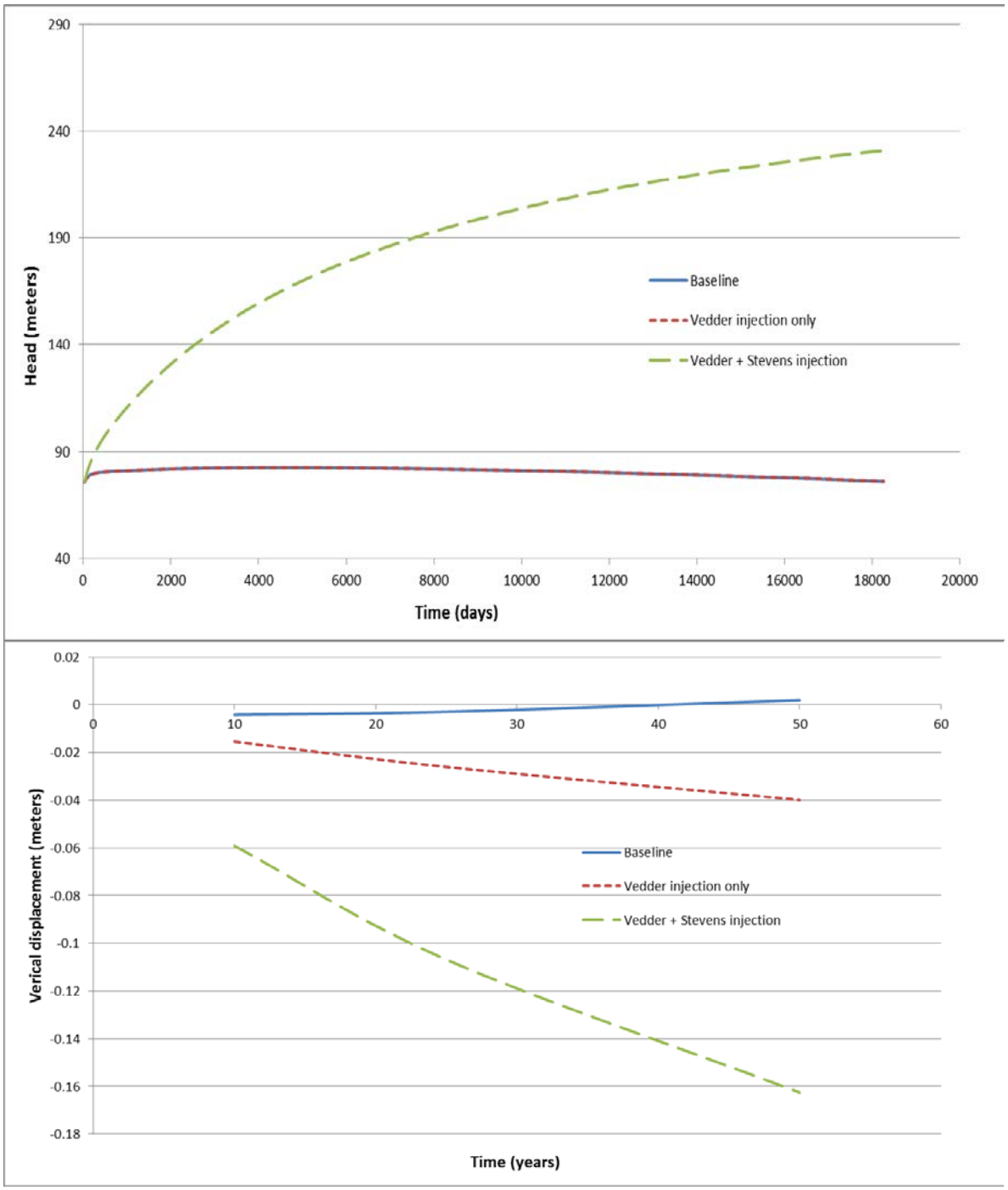

Figure 66: Pressure Head and Vertical Displacement in Layer 23 at the Stevens "Geo" Observation Location

Stevens "geo" is about 5 km northeast of the Stevens formation injection where the Stevens formation overlies a portion of the Vedder formation. At this location, Layer 23 is within the Stevens formation.

5.4.6 Contour Plots of Head at 0.1, 10, 25 and 50 Years

The spatial extent of head changes due to pumping in shallow units and CO_2 injection in deep reservoirs is shown below in contour plots for selected horizontal model layers. Figure 67 displays the head changes in Layer 6 for the baseline scenario at 0.1, 10, 25, and 50 years. In this layer, the head results for the baseline scenario are virtually identical with those for two CO_2 injection scenarios, which are therefore not included in this report. Shallow-formation aquifer dewatering from continued groundwater pumping shows up in mostly the center of the model as a reduction in hydraulic head, becoming very pronounced by 50 years. This same trend has been shown in the line graphs, as previously described. Layer 10, near the interface between the shallow model and the deeper vertical extension, shows a similar but slightly less pronounced behavior in terms of significant decline in hydraulic head due to groundwater pumping (Figure 68).

A very different picture of head changes can be observed in the deeper formations (Figures 69 through 71 for head changes in the baseline scenario, the Vedder-formation-only injection, and the combined Vedder and Stevens formation injection, respectively). Results are shown for Layer 21 of the model grid, which comprises a substantial fraction of the Stevens formation in the west and intersects the updipping Vedder formation further east. The baseline scenario in Figure 69 shows no considerable changes in hydraulic heads in this layer during the 50-year simulation period. This confirms again that shallow groundwater pumping has no effect on the deep hydrologic systems. In contrast, we observe in Figure 70 that CO_2 storage in the Vedder formation causes considerable and extensive head increases. As indicated by the elongated north-south trending zone where Layer 21 intersects the Vedder formation, the hydraulic head perturbation in the Vedder extends several tens of kilometers away from the injection location (see similar behavior in Figure 21). Figure 71 illustrates the added effect of injecting into both the Vedder and Stevens formations. A distinct area of head increase shows in the southwest portion of the model domain, where Layer 21 coincides with the Stevens formation. As observed before, the head changes in the Stevens are stronger than in the Vedder, because the same volume of CO_2 is injected into a smaller, more compartmentalized geologic unit.

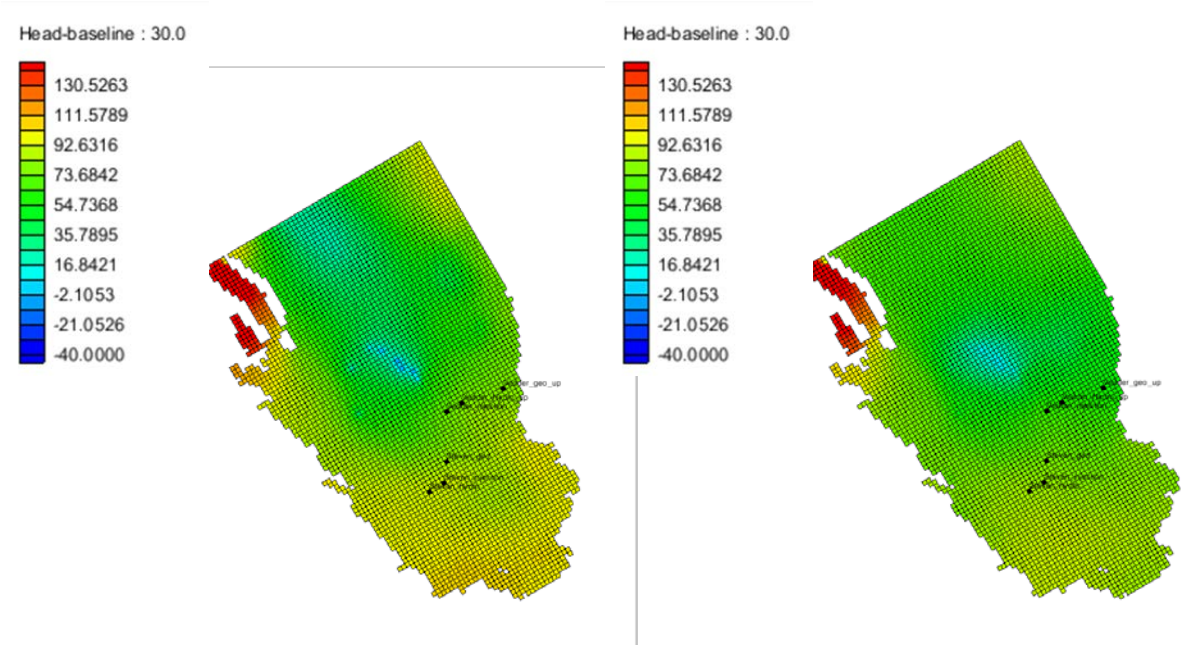

Baseline heads 0.1 years – Layer 6

Baseline heads – 10 years- Layer 6

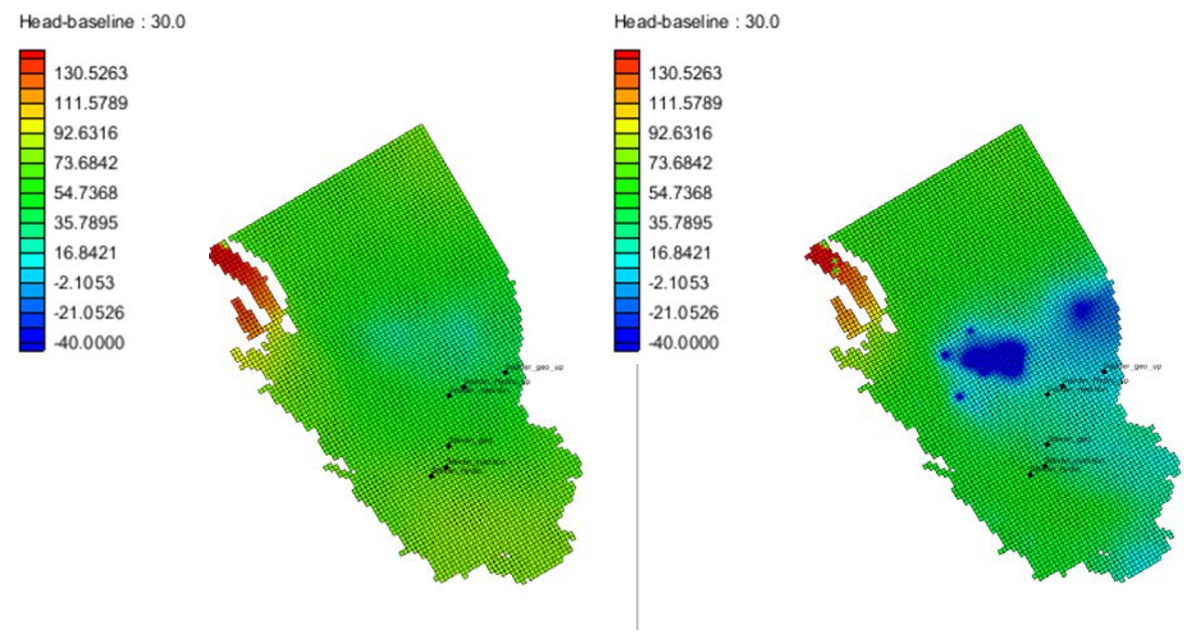

Baseline heads 25 years – Layer 6

Baseline heads – 50 years- Layer 6

Figure 67: Baseline Head Contours (Meters) for Layer 6 at 0.1 Years, 10 Years, 25 years, and 50 Years

Results are identical to the CO_2 injection scenarios (not shown in this report).

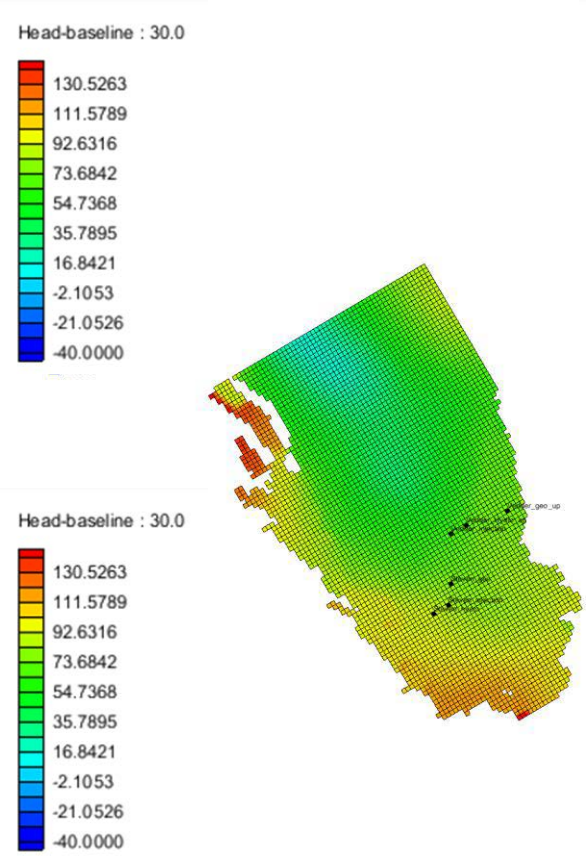

Baseline heads - 0.1 year – Layer 10

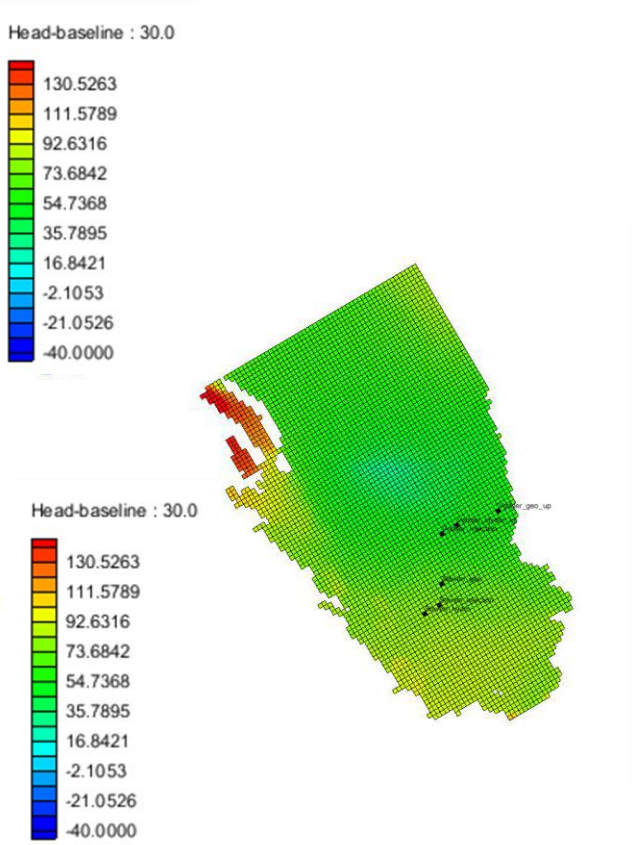

Baseline heads – 10 years - Layer 10

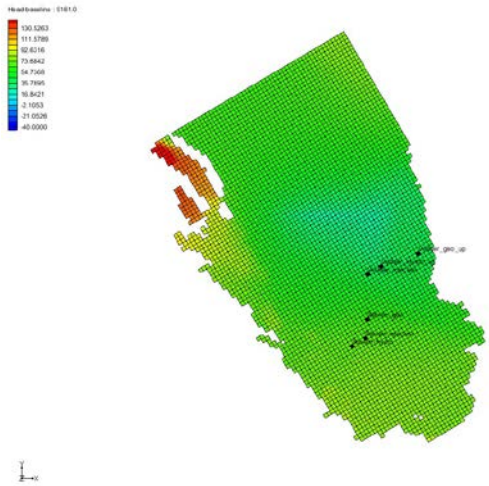

Baseline heads 25 years – Layer 10

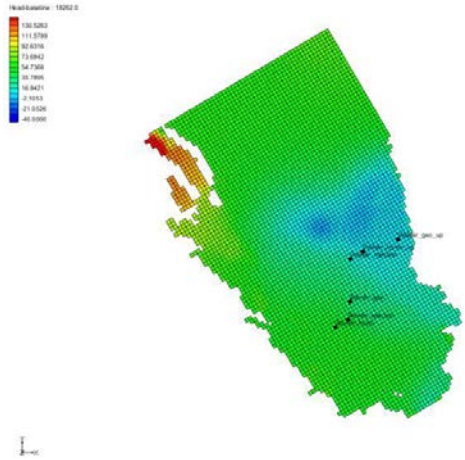

Baseline heads 50 years – Layer 10

Figure 68: Baseline Head Contours (Meters) for Layer 10 at 0.1 Years, 10 Years, 25 years, and 50 Years

Results are identical to the CO_2 injection scenarios (not shown in this report).

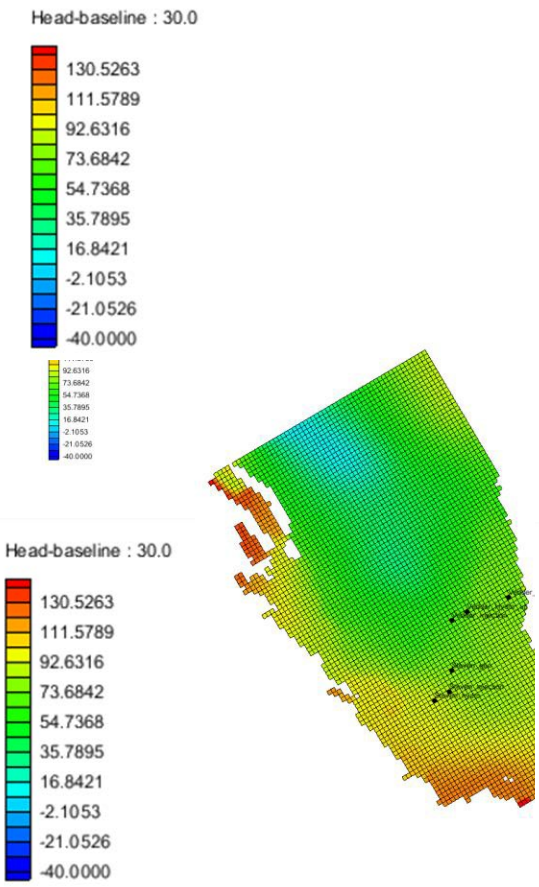

Baseline heads - 0.1 year – Layer 21

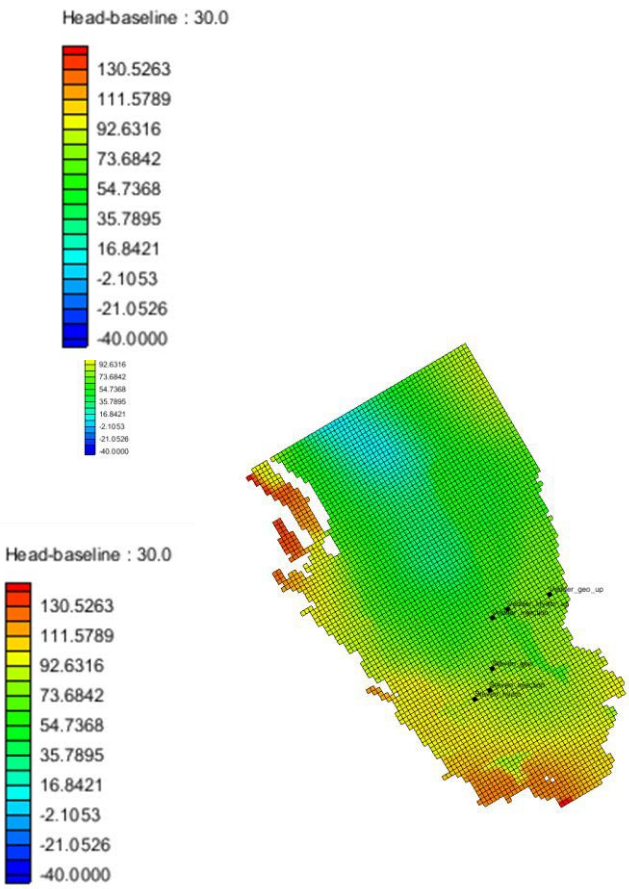

Baseline heads – 10 years - Layer 21

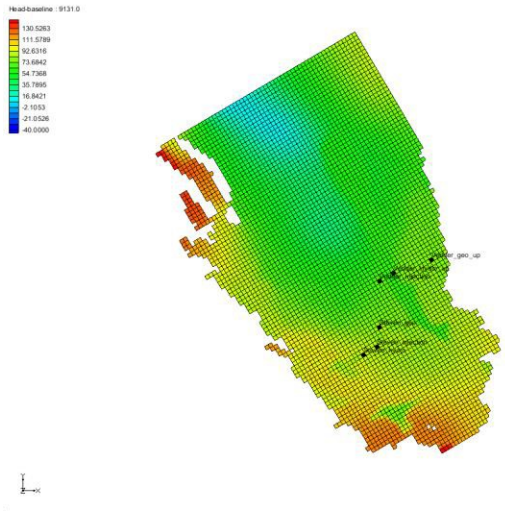

Baseline heads 25 years – Layer 21

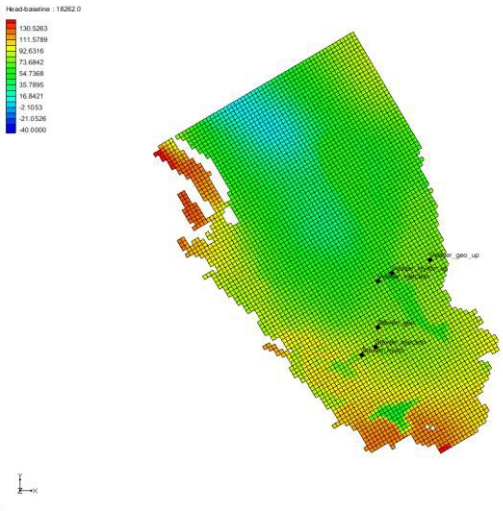

Baseline heads 50 years – Layer 21

Figure 69: Baseline Head Contours (Meters) for Layer 21 at 0.1 Years, 10 Years, 25 Years, and 50 Years

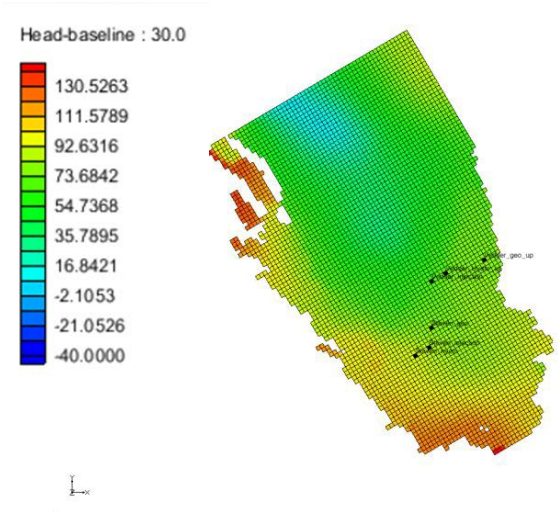

Vedder injection heads- 0.1 years – Layer 21

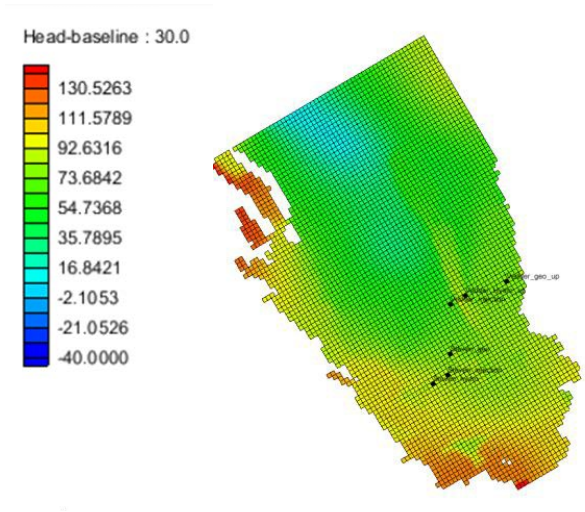

Vedder injection heads – 10 years- Layer 21

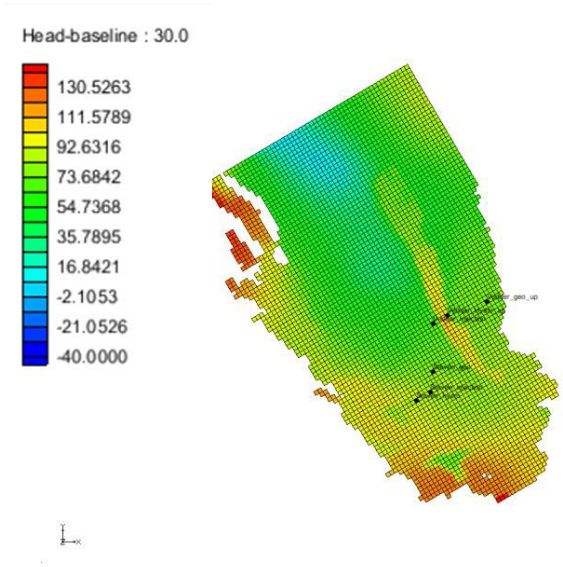

Vedder injection heads – 25 years- Layer 21

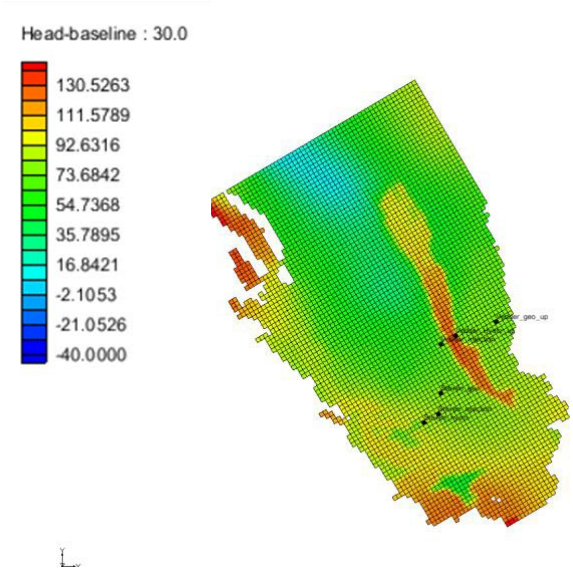

Vedder injection heads – 50 years - Layer 21

Figure 70: Vedder Injection Head Contours (Meters) for Layer 21 at 0.1 Years, 10 Years, 25 Years, and 50 Years

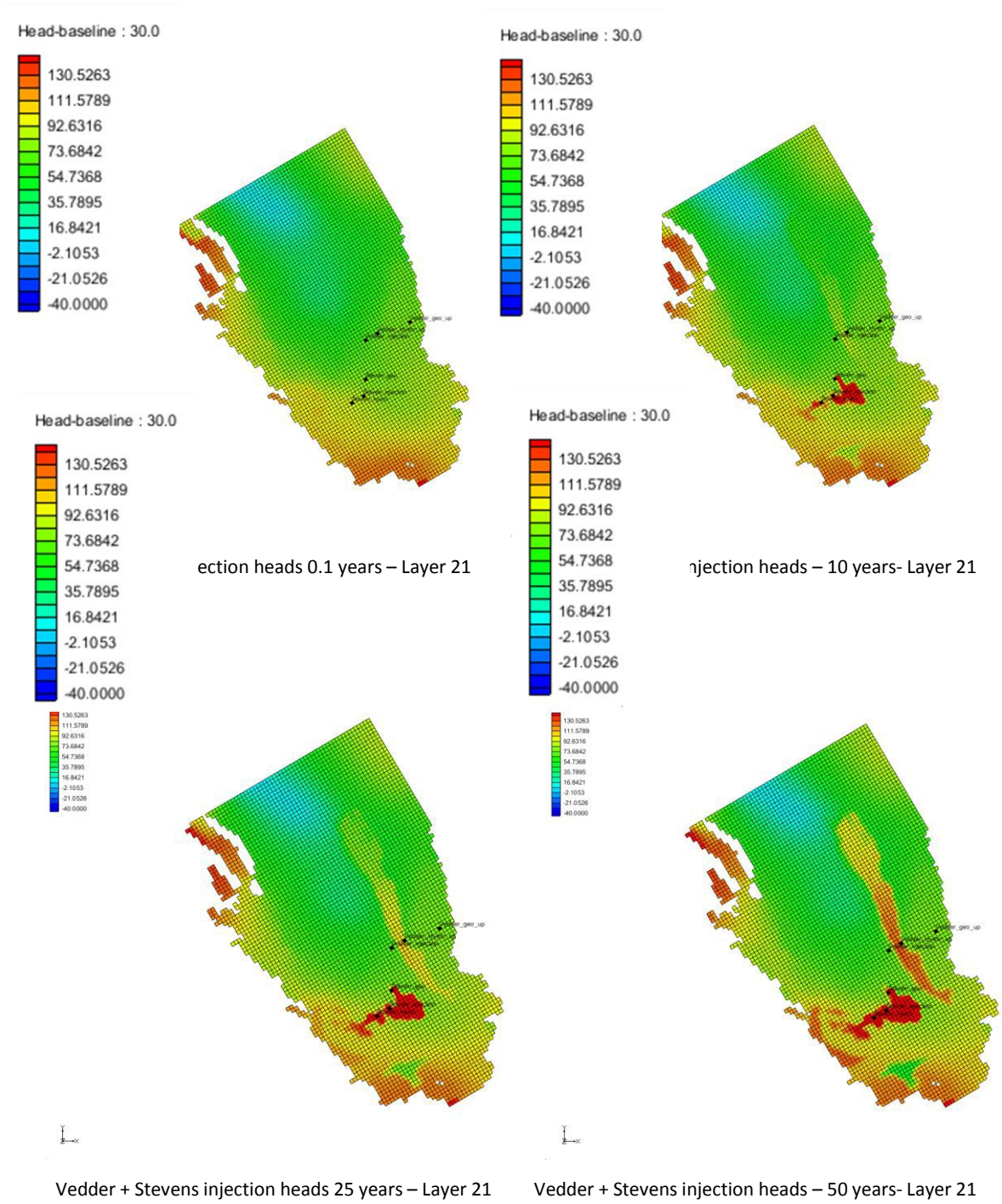

Figure 71: Vedder and Stevens Injection Head Contours (Meters) for Layer 21 at 0.1 Years, 10 Years, 25 Years, and 50 Years

5.4.7 Contour Plots of Displacement at 10, 25 and 50 Years

Here, we evaluate the spatial extent of displacement due to pumping in shallow units and CO_2 injection in deep reservoirs, showing contour plots for two selected horizontal model layers. Figure 72 illustrates vertical displacement in Layer 6 for the baseline scenario at 10, 25, and 50 years. We observe that a large area within the model domain may experience significant

subsidence, a result of the assumed continued pumping of groundwater without countermeasures. Subsidence is strongest after 50 years, with extended regions showing several meters of displacement. When selecting the same contour levels as in Figure 72, we find that the displacement plots for the two CO_2 injection scenarios are identical to the baseline scenario, and are therefore they are not included in this report. Compared to the meter-scale subsidence effects from groundwater pumping, the injection-induced upward displacement from deep storage of CO_2 is on the order of centimeters to perhaps decimeters.

Focusing on the displacement behavior in the deeper layers (Layer 21), we observe distinctly different results for the three simulation scenarios. The baseline displacements, while showing some simulation artifacts at the boundaries, are very small and mostly constant over the simulation period (Figure 73). Results for the Vedder injection show a wide north-south trending region of vertical uplift (up to 10 cm). This is the region where the Vedder formation underlies or intersects Layer 21 and where head increases are large enough to cause measurable uplift (Figure 74). Figure 75 for the combined Vedder and Stevens injection shows an additional area of relatively strong uplift (up to 20 cm) in the south, reflecting the spatial extent of head increase in the Stevens formation. As suggested above, though, the overall magnitude of uplift caused by deep injection is dwarfed by the meter-scale subsidence caused by pumping in the shallower units.

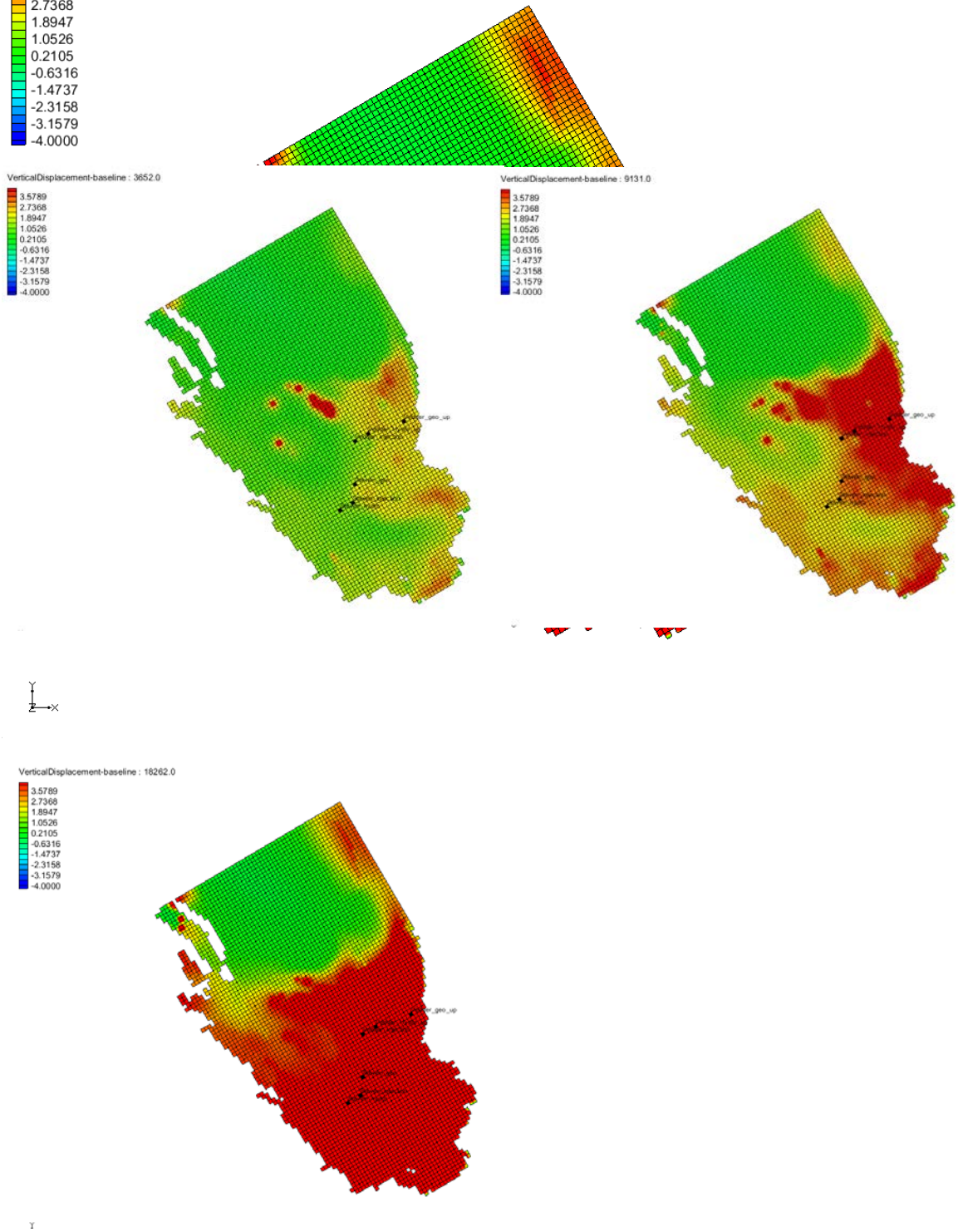

Baseline injection vert. displacement– 50 years Layer 6

Figure 72: Baseline Vertical Displacement Contours (Meters) for Layer 6 at 10 Years, 25 years, and 50 Years

Positive values indicate subsidence, negative values indicate uplift. This plot is identical to those for the CO_2 injection scenarios, which are therefore not shown in this report.

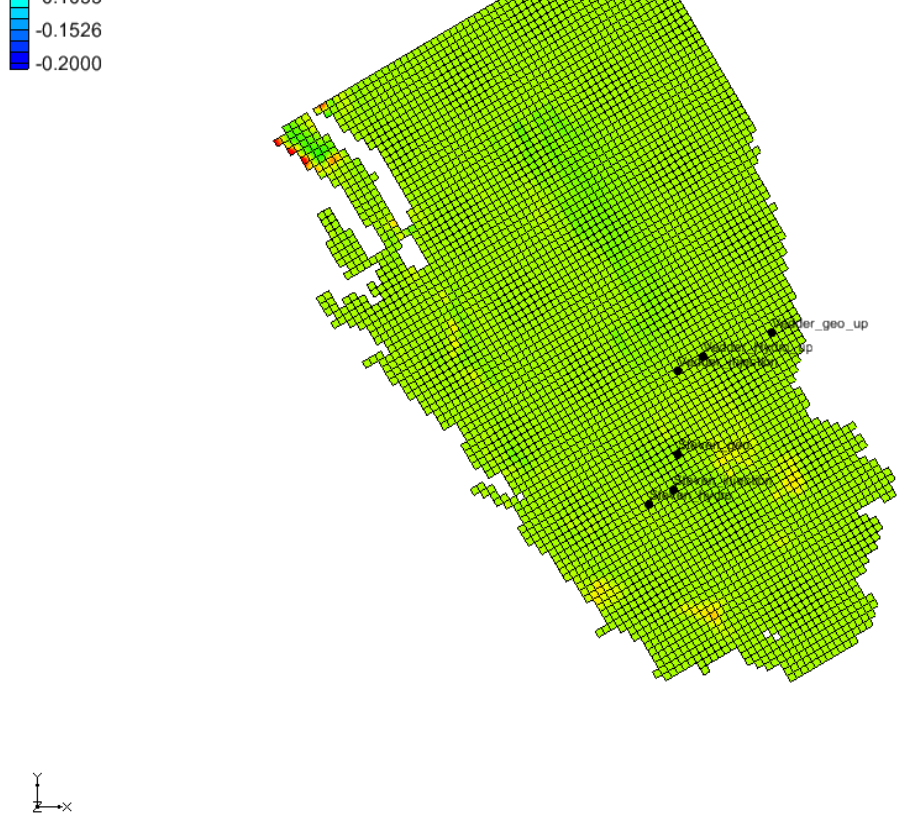

Baseline vertical displacement– 10 years Layer 21

Baseline vertical displacement– 25 years Layer 21

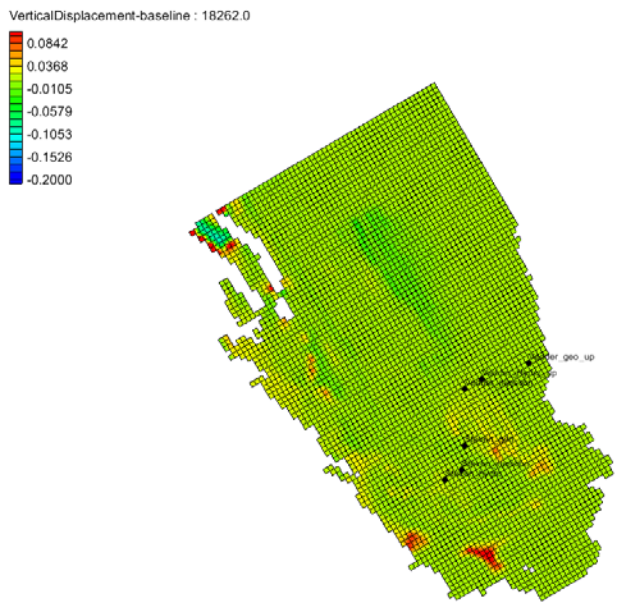

Baseline vertical. displacement– 50 years Layer 21

Figure 73: Baseline Vertical Displacement Contours (Meters) for Layer 21 at 10 Years, 25 Years, and 50 Years

Positive values indicate subsidence, negative values indicate uplift.

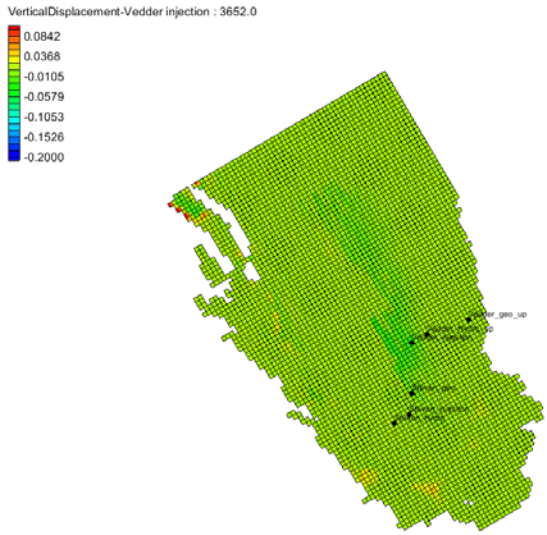

Vedder injection vertical displacement– 10 years Layer 21

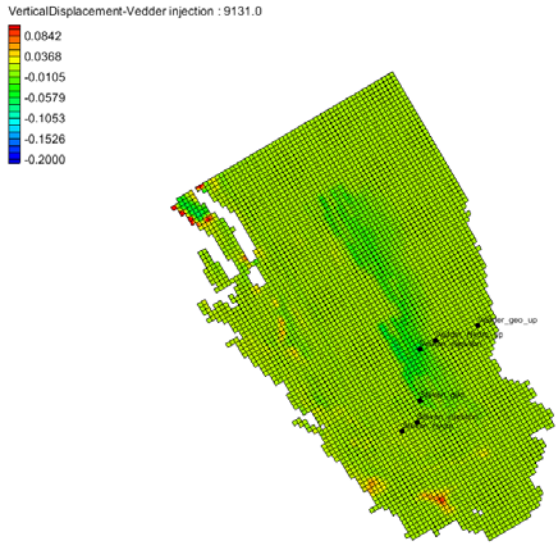

Vedder injection vertical displacement– 25 years Layer 21

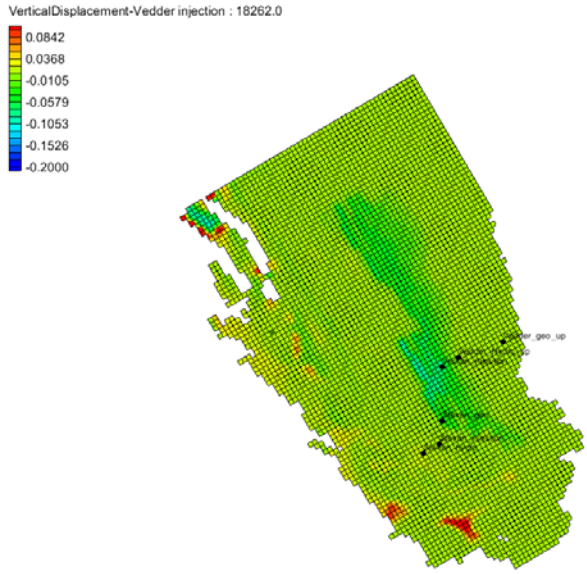

Vedder injection vertical displacement– 50 years Layer 21

Figure 74: Vedder Injection Vertical Displacement Contours (Meters) for Layer 21 at 10 Years, 25 Years, and 50 Years

Positive values indicate subsidence, negative values indicate uplift.

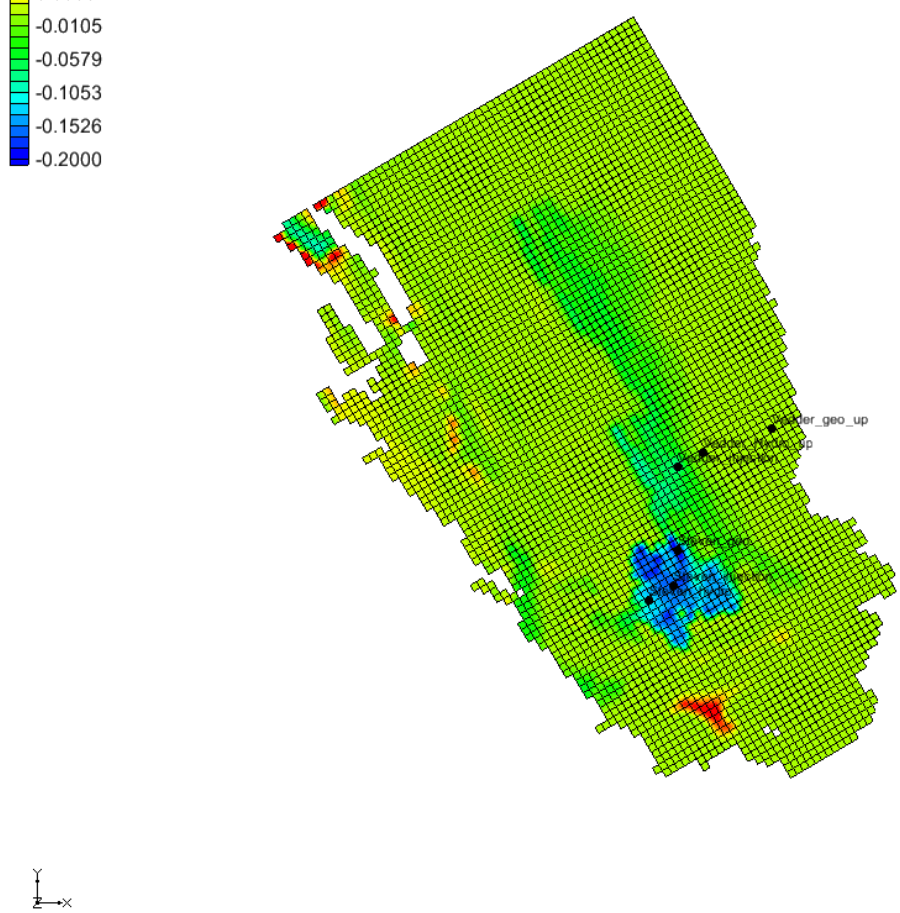

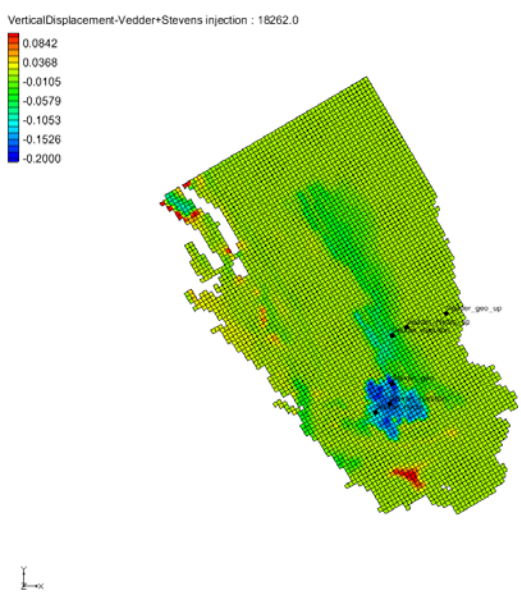

Vedder+Stevens injection vertical. disp.– 50 years Layer 21

Figure 75: Vedder and Stevens Injection Vertical Displacement Contours (Meters) for Layer 21 at 10 Years, 25 Years, and 50 Years

Positive values indicate subsidence, negative values indicate uplift.

5.5 Summary Results from Shallow Water Resources Impact Simulation Model

In this section, we used an accurate and well-calibrated simulation tool for surface water and groundwater resources in the southern San Joaquin Valley, and modified it by vertical extension to allow for modeling the injection of CO_2 into deep geological formations underlying the shallow model domain. The model was implemented (1) to evaluate the future water-level changes in the freshwater aquifers from ongoing water management with or without CO_2 sequestration, and (2) to evaluate similar trends for land-surface deformation with and without CO_2 sequestration. As to the spatial representation of the deeper hydrogeological formations and the description of the multi-phase flow processes in response to CO_2 sequestration, the Shallow Water Resources Impact Simulation Model is less sophisticated than the TOUGH2 simulation model described in Section 4. Thus a first task with the new model was to ensure that the simplified Shallow Water Resources Impact Simulation Model allows for a reasonable representation of CO_2 injection processes and related pressure and displacement impacts. We showed that results from the two models, within limits, are sufficiently similar.

The Shallow Water Resources Impact Simulation Model was applied to three simulation scenarios, the first one being a baseline scenario with ongoing shallow groundwater stresses due to pumping but no CO_2 injection. The first hypothetical CO_2 injection scenario is the same as the one in Section 4, with 5 million tons annually injected into the deep Vedder formation. The second scenario assumes additional injection of the same CO_2 volume into the Stevens formations, with injection occurring about 17 km away for the Vedder injection. For all scenarios, we compared the perturbations, namely head changes and vertical displacement, to shallow pumping and deep injection, at several locations throughout the domain and in various depths ranging from shallow to deep. The following observations were made:

- While ongoing stresses from pumping in shallow aquifers have strong effects on the shallow groundwater regime there, and CO_2 injection causes strong perturbation in the deep subsurface, these effects are largely independent of each other, at least in the absence of localized flow paths (such as leaky faults or fractures). The many geological layers between shallow aquifers in the CO_2 storage reservoirs, many of which are of very low permeability, effectively limit pressure changes from migrating far in vertical directions, downward or upward.
- There is a potential for CO_2 injection to cause extensive land-surface uplift; for the scenarios simulated in this section, the maximum vertical displacement caused by injection was about 20 cm. These upward deformations need to be considered in the context of ongoing subsidence from groundwater pumping. Our simulations demonstrate that such pumping-related deformations in the area might be one order of magnitude larger than those from CO_2 injection.
- The two injection scenarios allowed for some interesting observations with respect to neighboring CO_2 sequestration projects in stacked reservoirs. Overall, despite the Vedder and the Stevens formations being in relatively close proximity and having

partial overlap in the vertical direction, there was little interaction in terms of pressure perturbations, as a result of vertical separation by low-permeability units. With identical CO_2 injection rates and volumes in both units, the Stevens formation exhibited stronger head buildup than the Vedder, a result of the higher degree of compartmentalization in the Stevens. In terms of land-surface uplift, wherever the two formations overlapped vertically and exhibited head increases, the effect on overall vertical displacement was a cumulative one.

- Overall, we consider the above mentioned impacts of CO_2 storage on shallow water resources in the southern San Joaquin Valley to be minimal, in particular in comparison to the expected stresses on the groundwater and surface water systems from ongoing pumping. In other words, we should not expect significant additional effects on recharge and discharge areas, and stream flows, wetlands, and water uses. However, this might be different in regions that are more balanced hydrologically, i.e., where annual aquifer extraction is within the safe yield of the aquifer system and land subsidence issues are non-existent. In these circumstances, the land surface uplift caused by large CO_2 injection projects land deformation could have the potential to create reverse flow along certain canal reaches, or to reduce canal deliveries to agricultural land and managed wetlands (which tend to be located in bottom lands where flow gradients are minimal). The Shallow Water Resources Impact Simulation Model developed in this project is capable of simulating hydrodynamic surface water flows and could thus be a valuable tool for investigating such impacts in the future.

CHAPTER 6:
Conclusions and Outlook

This simulation study investigates the potential impacts of CO_2 injection and storage projects on shallow water resources in the southern San Joaquin Basin of California, including the possibility that such injection, if properly planned, might help to mitigate the land subsidence impacts related to over-pumping of groundwater. The thick marine sediments of this region have been identified as prime targets for future geological carbon sequestration. At the same time, the San Joaquin Valley has complex water management issues in light of increasing water demands, environmental concerns about wetlands, endangered species, and water quality, as well as land subsidence caused by groundwater pumping. In such a vulnerable and valuable system, any water resources impacts of large-scale CO_2 storage need to be evaluated and assessed before industrial-size storage projects get underway. Our study therefore was conducted to answer the following specific questions: (1) Can vertical pressure propagation caused by CO_2 injection through thick layers of shale and sands might have a significant impact on shallow water resources; (2) Can brine displacement through thick layers of shale and sands be an issue for shallow water resources; and (3) What is the degree of surface deformations expected from deep CO_2 storage? A hypothetical CO_2 injection scenario was assumed with industrial-scale injection occurring over an extended time period in the center of the region. The annual rate of CO_2 injected represents the captured and compressed emissions from medium to large coal-fired power plants.

Integration of shallow surface and groundwater simulation models with deep reservoir models has not often been attempted. In this study, we developed an integrated simulation approach that honors complex physical processes associated with supercritical CO_2 injections into a deep geologic information while also taking account of the important characteristics and imposed stresses on the near surface groundwater aquifers that support agricultural, industrial and municipal water supply uses. A two-pronged methodology was applied using two separate but complementary models, both of which covering the entire vertical thickness of interest from deep sequestration reservoirs to shallow water resources. The first model is the "Deep Basin Reservoir Simulation Model", built from a deep CO_2 sequestration reservoir model which was extended upward to include relevant shallow layers, albeit with little level of detail. The second model is the "Shallow Water Resources Impact Simulation Model", built from a shallow water management model which was extended downward to include additional deep sediments, among those sandstone units of interest for geologic carbon sequestration. Both models were applied in parallel efforts to look into CO_2 storage impacts, but the focus of one model was very different from the other.

The Deep Basin Reservoir Simulation Model, which accounts for the complex multiphase flow and buoyancy effects caused by injection of CO_2 and represents the geological structure in great detail, was used to investigate the possible impact of the CO_2 storage on the surface aquifer in terms of the pressure or head change, brine migration and surface uplift. Uncertainty quantification was performed to evaluate the impact of parameter uncertainties. The results

show that the caprock and overlying geological units have sufficient barrier attributes to prevent pressure propagation from the injection layer to the shallow aquifers. Although the updipping structure of the injection layer creates a hydrological connection with shallow surface aquifers several tens of kilometers east of the injection location, the pressure increase and brine flux decrease significantly before reaching this connection. We conclude that the potential concerns associated with the CO_2 storage would be relatively minor except possibly for land surface uplift effects. We note, however, that the Deep Basin Reservoir Simulation Model does not account for any of the dynamic shallow water resources changes in the region caused by groundwater pumping and other water management practices; thus above assessment is not based on a direct comparison of CO_2 injection impacts with other ongoing water system stresses.

The Shallow Water Resources Impact Simulation Model was built from a state-of-the-art surface water and shallow groundwater simulation model of the Central Valley. In addition to groundwater pumping, this model incorporates various important hydrologic inputs based on available land use, irrigation diversion, irrigation and drainage technology, groundwater level, streamflow and meteorological information. To investigate land surface deformation, a new algorithm resolves mechanical aquifer response into elastic and inelastic components and allows for the time delay that typically occurs as stresses propagate through thick impermeable zones. By comparison with results from the Deep Basin Reservoir Simulation Model, we confirmed that this second model was sufficiently accurate in terms of representing the salient CO_2 injection system responses (pressure changes, deformation) of the deep geological layers. Thus, the model could then be used to probe in more detail the possibility of these deep system responses impacting a complex and changing shallow water resources system.

Our simulation results obtained with the Shallow Water Resources Impact Simulation Model show that deep CO_2 injection would create only minor head change and surface uplift in the shallow model layers, which is consistent with the findings from the Deep Basin Reservoir Simulation Model. In fact, the projected changes in shallow groundwater levels and surface displacement as caused by CO_2 injection are much smaller than the significant groundwater drawdown and land subsidence effects that can result from ongoing pumping in shallow aquifers. In terms of surface deformation, the projected long-term subsidence would be slightly offset by the uplift provided by deep well injection of CO_2. This minor uplift is unlikely to cause any damage to existing conveyance facilities or to disrupt agricultural activities in any significant way; in fact, if carefully planned, such uplift could work against unwanted subsidence and could have a positive effect. We note that these conclusions are partly site-specific, since the geologic units in this study are capable of preventing substantial vertical pressure propagation, injection of CO_2 occurs fairly deep, and the overlying shallow water resources are already strongly impacted from over-pumping and thus affected by head decreases and land subsidence.

Overall, our simulations results suggests that even large CO_2 storage projects should have minimal impact on shallow groundwater and surface water systems if, as in the scenarios considered in here, thick layers of shales and sands separate the deep CO_2 injection layers from shallow aquifers. We note, however, that our study does not look into the potential for leakage

of CO_2 and/or brine in localized pathways nor does it consider the possibility of pressure-induced fault activation, or "induced seismicity". To investigate the feasibility and safety of CO_2 storage in the southern San Joaquin Basin, our study would justify that resources should be devoted to evaluating the potential impact from localized pathways or from induced seismicity. It would be a great interest to address such questions using the integrated shallow-to-deep models developed in this study.

REFERENCES

Bergmo, P.E., Grimstad, A.-A., Lindeberg, E. (2011). Simultaneous CO_2 Injection and Water Production to Optimize Aquifer Storage Capacity, *International Journal of Greenhouse Gas Control*, 5, 555-564.

Bertoldi, G.L., Johnston, R.H., Evenson, K.D. (1991). Ground Water in the Central Valley, California–A Summary Report, Regional Aquifer-System Analysis—Central Valley, California, U.S. Geological Survey Professional Paper 1401-A, U.S. Geological Survey.

Belitz K., Phillips, S.P., Gronberg, J.M. (1990). Numerical Simulation of Ground-water Flow in the Central Part of the Western San Joaquin Valley, California, U.S. Geological Survey Water-Supply Paper , 2396.

Birkholzer, J.T., Zhou, Q., Zhang, K., Jordan, P., Rutqvist, J., Tsang, C.-F. (2008). Research Project on CO_2 Geological Storage and Groundwater Resources: Large-Scale Hydrogeological Evaluation and Impact on Groundwater Systems, Annual Report October 1, 2007 to September 30, 2008, Lawrence Berkeley National Laboratory, Berkeley, CA.

Birkholzer, J.T., Zhou, Q. (2009). Basin-scale Hydrogeologic Impacts of CO_2 Storage: Capacity and Regulatory Implications, *Int. J. Greenh. Gas Con.,* 3(6), 745-756.

Birkholzer, J.T., Zhou, Q., Tsang, C.-F. (2009). Large-scale Impact of CO_2 Storage in Deep Saline Aquifers: a Sensitivity Study on the Pressure Response in Stratified Systems, *International Journal of Greenhouse Gas Control,* 3(2), 181-194.

Birkholzer, J.T., Zhou, Q., Cortis, A., Finsterle, S. (2011). A Sensitivity Study on Regional Pressure Buildup from Large-scale CO_2 Storage Projects, *Energy Procedia*, 4, 4371-4378.

Birkholzer, J.T., Cihan, A., Zhou, Q. (2012). Impact-Driven Pressure Management Via Targeted Brine Extraction – Conceptual Studies of CO_2 Storage in Saline Formations, *International Journal of Greenhouse Gas Control*, 7, 168-180.

Boyle Engineering Consulting Engineers Inc. (1990). Documentation and User Manual for Integrated Ground Water and Surface Water Model (IGSM).

Brush, C.F., Dogrul, E.C., Moncrief, M.R., Galef, J., Shultz, S., Tonkin, M., Wendell, D., Kadir, T.N., Chung, F.I. (2008). Estimating Hydrologic Flow Components of the Central Valley Hydrologic Flow System with the California Central Valley Groundwater-Surface Water Model, Proceedings of the California Central Valley Groundwater Modeling Workshop, Lawrence Berkeley National Laboratory, Berkeley, CA, July 10-11, 2008.

Brush C.F., Dogrul, E.C., Kadir, T.N., Chung, F.I. (2011). Applying C2VSIM, an Integrated Hydrologic Model of California's Central Valley, to Assess Local and Regional Impacts of Conjunctive Use Projects, California Department of Water Resources, Sacramento, CA.

Cihan, A., Zhou, Q., Birkholzer, J.T. (2013). Pressure Buildup and Brine Migration in CO_2 Storage Systems with Multiple Leakage Pathways – Application of a New Analytical Solution, *Ground Water,* 51(2), 252-267.

Court, B., Celia, M.A., Nordbotten, J.N., Elliot, T.R. (2011). Active and Integrated Management of Water Resources Throughout CO_2 Capture and Sequestration Operations, 10th International Conference on Greenhouse Gas Control Technologies, GHGT-10, *Energy Procedia*, 4, 4221-4229.

Dogrul, E.C., Brush, C.F., Kadir, T.N. (2011). Integrated Water Flow Model (IWFM), A Tool For Numerically Simulating Linked Groundwater, Surface Water And Land-Surface Hydrologic Processes, California Department of Water Resources, Sacramento, CA.

Doherty, J., 2010, PEST, Model-independent Parameter Estimation—User manual (5th ed., with slight additions), Brisbane, Australia, Watermark Numerical Computing.

Faunt, C.C., Hanson, R.T., Belitz, K. (2009a). Introduction, Overview of Hydrogeology, and Textural Model of California's Central Valley, in "Groundwater Availability of the Central Valley Aquifer, California," edited by Faunt, C.C., U.S. Geological Survey Professional Paper 1766, 225 p.

Faunt, C.C., Belitz, K., Hanson, R.T. (2009b). Groundwater Availability in California's Central Valley, in "Groundwater Availability of the Central Valley Aquifer, California," edited by Faunt, C.C., U.S. Geological Survey Professional Paper 1766, 225 p.

Faunt, C.C., Hanson, R.T., Belitz, K., Schmid, W., Predmore, S.P., Rewis, D.L., McPherson, K. (2009c). Numerical Model of the Hydrologic Landscape and Groundwater Flow in California's Central Valley, in "Groundwater Availability of the Central Valley Aquifer, California," edited by Faunt, C.C., U.S. Geological Survey Professional Paper 1766, 225 p.

Fjær, E., Holt, R.M., Horsrud, P., Raaen, A.M., Risnes, R. (2008). Petroleum Related Rock Mechanics. 2nd ed. Amsterdam: Elsevier.

Harbaugh, A.W. (2005). MODFLOW-2005, the U.S. Geological Survey Modular Ground-water Model -- the Ground-Water Flow Process: U.S. Geological Survey Techniques and Methods 6-A16, variously p.

Harter, T., Ruud, N.C., Lund, J.F., Marques, G.R., Jenkins, M. (2008). Water Management and Estimation of Groundwater Pumping as Closure to the Water Balance of a Semi-Arid, Irrigated Agricultural Basin: Tule River Basin (Southern Tulare County), Proceedings of the California Central Valley Groundwater Modeling Workshop, Lawrence Berkeley National Laboratory, Berkeley, CA, July 10-11, 2008.

Hosford Scheirer, A., ed. (2007). Petroleum Systems and Geologic Assessment of Oil and Gas in the San Joaquin Basin Province, California: U.S. Geological Survey Professional Paper 1713. (Available at http://pubs.usgs.gov/pp/pp1713/.)

Jaeger, J., Cook, N.G., Zimmerman, R. (2007). Fundamentals of Rock Mechanics, forth ed., Wiley-Blackwell.

Jung, Y., Zhou, Q., Birkholzer, J.T. (2013). Early Detection of Brine and CO_2 Leakage through Abandoned Wells Using Pressure and Surface-deformation Monitoring Data: Concept and Demonstration, *Advances in Water Resources*, doi:10.1016/j.advwatres.2013.06.008.

Kern County Water Agency (2013). Water Supply Report, 2011, Bakersfield, CA.

Laudon, J., Belitz, K. (1991). Texture and Depositional History of Late Pleistocene–Holocene Alluvium in the Central Part of the Western San Joaquin Valley, California, *Bulletin of the Association of Engineering Geologists*, 28(1), 73–88.

Miller, N.L., Brush, C.F., Dale, L.L., Vicuna, S.D., Kadir, T.N., Dogrul, E.C., Chung, F.I. (2008). Analysis of Droughts in the California Central Valley Surface-Groundwater-Conveyance Model, Proceedings of the California Central Valley Groundwater Modeling Workshop, Lawrence Berkeley National Laboratory, Berkeley, CA, July 10-11, 2008.

Namvar, R., Tijerina, E., Taghavi, A. (2008). An Analytical Tool for Integrated Regional Water Management Plan Development – Application to Kings Basin, Proceedings of the California Central Valley Groundwater Modeling Workshop, Lawrence Berkeley National Laboratory, Berkeley, CA, July 10-11, 2008.

Page, R.W. (1986). Geology of the Fresh Ground-Water Basin of the Central Valley, California, with Texture Maps and Sections, Regional Aquifer-System Analysis—Central Valley, California, U.S. Geological Survey Professional Paper 1401-C, U.S. Geological Survey.

Planert, M., Williams, J.S. (1995). Ground water atlas of the United States—California, Nevada, U.S. Geological Survey Hydrologic Atlas, HA 730–B.

Phillips, S.P., Belitz, K. (1991). Calibration of a Textured-based Model of a Ground-water Flow System, Western San Joaquin Valley, California, *Ground Water*, 29(5), 702–715.

PIER Collaborative Report (2006). An Overview of Geologic Carbon Sequestration Potential in California, California Energy Commission Report CEC-500-2006-088, prepared by California Geological Survey.

Pruess, K. (2005). ECO2N: A TOUGH2 Fluid Property Module for Mixtures of Water, NaCl, and CO_2. LBNL-57952, Lawrence Berkeley National Laboratory, Berkeley, CA, USA.

Rutqvist, J., Birkholzer, J.T., Tsang, C.-F. (2008). Coupled Reservoir–Geomechanical Analysis of the Potential for Tensile and Shear Failure Associated with CO_2 Injection in Multilayered Reservoir–Caprock Systems, *International Journal of Rock Mechanics and Mining Sciences*, 45(2), 132-143.

Rutqvist, J., Birkholzer, J.T., Cappa, F., Tsang, C.-F. (2007). Estimating Maximum Sustainable Injection Pressure during Geological Sequestration of CO_2 using Coupled Fluid Flow and Geomechanical Fault-Slip Analysis, *Energy Conversion and Management Journal*, 48(6), 1798-1807.

Rutqvist J. (2012). The Geomechanics of CO_2 Storage in Deep Sedimentary Formations, *Geotech Geol Eng*, DOI:10.1007/s10706-011-9491-0.

Ruud, N.C., Leffler, P., Dotson, L. (2008). Numerical Groundwater Flow Model for the Kaweah Delta Water Conservation District, Southern San Joaquin Valley, California, Proceedings of the California Central Valley Groundwater Modeling Workshop, Lawrence Berkeley National Laboratory, Berkeley, CA, July 10-11, 2008.

Schmid, W., Hanson, R.T., Mattock III, T.M., Leake, S.A. (2006). User's Guide for the Farm Process (FMP) for the U.S. Geological Survey's Modular Three-dimensional Finite-difference Ground-water Flow Model, MODFLOW-2000, *U.S. Geological Survey Techniques and Methods,* 6-A17, 127 p.

Schmid, W., Hanson, R.T. (2009). The Farm Process Version 2 (FMP2) for MODFLOW-2005 – Modifications and Upgrades to FMP1. U.S. Geol. Survey Techniques and Methods 6–A32.

Terzaghi, K., Peck, R.B. (1948). Soil Mechanics in Engineering Practice, New York, John Wiley & Sons, Inc. 566 p.

U.S. DOE (2012). The United States 2012 Carbon Utilization and Storage Atlas, Fourth Edition, U.S. Department of Energy, Office of Fossil Energy, Available at

http://www.netl.doe.gov/technologies/carbon_seq/refshelf/atlas/

USGS (1995). Groundwater Atlas of the United States, Segment 1, California and Nevada, Hydrologic Investigations Atlas 730-B, U.S. Geological Survey, Reston, VA.

Wagoner, J. (2009). 3D Geologic Modeling of the Southern San Joaquin Basin for the Westcarb Kimberlina Demonstration Project, Status Report, Lawrence Livermore National Laboratory.

Wainwright, H.M., Finsterle, S., Zhou, Q., Birkholzer, J.T. (2013). Modeling the Performance of Large-Scale CO_2 Storage Systems: A Comparison of Different Sensitivity Analysis Methods, *International Journal of Greenhouse Gas Control*, 17, 189-205, ISSN 1750-5836, http://dx.doi.org/10.1016/j.ijggc.2013.05.007.

Williamson, A.K., Prudic, D.E., Swain, L.A. (1989). Ground-Water Flow in the Central Valley, California, Regional Aquifer-System Analysis—Central Valley, California, U.S. Geological Survey Professional Paper 1401-D, U.S. Geological Survey.

Zhang, K., Wu, Y.S., Pruess, K. (2008). User's Guide for TOUGH2-MP – A Massively Parallel Version of the TOUGH2 Code. Report LBNL-315E, Lawrence Berkeley National Laboratory, Berkeley, CA, USA.

Zhou, Q., Birkholzer, J.T., Tsang, C.-F., Rutqvist, J. (2008). A Method for Quick-Assessment of CO_2 Storage Capacity in Closed and Semi-Closed Porous Formations, *International Journal of Greenhouse Gas Control*, 2(4), 626-639, DOI:10.1016/j.ijgcc.2008.02.004.

Zhou, Q., Birkholzer, J.T., Wagoner, J.L. (2011). Modeling the Potential Impact of Geologic Carbon Sequestration in the Southern San Joaquin Basin, California, The Ninth Annual Carbon Capture & Sequestration, Pittsburgh, PA.

Zhou, Q., Birkholzer, J.T. (2011). On Scale and Magnitude of Pressure Build-up Induced by Large-scale Geologic Storage of CO_2, *Greenhouse Gases: Sci. Technol*., 1, 11-20.